

## **UPWELLING HISTORY OF THE BENGUELA-NAMIBIA SYSTEM: A SYNTHESIS OF LEG 175 RESULTS<sup>1</sup>**

Wolfgang H. Berger,<sup>2</sup> Carina B. Lange,<sup>2</sup> and Gerold Wefer<sup>3</sup>

### **ABSTRACT**

Upwelling along the western coast of Africa south of the equator may be partitioned into three major areas, each having its own dynamics and history: (1) the eastern equatorial region, comprising the Congo Fan and the area of Mid-Angola; (2) the Namibia upwelling system, extending from the Walvis Ridge to Lüderitz; and (3) the Cape Province region, where upwelling is subdued. The highest nutrient contents in thermocline waters are in the northern region, the lowest in the southern one. Wind effects are at a maximum near the southern end of the Namibia upwelling system, and maximum productivity occurs near Walvis Bay, where the product between upwelling rate and nutrient content of upwelled waters is at a maximum.

In the Congo/Angola region, opal tends to follow organic carbon quite closely in the Quaternary record. However, organic carbon has a strong precessional component, while opal does not. Despite relatively low opal content, sediments off Angola show the same patterns as those off the Congo; thus, they are part of the same regime. The spectrum shows nonlinear interference patterns between high- and low-latitude forcing, presumably tied to thermocline fertility and wind.

On Walvis Ridge, as in the Congo-Angola region, the organic matter record behaves normally; that is, supply is high during glacial periods. In contrast, interglacial periods are favorable for opal deposition. The pattern suggests reduction in silicate content of the thermocline during glacial periods. The reversed phase (opal abundant during interglacials) persists during the entire Pleistocene and can be demonstrated deep into the Pliocene, not just on Walvis Ridge but all the way to the Oranje

<sup>1</sup>Berger, W.H., Lange, C.B., and Wefer, G., 2002. Upwelling history of the Benguela-Namibia system: a synthesis of Leg 175 results. In Wefer, G., Berger, W.H., and Richter, C. (Eds.), *Proc. ODP, Sci. Results*, 175, 1–103 [Online]. Available from World Wide Web: <[http://www-odp.tamu.edu/publications/175\\_SR/VOLUME/SYNTH/SR175SYN.PDF](http://www-odp.tamu.edu/publications/175_SR/VOLUME/SYNTH/SR175SYN.PDF)> [Cited YYYY-MM-DD]

<sup>2</sup>Geosciences Research Division, Scripps Institution of Oceanography, University of California, San Diego, La Jolla CA 92093, USA. Correspondence author: [wberger@ucsd.edu](mailto:wberger@ucsd.edu)

<sup>3</sup>Geowissenschaften, University of Bremen, Postfach 330440, Bremen D-28334, Germany.

Initial receipt: 27 November 2000

Acceptance: 24 October 2001

Web publication: 5 February 2002

Ms 175SR-235

River and off the Cape Province. From comparison with other regions, it appears that silicate is diminished in the global thermocline, on average, whenever winds become strong enough to substantially shorten the residence time of silicate in upper waters (Walvis Hypothesis, solving the Walvis Paradox of reversed phase in opal deposition).

The central discovery during Leg 175 was the documentation of a late Pliocene opal maximum for the entire Namibia upwelling system (early Matuyama Diatom Maximum [MDM]). The maximum is centered on the period between the end of the Gauss Chron and the beginning of the Olduvai Chron. A rather sharp increase in both organic matter deposition and opal deposition occurs near 3 Ma in the middle of the Gauss Chron, in association with a series of major cooling steps. As concerns organic matter, high production persists at least to 1 Ma, when there are large changes in variability, heralding subsequent pulsed production periods. From 3 to 2 Ma, organic matter and opal deposition run more or less parallel, but after 2 Ma opal goes out of phase with organic matter. Apparently, this is the point when silicate becomes limiting to opal production. Thus, the MDM conundrum is solved by linking planetary cooling to increased mixing and upwelling (ramping up to the MDM) and a general removal of silicate from the upper ocean through excess precipitation over global supply (ramping down from the MDM).

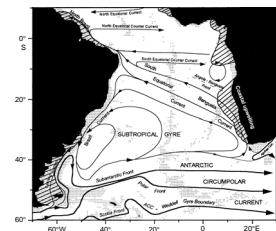
The hypothesis concerning the origin of the Namibia opal acme or MDM is fundamentally the same as the Walvis Hypothesis, stating that glacial conditions result in removal of silicate from the thermocline (and quite likely from the ocean as a whole, given enough time). The Namibia opal acme, and other opal maxima in the latest Neogene in other regions of the ocean, marks the interval when a cooling ocean selectively removes the abundant silicate inherited from a warm ocean. When the excess silicate is removed, the process ceases. According to the data gathered during Leg 175, major upwelling started in the late part of the late Miocene. Presumably, this process contributed to the drawing down of carbon dioxide from the atmosphere, helping to prepare the way for Northern Hemisphere glaciation.

## INTRODUCTION AND OVERVIEW

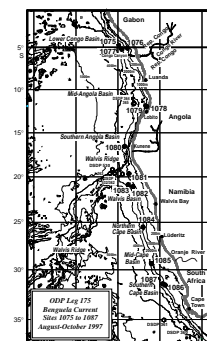
### Leg 175

The goal of Leg 175 of the Ocean Drilling Program (ODP) was to provide for the reconstruction of the late Neogene history of the great eastern boundary current off Namibia and of the upwelling regimes north and south of the Walvis Ridge. Upwelling north of the Walvis Ridge is dominated by the Congo River outflow and the influence of a large cyclonic gyre, the Angola Dome. Upwelling on the landward side of Walvis Ridge and off southwestern Africa in general is intimately tied to the dynamics of the Benguela Current. The front between the two systems runs southeast to northwest just north of the Walvis Ridge (Fig. F1). On 12 August 1997, the *JOIDES Resolution* left Las Palmas (Canary Islands) on a course for the first site (1075) on the Congo Fan. During the 57-day expedition, we occupied 13 sites (Fig. F2) and drilled 40 holes. Overall penetration totaled 8210.5 m, with 8003.2 m of recovery (see the "Appendix," p. 54, for a summary of drilling results). On 9 October 1997, the vessel entered the port of Cape Town, South Africa, ending the leg.

F1. South Atlantic circulation and areas of high productivity, p. 55.



F2. Locations of Sites 1075–1087, p. 56.



Like other eastern boundary upwelling systems studied during recent ODP legs (Peru and California), the Angola-Namibia regimes are characterized by organic-rich sediments that contain an excellent record of productivity history that can be read on a very fine scale, thanks to high sedimentation rates. In addition, this environment is a prime setting for natural experiments in diagenesis, driven largely by bacterial action, including the formation of dolomite and the production of methane and carbon dioxide. The drilling transects realized represent a compromise between geographic coverage, likelihood of continuous stratigraphy, hydrocarbon hazards, and time constraints. Off the Congo and off Angola, where active exploration for offshore hydrocarbons is in progress, drilling was limited to a maximum of 200 meters below seafloor (mbsf) (six sites), and some of the sites initially proposed were rejected altogether for safety reasons. On the Walvis Ridge and off Namibia and South Africa, we drilled to refusal of advanced hydraulic piston coring (APC) at two sites and down to between 400 and 600 mbsf at five more sites.

This overall drilling strategy resulted in the recovery of Quaternary sediments at the sites north of the Walvis Ridge and of upper Neogene sediments on the Walvis Ridge and south of it. At some of the southern sites, the drill reached Miocene deposits. Site 1087 (the last drilled) includes upper Eocene sediments, but the record in the lower section has large gaps. The chief types of facies encountered are diatomaceous clays (Congo sites) and diatomaceous calcareous clays (Walvis Ridge and Walvis Bay sites). The southernmost three sites in the Cape Basin (Cape Basin group sites) had calcareous ooze with very little opal.

### **Scientific Objectives and Principal Results**

The main scientific objectives of Leg 175 were concerned with paleoceanographic reconstruction, but also included diagenetic processes within upwelling sediments. Extensive preparations for the drilling expedition, in addition, yielded much information on seismic stratigraphy and Quaternary sediment patterns. The major questions driving Leg 175 research were formulated based on this preparatory work (carried out by Bremen scientists) (Bleil et al., 1995, 1996) and on previous studies by many others (see Summerhayes et al., 1992, 1995; Wefer et al., 1996) and by the scientists of cruises of the Deep Sea Drilling Project (see Bolli, Ryan, et al., 1978; Moore, Rabinowitz, et al., 1984; Hay, Sibuet, et al., 1984; Hsü and Weissert, 1985). They may be summarized as follows (cf. Shipboard Scientific Party, 1998a):

1. Regarding Quaternary upwelling cycles, what is their precise nature, what is their relationship to Milankovitch forcing, and what are the implications for changing heat transport from south to north across the equator?
2. What can the sediments deposited off the mouth of the Congo River tell us about the evolution of climate in central Africa in the late Neogene?
3. In what ways does the Benguela Current change its course and strength through geologic time, and how are such changes related to the general circulation in the South Atlantic?
4. Are there fundamental differences in the dynamics of upwelling through time off the coast of Namibia?

5. How do the Namibia upwelling system and the Benguela Current respond to known climate shifts on various geologic time-scales?
6. What kinds of diagenetic processes help determine the nature of the deposits off southwestern Africa, and how fast does diagenesis proceed?

Many new insights have been gained regarding these and related questions in the wake of Leg 175. The principal results may be summarized as follows:

1. The Congo Fan sediments contain clues to wet-dry cycles in the interior of Africa; a major change in climatic conditions was initiated somewhat earlier than 1 m.y. ago (Uliana et al., [Chap. 11](#), this volume).
2. Monsoon winds forced by North African summer insolation modify the southeast trade winds and affect upwelling intensity well south of the equator.
3. Increased upwelling does not necessarily imply increased deposition of diatom debris. Over much of the time span studied, the reverse is the case, for reasons yet unknown (presumably low silicate content in the thermocline).
4. The great cooling steps between 3 and 2 Ma and the climate shift near 1 Ma (toward large-amplitude glacial-interglacial cycles) affected the upwelling history in fundamental ways and resulted in marked changes in the pelagic and benthic environments.
5. Chemical activity within the sediments is driven by the availability of reactive organic matter; where it is abundant, there is intense production of methane and carbon dioxide and formation of new minerals, especially dolomite.

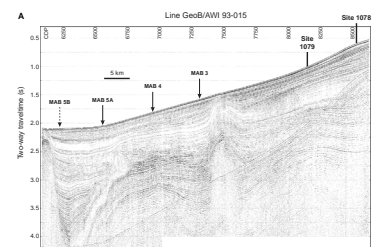
### Sediment Recovery and Gas Content

Many or most of the sections drilled showed continuous sequences with high rates of sedimentation. This was a result not of a lack of disturbance along the margin of southwestern Africa (slumping is common, in fact) but of good control from seismic stratigraphy, gained through the efforts of Volkhard Spiess and his collaborators. An outstanding difference between the sites north and south of the Walvis Ridge is that sites to the north show the effects of salt tectonics and those to the south do not (Fig. [F3](#)). The salt tectonic structure is a reminder that back in the Aptian, when the Walvis Ridge and the Rio Grande Rise formed a continuous barrier across the opening South Atlantic, there was a restricted evaporite basin north of this barrier.

Continuity of recovery was affected, in many cases, by the strong development of gas pressure from abundant methane and carbon dioxide, which produced sediment expansion and created voids and cracks. This process also impacted the measurement of physical properties. Although the high gas content had its drawbacks (besides posing a hazard in cases), it also retarded compacting of sediments, permitting fast drilling. Because of this, 13 sites were ultimately occupied, rather than 8 as planned.

The detailed guidance from seismic profiles and the strict application of safety principles resulted in the avoidance of clathrates. We found no evidence for the decrease in salinity (or chlorinity) corresponding to an addition of freshwater from melting of clathrates in sediments recov-

**F3.** Nature of deposition on Walvis Ridge, p. 57.



ered from areas where clathrates might be expected (Murray et al., 1998). Presumably, the highly reflective “cloud” structures seen in the seismic profiles over anticlinal features in the Congo Fan region (Shipboard Scientific Party, 1998b, p. 56) indicate the presence of clathrates. Also, narrow disturbed zones where sound is dispersed (leaving a blank record) are seen, suggesting venting of gas from some depth. Clearly, the formation of gas within margin deposits and the return of gas to the atmosphere are problems of prime importance, but owing to the limitations of the *JOIDES Resolution*, we have but little to contribute in this regard.

### Focus of the Review

Our focus in this overview is entirely on paleoceanographic problems, from the nature of Quaternary sediment cycles to the response of the upwelling systems to global cooling in the late Neogene. The outstanding issue in this context is the “Walvis Paradox,” that is, the observation that increased upwelling during glacial stages results in decreased deposition of opal. The paradox manifests itself on two levels: within the scale of glacial–interglacial fluctuations and within the scale of the last 4 m.y., where the onset of strong glaciations within the Quaternary results in reduced deposition of diatoms during the last ~2 m.y. off Namibia. The complex evidence surrounding the Walvis Paradox makes interpretation difficult.

## OCEANOGRAPHY, NOMENCLATURE, PROXIES, AND SEDIMENT PATTERNS

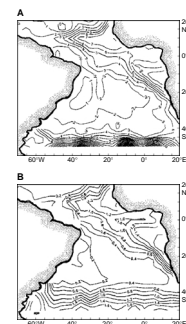
### Thermocline Fertility and Upwelling

The goal of Leg 175 was to provide for the reconstruction of the history of currents and of mixing and upwelling dynamics off the margin of western Africa south of the equator. To this end, we largely use the deposits generated by biologic production in surface waters (that is, microfossils and nannofossils), assuming certain responses to varying productivity. Also, the preservation state of the fossils is useful; it can track chemical properties of bottom waters and early diagenetic reactions.

Of special interest, in the context of upwelling, is the distribution of nutrients in subsurface waters. Surprisingly, waters with high phosphate and silicate content underlie the region off Angola, where productivity is low relative to that off Namibia. The high productivity regions—off the Congo and south of Walvis Ridge—are at the very edge of a high-nutrient region, rather than in its center (Fig. F4). One may readily conclude that the nutrient content of thermocline waters is not the crucial factor, or at least not the only important factor, in determining the productivity of overlying waters. The nutrients also have to be brought upward into the sunlit zone. This is the work of upwelling and mixing. It is the combination of the two factors, high nutrient content and vigorous mixing, that results in high productivity. The general formulation of this concept may be given as follows:

$$PP \equiv NCT \times \text{wind}, \quad (1)$$

F4. Silicate and phosphate patterns in subsurface waters, p. 59.



where PP is the primary productivity, and “wind” represents mixing intensity (that is, the flux of thermocline water to the sunlit layer). NCT stands for nutrient content of the thermocline. The symbol expresses equivalence.

The obvious corollary of Equation 1 is that “wind” is equivalent to the ratio between productivity and nutrient content. For these two parameters, estimates are possible from the study of sediments, but only if flux proxies and nutrient proxies are kept separate when discussing paleoproductivity. Flux proxies represent an important fraction of the material delivered to the seafloor, while nutrient proxies contain information about the chemistry of the seawater that provides the nutrients (for a discussion of proxies see Wefer et al., 1999.) Thus, in principle, it is possible to make estimates of relative wind stress through time in the upwelling regions off Namibia. Such estimates can then be compared with the supply of dust from the Namibian Desert (which is itself a result of Namibian upwelling dynamics). This has not been done, but the first steps in this direction have been made (see Anderson et al., [Chap. 21](#), this volume).

### Temperature Anomalies and Namibia Upwelling System

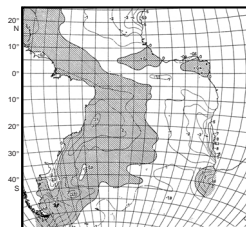
Vigorous vertical mixing brings cold waters to the surface and results in temperature anomalies in surface waters. Such anomalies have been mapped in the South Atlantic since the German *Meteor* Expedition (1925–1927) (Fig. [F5](#)). The pattern shows large anomalies off Namibia in the vicinity of Lüderitz. Since the nutrient content of upwelled waters decreases rapidly south of 25°S (Fig. [F4](#)), optimum conditions for high productivity should occur just north of that latitude (that is, north of Lüderitz) in Walvis Bay.

We shall refer to this upwelling region as the “Namibia” or “Walvis” upwelling system because of its location. The name “Benguela upwelling system,” which is commonly used to describe upwelling in regions from the coast of Angola to that of the cape is retained as a term with that broader meaning. Strictly speaking, there is no well-defined “Benguela upwelling system.” The three upwelling regions (Congo-Angola, Walvis-Namibia, and Cape Province) are quite distinct (e.g., Chapman and Shannon, 1987; Hay and Brock, 1992; Berger et al., 1998a; Giraudeau et al., in press).

The front just north of the Walvis Ridge (“Angola-Benguela” Front) should be referred to, more rationally, as the “Angola-Namibia” Front. This would have the benefit of describing its location quite accurately, in contrast with present usage. In fact, there is no front off Benguela, which is close to the center of the Angola coast (12°S). The great current off Namibia turns toward the open sea and northward and westward at ~15°S (Figs. [F1](#), [F5](#)). It never gets close to Benguela (Peterson and Stramma, 1991; Tomczak and Godfrey, 1994), whose name it carries.

The negative temperature anomaly off Namibia (Fig. [F5](#)) reflects mixing, as mentioned, and hence, is a measure of wind action, shown as “wind.” In principle, it should be possible to capture the gradient of the anomaly along the Walvis Ridge (as here the seafloor is sufficiently elevated to preserve carbonate well offshore). Alternatively, or in addition, the negative anomaly within the Namibia upwelling system, as seen in the sediments, should provide a good guide to wind action, that is, intensity of upwelling and mixing. Clearly, additional information (be-

[F5](#). Annual mean of surface temperature anomalies, p. 60.



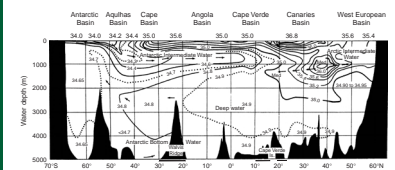
sides a temperature gradient) is needed to define wind fields; the point is that upwelling needs to be separated conceptually from productivity to make progress in that direction.

### Carbonate Preservation and NADW Production

Preservation of calcareous fossils (nannofossils and foraminifers) on the seafloor depends on the depth of the seafloor and the position of the carbonate compensation depth and the lysocline level. In turn, the lysocline is tied to the lower boundary of the North Atlantic Deep Water (NADW), where it meets the underlying Antarctic Bottom Water (AABW). The distribution of salinity nicely reflects the overall pattern of flow (Fig. F6). In fact, the hydrographic boundary near 2°C, first mapped by Georg Wüst of the *Meteor* Expedition, is virtually congruent with the lysocline, except where organic matter supply increases the dissolution of carbonate on the continental margin. The present distribution of NADW puts this boundary between 4 and 4.8 km west of the Mid-Atlantic Ridge (going north from the Rio Grande Rise to the equator). In the eastern trough, the situation is different for the basins north and south of the Walvis Ridge, which blocks the AABW from entering the Angola Basin. (AABW enters, but through the Romanche Trench near the equator, where it mixes with NADW.) In the Cape Basin, then, we expect a sharp boundary somewhere near 4 km. In the Angola Basin, the boundary is likely to be fuzzy and closer to 5 km.

Where the seafloor is bathed by NADW, preservation of carbonate tends to be good for a given depth of deposition. The production of NADW varies greatly through time, as can be documented by using carbonate preservation stratigraphy or carbon isotope stratigraphy or both (e.g., Bickert and Wefer, 1996; Curry, 1996). The preservation stratigraphy on the outer Walvis Ridge suggests a rapid rise of NADW production (that is, better preservation of carbonate) sometime within the late Miocene and another step of increase near the beginning of the Pliocene (e.g., Moore et al., 1984, p. 15). In essence, this pattern agrees with the great shift of silica from the North Atlantic to the North Pacific at the end of the middle Miocene (Keller and Barron, 1983; Baldauf and Barron, 1990), which is another expression of NADW production (NADW removes silicate from the deep North Atlantic). The carbonate trends and the silica shift run parallel to the overall cooling of the planet as seen in oxygen isotopes (Shackleton and Kennett, 1975; Miller et al., 1987; see review in Berger and Wefer, 1996b). Thus, increased production of NADW on this late Neogene timescale is seen to result from cooling. With the onset of glaciation in the Northern Hemisphere, that is, ice surrounding the high-latitude margins of the North Atlantic, an optimum situation is reached whereby vigorous evaporation combines with strong cooling to make plenty of deep water. However, as cooling proceeds into severe glacial periods, the optimum is exceeded, which results in a decrease of carbonate preservation upon cooling on glacial-interglacial timescales of the late Quaternary. (At this point, opaline deposits return, sporadically, to the North Atlantic; see Baldauf and Barron, 1990; their fig. 13.) Thus, we have another paradox, this time referring to the preservation of carbonate, whereby cooling first results in improved preservation, but further cooling beyond an optimum results in increased dissolution. One important task is to find out where the optimum is located along the cooling curve and within the glacial-interglacial cycles.

F6. Deepwater circulation as seen in the distribution of salinity, p. 61.



## Concept of Optimum

We shall make use of the concept of “optimum” in several contexts: carbonate preservation, organic matter supply, and opal deposition. The simplest way to envisage an optimum situation is to think of it as a product of two factors that are varying out of phase with each other:

$$\text{Optimum} = \max(f_1a, f_2b), \quad (2)$$

where  $f_1a$ ,  $f_2b$  stands for some interaction between two variables (for example, a product). The task is to identify the two (main) factors involved. The two factors may be antagonistic, at least over some relevant range. In the case of productivity, it is thermocline fertility and mixing intensity (Berger et al., 1994; Herguera and Berger, 1994). In the case of carbonate preservation, it is evaporation and cooling of surface waters in the North Atlantic. Evaporation needs dry, warm winds; cooling needs temperatures near freezing. Best results are obtained when both conditions prevail in series (Sargasso to Iceland), or seasonally, or both. In the case of opal deposition, it is silicate content of the thermocline and deep mixing and, possibly, the presence of a shelf. Planetary cooling enhances deep mixing, but buildup of ice removes shelves.

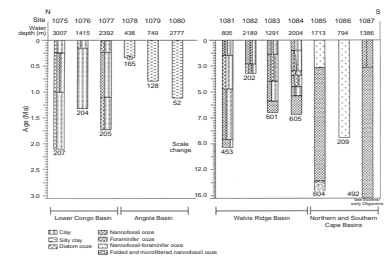
## Sediment Patterns

The sediments accumulating along the margin of southwestern Africa are well suited to study carbonate preservation and the deposition of organic matter and opal as a function of time. Surveys of sediment patterns recorded during Leg 175 are given by Wefer et al. (1998), Pufahl et al. (1998), and Berger et al. (1998a) in the Leg 175 *Initial Reports* volume, as well as in the site reports therein. Four different major sedimentary facies regimes characterize the region drilled during Leg 175 (see Fig. F7). Off the mouth of the Congo, sediments have a large terrigenous component. This is also true for the silts and clays recovered off Angola at sites close to the shelf edge, where very high sedimentation rates prevail. On the Walvis Ridge and in its vicinity, sediments have a strong pelagic aspect, although organic matter contents remain high. South of the ridge in Walvis Bay and near Lüderitz Bay, sediments are unusually rich in opal and organic matter, reflecting the high coastal ocean productivity here. In the southern Cape Basin away from the high-productivity regions off Namibia, sediments are dominated by pelagic carbonates.

Generally, organic carbon contents were quite high at all sites, ranging from a few percent to as much as 20% by weight. North of Walvis Ridge, values were between 1 and 5 wt%. South of the ridge, values were typically <5 wt%, but reached values well over 10 wt% at sites near the coastal upwelling areas. Black layers extremely rich in organic carbon (as much as 20 wt%) are common in sediments from the Lüderitz site (1084). There is, at all sites, an overall decrease in downhole percentages of organic carbon. Continued diagenetic destruction of organic matter and an increase in upwelling and productivity in the last 10 m.y. are thought to be responsible for this pattern. Sedimentation rates ranged from 30 to 600 m/m.y., with the most common values located between 50 and 100 m/m.y., roughly three to four times the values typical for deep-sea carbonates.

A high supply of organic matter at all but the southern Cape Basin sites drives intense diagenetic activity. Besides reactions directly affect-

F7. Summary of major facies patterns, p. 62.



ing organogenic compounds, there is dissolution of biogenic carbonates and opal, formation of calcite and dolomite, and precipitation of glauconite, pyrite, and phosphate. One of the more conspicuous discoveries during Leg 175 was the presence of several decimeter-thick dolomite layers that were found as fragments in some cores and could be located precisely within the holes using various logging tools. If dolomites are widespread, seismic profiles will have to be reinterpreted. Also, the presence of dolomite layers in sediments <1 Ma in age indicates rapid development of such layers under the high-productivity conditions encountered (see Pufahl et al., 1998; Wefer et al., 1998).

## AGE ASSIGNMENTS AND SEDIMENTATION RATES

### Overview and Summary

The discussion of the history of upwelling requires age models of sufficient resolution for comparison between sites and with records from other regions. On the whole, time resolution at the Leg 175 sites is excellent, mainly because of high sedimentation rates and the ubiquitous presence of nannofossils. The available information on biostratigraphic and magnetostratigraphic control is summarized in the Leg 175 *Initial Reports* volume (Giraudeau et al., 1998; individual site reports in Wefer, Berger, Richter, et al., 1998). Those interested in refining stratigraphic resolution will wish to consult these published data. For the purposes of this synthesis, ages are reassigned using one additional (arbitrary) criterion: avoidance of jumps in sedimentation rates. These assignments are then used to combine sediment properties of all kinds from several sites to detect trends and fluctuations. Events based on diatoms, radiolarians, and foraminifers were of secondary importance in age assignments, although these microfossils deliver important information concerning paleoceanographic history. Supplementary information useful in detailed age assignments within the late Quaternary, in cases, comes from the study of sediment cycles (magnetic susceptibility and color). The latter is only useful if independent age determinations are available, especially for sediments older than 1 Ma.

The assignments given here differ from the straight-line method of the Leg 175 *Initial Reports* volume (Wefer, Berger, Richter, et al., 1998) in that the sedimentation rate is taken to change gradually rather than abruptly at the point of stratigraphic control. They are similar because no additional data were used beyond those available in the Leg 175 *Initial Reports* volume (additional work on age models is provided in several papers in this volume, but these data could not be incorporated here). The modified age models are summarized in Table T1 ("Age models for Congo and Angola sites") and Table T2 ("Age models for Namibia and South Africa sites"). Table T1 refers to Sites 1075–1079, Table T2 to Sites 1081–1087. (Site 1080 had stratigraphic problems and is not considered.) The intent is to provide a convenient means of initial age assignment for any set of samples from the Leg 175 sites. Such samples are tagged by depth below seafloor, which is the reason that ages are assigned to a regular succession of depths (in meters below seafloor). Values are given to three digits after the decimal point, not to claim (unrealistically) high precision, but because sedimentation rates are very sensitive to differences in age assignments. Errors are routinely of magnitude 0.01 m.y. and greater.

---

T1. Age models for Congo and Angola sites, p. 97.

---



---

T2. Age models for Namibia and South Africa sites, p. 98.

---

The age models for the Congo sites show that the oldest sediment reached on the Congo Fan is somewhat greater than 2 m.y. old. Site 1076 does not reach that far back because of a doubled section, owing to slumping. A period of high sediment influx, presumably a debris flow, is apparent at Site 1079 off Angola. But for this disturbance, sedimentation rates would be similar to those of the other sites. An unusually high rate of accumulation is seen at Site 1078 throughout the section. (For reassessment of composite depths at Site 1077, see Jansen and Dupont, [Chap. 20](#), this volume.)

The age models for the sites on Walvis Ridge and off Walvis Bay (Sites 1081–1084) show similar sedimentation rates, reaching an age of 2 Ma at depths between 130 and 200 mbsf, which is normal for continental slope deposition. Rates for Site 1084 are distinctly greater, with 2 Ma occurring at 340 mbsf. This site, off Lüderitz Bay, has exceptionally high contributions of plankton remains (including diatom debris) as a result of being in the sphere of influence of a strong upwelling cell (perhaps the strongest off Namibia). In keeping with this influence, Site 1084 also displayed unusual chemical properties, with exceptionally high levels of phosphate and ammonia in interstitial waters (Murray et al., 1998), as well as strong development of biogenic gases (Meyers et al., 1998).

It cannot be assumed that when using Tables [T1](#) and [T2](#) in assigning ages to a series of samples taken at high density from several adjacent cores in the same hole that a continuous stratigraphy is thereby obtained. Setting aside errors within each model, it is also necessary to make allowance for core expansion and loss of sediment between adjacent cores, the “core gaps.” A first estimate of the size of gaps between cores is readily made by using the “growth” percentages when matching adjacent holes to determine “composite depth” (see individual site chapters in Wefer, Berger, Richter, et al., 1998). These percentages reflect core expansion. Such expansion makes it necessary to add depth increments beyond the driller’s depths when correlating physical properties markers from one hole to another at the same site. Expansion percentages differ from one hole to another, and they change downhole. The values shown in [Table T3](#) are estimates taken from the graphic summaries in the site chapters (except for Site 1087, which has a drafting mistake) and have a typical error of ~1%.

The size of a core gap may be estimated as follows. Let us say we are interested in the likely gap between two cores taken near 150 mbsf at Site 1075. First, we note that the growth rate is 9% at 100 mbsf and 11% at 150 mbsf. A similar change of 2% is obtained for the next deeper 50 m ([Table T3](#)). Thus, the composite depths are 109, 166.5, and 226 meters composite depth (mcd). The difference between the top and bottom of this section is 100 mbsf and 117 mcd, for an expansion of 17%. A core whose in situ length is 9.5 m (as is typically the case) consequently expanded by ~1.6 m, for a total length of 11.1 m. Given a core recovery of 10.2 m (see the “Site Summary,” section in the individual site chapters in Wefer, Berger, Richter, et al., 1998), the gap is 0.9 m of expanded sediment, or ~0.75 m (8%) of the original record. For an instantaneous rate of sedimentation near 8 cm/k.y. (see below), the length of the missing time span is just under 10 k.y. When growth percentages do not change, the calculations are much simpler. For Site 1082, the percent growth values stay near 10%. Thus, the expansion of each individual core is near 10%. Recovery of 107.8% of length cored in Hole 1075C (see [table 1](#) in Shipboard Scientific Party, 1998b) implies that gaps are minor (typically a few tenths of meter). For a sedimenta-

---

[T3](#). Approximate percentages for integrated core expansion, p. 99.

---

tion rate of 10 cm/k.y. (see below), the typical gap has but a few thousand years in Hole 1075C (recovery in Hole 1075A was much less satisfactory).

We recommend the following procedures in assigning age to any given sample:

1. Estimates for single samples: simple linear interpolation between 10-m check points of Tables T1 and T2, using “sample depth” as given by ODP.
2. Estimates for continuous samples:
  - a. Assume that the bottom depth of the core is the correct in situ depth, as shown in the “Coring Summary” table;
  - b. Assign an age to that depth from Table T1 or Table T2;
  - c. Assume that the core expanded upward by the amount implied in assigning a composite depth (Table T3);
  - d. Calculate the original distance of each sample from the bottom of the core before expansion; and
  - e. Assign ages to samples using the original distance from the bottom and dividing it by the instantaneous sedimentation rate appropriate for the position in the hole (taken from Table T1 or Table T2, or from the figures given below).

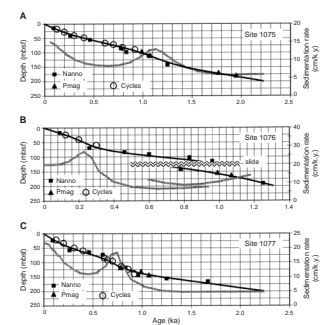
The procedure results in initial age models for sequences of samples, which can then be refined according to additional information, for example, based on oxygen isotope stratigraphy (e.g., see Giraudeau et al., Chap. 7, this volume; Uliana et al., Chap. 11, this volume).

### Congo and Angola Sites (Sites 1075–1077 and 1078–1079)

The first three sites of Leg 175 (Sites 1075, 1076, and 1077) were drilled off the Congo and contain sediments typical for a distal fan-type environment (Wefer, Berger, Richter, et al., 1998). Age control was excellent, especially for Site 1075, which has a well-behaved stratigraphy (Fig. F8A). For Site 1075, nannofossil events (“Nanno” in Fig. F8) and magnetic reversals (“Pmag” in Fig. F8) are available (Shipboard Scientific Party, 1998b), as well as a detailed study of cycles of magnetic susceptibility and color (“Cycles” in Fig. F8) (Berger et al., 1998b). In plotting the line representing the age model, here and in the following instances, it was assumed that nannofossil events will give approximate but absolute time control, magnetic reversals will yield refinement, as long as they can be assigned with confidence to a stratigraphic position, and cycles will yield further refinement once the proper time frame is agreed on. Tie points determined for different holes of the same site were treated the same; that is, depths given (in meters below seafloor) were taken as is, without adjustment for any differences in sequences between holes. Mostly, the error is within the bounds set by biostratigraphic resolution in the Leg 175 *Initial Reports* volume.

Sudden jumps in sedimentation rate were avoided as much as possible within the constraints set by the age tie points. Tie points have errors from several sources: uncertainties arising from the original age assignments to events, proper recognition of events, or unusual position of events within the regional framework of sedimentation (e.g., early regional extinction or dissolution or else unfavorable conditions delaying first occurrences or redeposition delaying last occurrences). Magnetic reversal stratigraphy has to deal with diagenetic interference

F8. Graphic age models for Congo Fan sites, p. 63.



(see Frost and Yamazaki, [Chap. 8](#), this volume). Cycles may be improperly assigned to known periods of orbital forcing. This problem arises especially when the response is complex, as in color cycles in the case at hand. As it happens, the stratigraphy derived from Milankovitch-based cyclostratigraphy for Site 1075 (Berger et al., 1998b) agrees very well (within error limits) with the biostratigraphy and the magnetic stratigraphy (Fig. [F8A](#)). Obviously, if this were not so, the cyclostratigraphy would have to be rejected.

The available data for Site 1075 can be accommodated with a sedimentation rate stratigraphy ranging from just over 5 cm/k.y. near the bottom to 15 cm/k.y. at the top of the record (shaded line in Fig. [F8](#)); that is, there is a general increase in sedimentation rate throughout the Quaternary (which is distinctly greater than expected from increasing water content only). Also, there is evidence for a maximum in sedimentation rate centered between 1.2 and 1.1 Ma, a time of distinct change in climate and vegetation in the drainage basin of the Congo (L. Dupont, pers. comm., 2001; Uliana et al., [Chap. 11](#), this volume). A change toward drier conditions would readily explain a pulse of increased erosion and sedimentation. However, without confirmation from other sites, effects from regional shifting of depocenters on the Congo Fan cannot be excluded.

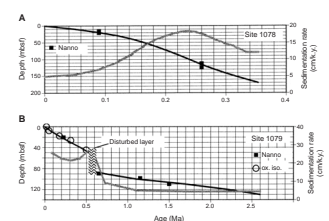
The dating of cycles of magnetic susceptibility in terms of Milankovitch forcing (a method supported by recent results from throughout the South Atlantic) (von Dobeneck and Schmieder, 1999; Schmieder et al., 2000) is readily ported from Site 1075 (Berger et al., 1998b) to the other Congo sites (Fig. [F8B](#), [F8C](#)), especially to Site 1077. Site 1076 seems disturbed (Giraudeau et al., 1998); the stratigraphy suggests large-scale coherent sliding, doubling the section in the central part of the site (Fig. [F8B](#)). Again, sedimentation rates increase within the Quaternary, from ~7 to ~20 cm/k.y. A distinct maximum is centered near the age of 220 ka. Before 0.5 Ma, rates hover around 6 to 10 cm/k.y., both above and below the slide contact. Site 1077 likewise shows the general increase within the Quaternary (from 5 to >15 cm/k.y.), with a distinct acceleration near 1 Ma. A maximum is centered near 0.75 Ma (following the mid-Pleistocene climate shift). The onset of 100-k.y. climate cycles (after 0.7 Ma) (Berger and Wefer, 1992) is accompanied by a decrease in sedimentation rate, which increases again after 0.3 Ma. (Increased water content contributes to the rate increase in the upper portion of the record.)

The Angola Sites 1078 and 1079 show very different patterns in sedimentation rate history. Site 1078 (Fig. [F9A](#)) shows decreasing rates from near 60 cm in the early part of the record to near 20 cm in the late part. Maximum penetration at 165 mbsf is estimated to have been reached at 0.35 Ma. Site 1079 (Fig. [F9B](#)) has three distinct sections with respect to sedimentation rate: one below 90 mbsf, with rates near 5 cm/k.y., one between 90 and 50 mbsf, with apparently redeposited material of an age near 0.22 Ma, and one above 50 mbsf, with rates slightly greater than 20 cm/k.y. The tie points from oxygen isotopes are based on analysis of *Uvigerina auberiana* and *Globobulimina* spp. at Scripps Institute of Oceanography (SIO) (Pérez et al., [Chap. 19](#), this volume).

### Walvis Sites and Lüderitz Site (Sites 1081–1083 and 1084)

Sites 1081–1083 are referred to as the Walvis sites because they are either on Walvis Ridge (Site 1081) or on the slope of Walvis Basin (Sites

**F9.** Graphic age models for Angola sites, p. 64.



1082 and 1083). The closely related Lüderitz site is in the spheres of influence of both Walvis Bay and Lüderitz Bay, reflecting strong Namibian upwelling activity.

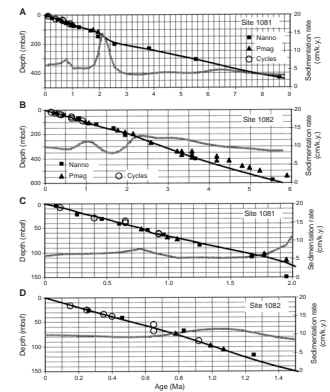
Site 1081 reaches back well into the late Miocene to ~9 Ma (Shipboard Scientific Party, 1998g). Judging from the constancy of the apparent sedimentation rate (Fig. F10A), the record is expected to be continuous. Stratigraphic control is excellent back to 2 Ma (Fig. F10B), with nannofossil events and magnetic reversal stratigraphy in good agreement. The addition of tie points from cycles of magnetic susceptibility adds nothing to the resolution but suggests that magnetic susceptibility is tied to glacial–interglacial cycles, as at the Congo sites.

There is one serious discrepancy between nannofossil stratigraphy and magnetic reversal stratigraphy at Site 1081: the last occurrence of *Discoaster brouweri*, dated at 1.95 Ma, occurs at 149 mbsf  $\pm$  2.2 m. According to the paleomagnetic data, this age level (1.95 Ma) is crossed above 120 mbsf (Fig. F10B; tie points at 1.95 Ma). An assumption that *D. brouweri* became regionally extinct at ~2.1 Ma (which would help resolve the discrepancy) is attractive, considering that at each of the Walvis sites (but not at the Lüderitz site) the last occurrence (LO) of *D. brouweri* is well below the corresponding reversal (bottom of the Olduvai Chron). Once this assumption is made, sedimentation rates for the three sites are relatively steady (4 cm/k.y. for Site 1081, rising to 6 cm/k.y. in the Quaternary; 8–2 cm/k.y. for Site 1082; and 6–8 cm/k.y. for Site 1083). The one exception is a pulse of high sedimentation rates at Site 1081 centered at 2.3 Ma (following cooling and ice buildup in the Northern Hemisphere) (Tiedemann et al., 1994; Mix et al., 1995; Bickert et al., 1997; Haug and Tiedemann, 1998; Maslin et al., 1998). The significance of this apparent pulse is not clear; it is not seen at the other Walvis sites, at least not when the stratigraphic data are interpreted as here proposed, which minimizes steps and pulses.

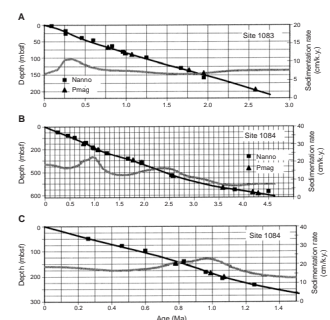
Another discrepancy between nannofossil stratigraphy and magnetic reversal stratigraphy arises at Site 1082 below 400 mbsf in sediments older than 3.5 Ma. According to the “Site 1082” chapter (Shipboard Scientific Party, 1998h), the magnetostratigraphy is ambivalent between 3 and 5 Ma and two differing models are proposed as viable. The straight-line biostratigraphic interpolation (Fig. F10C) favors “1082A-Model 1” (Shipboard Scientific Party, 1998h, p. 294, fig. 12). This discrepancy must not be confused with the one discovered for Site 1086, whereby paleomagnetic tie points are systematically younger than assigned nannofossil ages between 3.5 and 5 Ma. That situation is the reverse of the one described here and is owing to the use of different timescales (Berggren et al., 1995, vs. Lourens et al., 1996) (see Shipboard Scientific Party, 1998m). Site 1083 shows excellent agreement between nannofossil tie points and magnetic stratigraphy (Fig. F11A). The sedimentation rate is near 7.5 cm/k.y. throughout the sequence.

Site 1084 has the highest sedimentation rates of any of the sites between Walvis Ridge and the cape; rates range from ~8 cm/k.y. in the Pliocene portion of the record to well above 15 cm/k.y. in the late Quaternary. Periods of increase are centered near 2.8 Ma (a Northern Hemisphere cooling step) (Whitman and Berger, 1992; Tiedemann et al., 1994; Mix et al., 1995; Bickert et al., 1997; Haug and Tiedemann, 1998; Maslin et al., 1998) and near 1.1 Ma (a time of climate change in central Africa) (L. Dupont, pers. comm., 2001; Uliana et al., Chap. 11, this volume). The sedimentation rate maximum between 2.5 and 2.2 Ma coincides with a maximum in opal content (the Matuyama Diatom Maximum) (Lange et al., 1999; Pérez et al., Chap. 4, this volume). The

F10. Graphic age models for Walvis Ridge and Basin sites, p. 65.



F11. Graphic age models for Walvis and Lüderitz Bay sites, p. 66.



maximum near 1 Ma marks a secondary diatom maximum associated with a carbonate minimum. The sediments of Site 1084, as mentioned, bear a strong imprint of hyperproductivity; they also show the greatest expansion of any of the Leg 175 sections (owing to high gas pressure). Thus, it is reasonable to assign much of the fluctuations in sedimentation rate (and the overall increase since the early Pliocene) to changes in supply of biogenous matter. Terrigenous contributions may vary similarly; only detailed analysis can resolve the question of the relative importance of the two components.

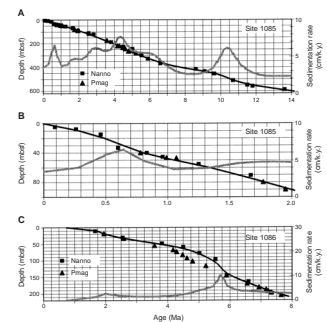
### Cape Basin Sites (Sites 1085–1087)

The Cape Basin sites (1085, 1086, and 1087) have records consisting of calcareous ooze, with carbonate values typically well over 60 wt% (Shipboard Scientific Party, 1998m, 1998k; Meyers and Robinson, Chap. 2, this volume, for Site 1087). Sedimentation rates at Site 1085 are higher than in typical pelagic carbonate oozes, varying from ~2 cm/k.y. in the middle Miocene to >5 cm/k.y. in the Pliocene (Fig. F12A, F12B). Maximum values appear just before 10 Ma (at the very time of a distinct carbonate minimum and a total organic carbon [TOC] maximum) (Shipboard Scientific Party, 1998k) and between 4 and 4.5 Ma (a secondary TOC maximum). A generalized increase is centered on 6.5 Ma, at the time of early glaciation pulses in the Northern Hemisphere (Larsen et al., 1994) when the Mediterranean dried up (Hsü et al., 1973a, 1973b) and the Himalayas first experienced considerable uplift (Raymo, 1994). It is reasonable to speculate that increases in sedimentation rates resulted from increases in export production and biogenic supply resulting from wind-forced upwelling and mixing.

The record of Site 1086 (Fig. F12B) suggests one way how sedimentation rates are decreased during times of increased upwelling. Site 1086 shows effects of winnowing in the uppermost portion of the record and a hiatus comprising most of the Brunhes Chron. Overall, sedimentation rate is low (<2 cm/k.y.), with the exception of a maximum centered near 5.7 Ma. The data for nannofossil stratigraphy and magnetostratigraphy provide for alternative age models, as mentioned. This is not because of an inherent discrepancy but because of the use of different timescales by physicists and geologists during Leg 175 (Berggren et al., 1995, for reversals; Lourens et al., 1996, for nannofossil events). The difference is as expected, given the two timescales. Using exclusively the timescale of Lourens et al. and making the corresponding correction to the depth-age line for Site 1085 (Fig. F12A) results in removal of the sedimentation-rate peak near 4.3 Ma and appearance of another peak near 5.3 Ma, that is, a position close to the peak at Site 1086. This illustrates the hazards of elaborating on changes in sedimentation rate (or using mass-flux rates in plotting sedimentation patterns) when age models are subject to substantial revision.

The stratigraphy of Site 1087 is well constrained by nannofossil events; magnetic data are useful back to 3.5 Ma (where the discrepancy noted at Site 1086 first becomes important). A continuous record apparently reaches deep into the upper Miocene; middle Miocene and pre-Neogene sediments also are present below disconformities. Sedimentation rates typically vary between 5 cm/k.y. in the late Miocene to ~4 cm/k.y. in the Pliocene and Pleistocene, where the variability may be greater. (Higher stratigraphic resolution also can result in greater variability of apparent sedimentation rates.) A pronounced maximum of sedimentation rate is centered near 3.2 Ma (the first strong cooling

F12. Graphic age models for Cape Basin sites, p. 67.



event of a series of cooling steps leading into Northern Hemisphere glaciation) (see Tiedemann et al., 1994; Mix et al., 1995; Bickert et al., 1997; Haug and Tiedemann, 1998; Maslin et al., 1998). The period is characterized by a strong TOC maximum centered near 140 mbsf (Meyers and Robinson, [Chap. 2](#), this volume).

### Observations on the Relative Stratigraphic Positions of Microfossils and Nannofossils

Given the age models here derived from the shipboard data of Leg 175, by allowing for uncertainties in position of events and by minimizing abrupt changes in sedimentation rates, “most likely” ages can now be assigned to the events used to produce the depth-age models and also to the events not used. The latter include all determinations based on radiolarians, diatoms, and foraminifers. Our concern was that the lesser abundance of guide fossils in these groups and their greater sensitivity to problems arising from poor preservation introduces additional uncertainties into the age models, which might as well be avoided.

Separate tabulations were made for the position of biostratigraphic events at the Congo and Angola sites (1075–1079), the Walvis sites (1081–1084), and the Cape Basin sites (1085–1087) (Tables [T4](#), [T5](#), [T6](#)). The three regimes were then compared to check for possible asynchrony (Table [T7](#)).

In Table [T4](#) (as in the companion tables), there are three entries for age estimates for each stratigraphic event. The first is the age used in making the age models during Leg 175 (see Giraudeau et al., 1998). These are based on various earlier studies tying fossil events to age scales of varying reliability. The last serious change to the Quaternary age scale was in 1990 (Shackleton et al., 1990), and the scale for the last 3 m.y. or so now seems stable (e.g., Tiedemann et al., 1994; Mix et al., 1995; Bickert et al., 1997; Haug and Tiedemann, 1998; Maslin et al., 1998). Uncertainties in the early Pliocene were discussed above in connection with the age model of Site 1086. (Uncertainties for pre-Pliocene age determinations may still be substantial in places; T. Bickert, pers. comm., 2001.) The “effective ages” listed are valid within the framework of the stratigraphy of Leg 175, with emphasis on the nannofossil record and the minimizing of abrupt changes in sedimentation rate. The first of these “effective ages” is weighted by the time range within which the event occurs, given the depth range that constrains it. If the depth range is small (and the sedimentation rate high), the weight is correspondingly great. (The weight is taken as a function of 1/range.) The second “effective age” listing is based on the same data but without weighting. Differences resulting from the two methods are minor.

On the whole, the “effective ages” closely follow the “defined ages” in all three regions, as expected. Deviations are typically <50 k.y., corresponding to a depth difference of <5 m in deposits with a sedimentation rate of 10 cm/k.y. Five meters is also the typical range of uncertainty in assigning a depth position to an event when studying core catcher samples. If datums from different holes are used as though they were from the same hole (as we did), the uncertainty roughly doubles for any one sample. For several samples, there should be a convergence on the “defined age.”

A number of discrepancies between “defined” and “effective” ages stand out and may be significant in terms of asynchronous first appearance or last occurrence relative to the biostratigraphic standard used.

---

[T4](#). Ages of biostratigraphic events at the Congo and Angola sites, p. 100.

---



---

[T5](#). Ages of biostratigraphic events at the Walvis and Lüderitz sites, p. 101.

---



---

[T6](#). Ages of biostratigraphic events at the Cape Basin sites, p. 102.

---



---

[T7](#). Comparison of ages of biostratigraphic events at Congo, Walvis, and Cape Basin sites, p. 103.

---

For example (Table T7), the LO of *Axoprunum angelicum* (0.46 Ma) may be diachronous, occurring later than expected at the Congo and Walvis sites but not at the Cape Basin sites. Redeposition can move LO events upward. Alternatively, the LO valid for the open ocean is not valid for the coastal ocean.

## QUATERNARY RECORD OF THE CONGO AND ANGOLA SITES

### Congo Group (Sites 1075, 1076, and 1077)

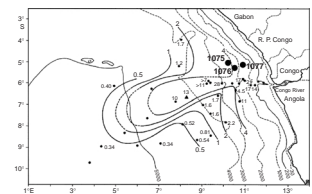
The northernmost sites of Leg 175 are situated near 5°S on the Congo Fan. They contain the record of sediment supply by the Congo, intercalated with the oceanic record. Pollen, freshwater diatoms, phytoliths, and clay minerals provide clues to climatic change in the inner Congo drainage basin in central Africa. Fluctuations in the accumulation of pelagic diatoms and marine organic matter track the changes in productivity in this periestuarine environment. Much of the sediment here consists of diatomaceous clay with varying admixtures of nannofossil carbonate. Sedimentation rates are high; typically near 10 to 15 cm/k.y., on the high side of the depositional rates mapped for the late Quaternary (Fig. F13). The deepest site (1075; near 3000 m water depth) penetrated the entire Quaternary, reaching roughly 2 Ma at 200 mbsf.

Shipboard studies showed pronounced cyclic sedimentation, evidenced in the stratigraphy of physical properties, notably magnetic susceptibility and reflectance of the sediment surface. For Site 1075, reflectance clearly demonstrates response of the Congo upwelling region to precessional forcing (Berger et al., 1998b). The record of magnetic susceptibility, in turn, is closely allied to a standard oxygen isotope curve, suggesting a strong link to sea level variation. The nature of the links of Congo sedimentation to Quaternary climate has been discussed in previous studies (Jansen et al., 1984; Schneider et al., 1995).

### Background: Deepwater Record

For the deepest site (Site 1075; ~3000 m water depth), the possibility must be considered that a general deep Atlantic signal is present within the record for carbonate, organic carbon, and opal. To compare the actual record found at this site, we should first get an idea of what the general deep Atlantic record looks like. Such a deepwater record is reflected in the results from Site 663 in the eastern equatorial Atlantic (deMenocal et al., 1993). The late Pleistocene record shows an excellent correspondence between carbonate content (plotted as negative log of noncarbonate percent) and the deepwater oxygen isotope curve (Fig. F14). Carbonate is high during interglacials and low during glacial periods. In fact, the record is quite similar to the  $\delta^{13}\text{C}$  stratigraphy of *Cibicides wuellerstorfi* in the deep western equatorial Atlantic (Curry, 1996) (Fig. F10). The  $\delta^{13}\text{C}$  record in that region was interpreted in terms of fluctuations of the lower NADW boundary, such that the boundary rises during glacial periods in response to decreased NADW production (Curry, 1996). However, studying the sand content in calcareous Quaternary sediments from the Guinea Basin in the deep west-equatorial Atlantic, Bickert and Wefer (1996) note the strong precessional component and ascribe the changing preservation of foraminifers (that is,

**F13.** Position of Congo sites relative to present-day sedimentation rates on the Congo Fan, p. 69.



sand) to dissolution effects from varying productivity. Increased glacial-time productivity, thus their hypothesis, increases dissolution and destroys sand. The third possible factor, fluctuations in the dilution from the supply of noncarbonate matter, is emphasized by deMenocal et al. (1993) in their explanation of the carbonate cycles.

We may conclude from these contrasting views that while we should expect low carbonate content for glacial periods in deepwater sediments, we might not be able to attribute a mechanism to the fluctuations without further detailed study. The  $\delta^{13}\text{C}$  stratigraphy of the Guinea Basin cores studied by Bickert and Wefer (1996) shows similar fluctuations to those from Ceara Rise (Curry, 1996), with amplitudes exceeding 1‰ (more than twice the global-ocean background fluctuation). The most parsimonious explanation is that both sets of cores reflect changes in NADW production, although an additional effect from productivity variation is likely in the eastern set (making up for a reduced influence from NADW).

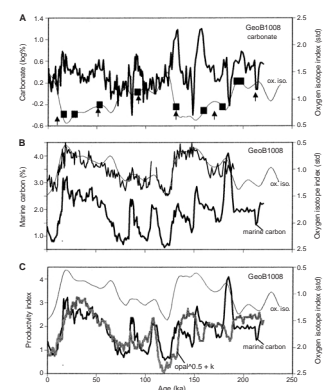
The opal record at Site 663 (Fig. F14B) also is in synchrony with the oxygen isotope stratigraphy, such that high values of opal (plotted in reverse as log opal percent, standardized) coincide with glacial periods. The agreement between carbonate and opal is virtually perfect, provided one of the two is plotted in reverse and the log transforms are used before standardization (Fig. F14C). This remarkable match in amplitude and phase supports the proposition of Bickert and Wefer (1996) that dissolution effects are caused by varying productivity. Note that this is not simply a matter of most of the noncarbonate consisting of opal. This is not the case. The opal expands into the noncarbonate space during glacial periods. A plot of  $\log(\text{opal}/\text{noncarbonate})$  is virtually identical to the opal record shown, signifying that variation of carbonate is unimportant as far as variation of opal. (The high correlation shown only appears after some smoothing.)

### Productivity Cycles off the Congo

In contrast to the deepwater environment well west of the Congo Fan, the carbonate variations off the Congo are much less regular and therefore more difficult to describe and interpret (Fig. F15). High carbonate values encountered in core GeoB1008 ( $6^{\circ}44.9'S$ ,  $10^{\circ}19.1'E$ ; 4124 m water depth), which was taken during preparatory work for Leg 175, are concentrated in glacial intervals (position of peaks is marked by black rectangles on the oxygen isotope curve). However, the relationship is not a simple one: peaks tend to move to the positions of warmings and coolings and apparently avoid maximum glacial conditions. The water depth of the location of core GeoB1008 is distinctly deeper than that of Site 1075 (4124 vs. 2995 m). Nevertheless, any influence from abyssal lysocline fluctuations (good carbonate preservation during interglacials) apparently is eclipsed through effects prevailing above the lysocline. These include, apparently, increased preservation during glacials well above the lysocline (even though that level is now shallower) and changing productivity (which provides for increased dissolution at peak glaciations).

The record of productivity is well reflected in the marine organic carbon within the core, with abundance of organic matter following the oxygen isotopes rather precisely, at least for the last 140 k.y. or so (Fig. F15B). A tendency for large amplitudes in the precessional band in the organic carbon decreases the match with the oxygen isotopes, although the long-period response (glacial periods have high productivity) per-

**F15.** Carbonate, marine organic carbon, and opal in the Congo Fan, p. 71.



sists. The opal content follows the organic matter content nicely back to ~140 ka but moves out of phase before that (shaded line in Fig. F15C). Evidently, precessional forcing is less important for the opal deposition than for organic matter deposition. To some degree, the two processes are decoupled. (Uliana et al., Chap. 11, this volume, propose adjustments to the timescale before 150 ka, but this does not affect the match between organic carbon and opal, or lack thereof.)

A strongly dominant eccentricity signal was found at Site 1077 in the opal abundance series by Uliana et al. (Chap. 11, this volume) (power near 98 k.y.) for the late Quaternary. Interestingly, the 400-k.y. cycle is clearly reflected (i.e., Stage 11 and adjacent glacial periods are not clearly expressed). This means that the opal cycle here feeds off precessional amplitudes. Surprisingly, however, precessional periods are not clearly expressed. Neither is the obliquity cycle. Indications are, therefore, that the energy from these forcings ends up in periods produced by interference (that is, 70 k.y. and its harmonic, 35 k.y.). Such interference might be expected at the sites of production of intermediate waters at latitudes where interaction of precessional (eccentricity) forcing and obliquity forcing would be optimal. If so, the silicate content of subsurface waters (and the opal deposition off the Congo) would reflect this interaction.

The precessional effect is commonly attributed to the competing effects from monsoon winds and trade winds (Schneider et al., 1996, and references therein). In the present case, the competition reaches across the equator, with North African monsoon interfering with southwest trade winds. Enhanced heating of the North African land masses by a close-by sun in northern summer (June, July, or August perihel) weakens both the trade winds off northwest Africa and the South Atlantic ones, thereby reducing forcing for upwelling (Kutzbach and Liu, 1997). Relevant land areas being much smaller in the south, the reverse effect (monsoon over southern Africa) is much less important. Thus, the precessional tone of the forcing is preserved in the Congo sediments, as productivity variation, in phase with northern summer monsoon maxima and minima.

### Freshwater Input from the Congo

Schneider et al. (1997) suggest that much of the opal results from the delivery of dissolved silicate by the river itself rather than from oceanic upwelling (which is shown to dominate the organic production).

As an alternative to the hypothesis of Schneider and co-workers (riverine silicate supply), we propose that the ratio between silicate and phosphate within thermocline waters changes in such a fashion as to counteract the precessional upwelling effect as far as opal production. That is, the silicate content would have to be decreased during glacial periods relative to phosphate. Such a change implies a drop of all nutrients during the glacial period (Berger and Lange, 1998). We envisage increased dust supply during glacials to the areas of convergence, where intermediate waters are formed, with corresponding precipitation of opal from increased availability of iron and of dust particles providing for fecal ballast (Berger and Wefer, 1991, and references therein; see also Young, 1991; Martin, 1994; Harrison, 2000, and references therein).

The question of river input is addressed by Uliana et al. (Chap. 11, this volume) in a comprehensive study of siliceous components of continental and marine origin within the sediments of Site 1077 for the last 460 k.y. Uliana and colleagues find that marine siliceous microfossils

entirely dominate opal deposition, especially during glacial periods. Uliana et al. also find that there is considerable pulsed input of freshwater to the surface waters above Site 1077 during certain periods, with a distinct increase in brackish water diatom species. Abrupt changes are observed during Termination II, near 130 k.y. ago, where the assemblage composition varies from predominantly marine to marine/brackish. In addition, evidence obtained from freshwater diatoms and chrysophycean cysts points to changes in the drainage basin from more arid conditions to more humid conditions at that time (a change since reversed). Presumably, two effects have to be considered: increased monsoonal rains in the northern parts of the drainage area, during times when perihelion occurs during the monsoon season (precession effect), as well as changes in current direction offshore, which may redirect the freshwater outflow off the Congo River toward the area of Site 1077.

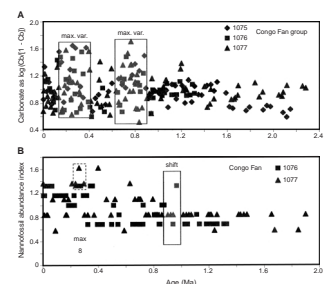
### Mid-Pleistocene Climate Shift

There is a major shift in global climate close to 0.9 Ma following a cooling initiated near 0.95 Ma. This event is referred to as the mid-Pleistocene climate shift. It marks the initiation of high-amplitude glacial-interglacial cycles, which start as 80-k.y. cycles and then move into 100-k.y. cycles upon entering Stage 16, ~700 k.y. ago (Berger and Wefer, 1992; Berger and Jansen, 1994). It is of great interest to find the response of the various upwelling systems to this event. In the case of the Congo group, we would like to know what kind of climate shift may have occurred in central Africa and how the large-scale pattern of sedimentation responded to this event.

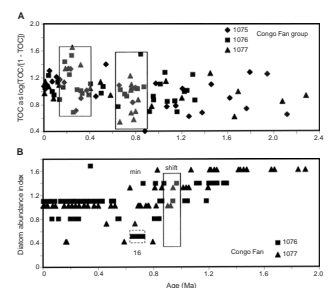
The shipboard data allow some statements of a general nature (Fig. F16). Regarding carbonate deposition, it seems that variability of carbonate content increased drastically at the time of the mid-Pleistocene shift, indicating much larger fluctuations in productivity after the shift. The range expands both toward lower values and toward higher values, compared with preshift time. There is a slight relaxation for the period containing isotope Stages 12–15 and a similar reduction of range for the last 100 k.y. However, overall, the range of variation is distinctly greater after the shift than before it. The same kind of range expansion is also seen in the nannofossil abundance, as recorded in smear slides (the index values from the Leg 175 report are log-transformed). Highest carbonate values, according to these visual estimates, are reached between Stage 11 and Stage 8.

Organic matter content at the Congo sites also shows a change at the time of the mid-Pleistocene climate shift but much less prominent than for carbonate. Again, the range expands right after the shift, at 0.9 Ma (Fig. F17A). However, on entering the Milankovitch Chron (at 0.65 Ma), the range tends to contract again. A loss of low values and a gain in higher ones (seen between 0.1 and 0.4 Ma) reflects a general increase in productivity (or better preservation of organic matter within the less-aged sediments). The range of values even before the shift is quite remarkable (a factor of four; note the logarithmic scale). Diatom abundance also shows a distinct expansion of range at the time of the shift. Before the shift, diatom abundances are high (in fact, they tend toward a maximum because of the way the visual index is used when describing smear slides). After the shift, they cluster around an intermediate value, with occasional low values. In the 400 k.y. after the mid-Pleistocene climate shift (0.9–0.6 Ma) the range varies between low and high

F16. Carbonate sedimentation at the Congo group sites, p. 72.



F17. Organic carbon and diatom abundance at the Congo group sites, p. 73.



values, with the lowest sustained values (marked by a dashed-line box) centered on the maximum glacial period of the late Quaternary, isotope Stage 16 (Fig. F17B).

From the increase in variation in productivity-related indices, we conclude that the sensitivity of the Congo upwelling system to precessional forcing increased at the time of the mid-Pleistocene climate shift. If so, this would indicate that developments in high latitudes (ice buildup) and global cooling (desert development) provided for changes in response of tropical systems to (comparatively invariant) astronomical forcing. In turn, the greater sensitivity of the tropical systems would have resulted in increased feedback to the high-latitude ice dynamics, with implications for runaway amplification and accelerated melting (terminations).

Lydie Dupont et al. (Bremen) has made a detailed study of changes in the terrestrial record of Sites 1075 and 1077, especially with a view to pollen and dinoflagellate cysts (pers. comm., 2001). She finds that the variation of river discharge increased after 0.94 Ma, suggesting larger contrasts in rainfall between glacial and interglacial periods within the African interior. Before 1.05 Ma, she finds, there is no strong glacial–interglacial rhythm within the pollen record. A strong rise of *Podocarpus* pollen occurs at 1.05 Ma, suggesting a cooling, in synchrony with distinct changes in the dinoflagellate record. While the dinoflagellate cysts indicate a reduction in river discharge, the contrast between pollen spectra of glacial and interglacial periods increases after 1.05 Ma. Thus, the expansion in the range of fluctuation of productivity off the Congo goes parallel (more or less) with an increase in the range of variation in the vegetation cover in the interior of the continent. The connection, presumably, is the tie-in of both marine and terrestrial photosynthesis to the monsoon/trade wind contrast, at least for the latest Pleistocene. A complication arises for the earlier glacial cycles after the climate shift. Those glacials, according to Lydie Dupont, may have been cool and wet, rather than cool and dry.

### Angola Group (Sites 1078 and 1079)

The Angola or Lobito sites are situated off the central part of the Angolan coast, near 12°S. They might also be called, with more justification than all others, the “Benguela sites,” since they are located not so distant from the port of Benguela. However, the “Benguela Current” does not reach this far north and they are not within the region off Namibia and South Africa usually referred to as the “Benguela upwelling system.” The deposits of the Angola group document high productivity, albeit these are low when compared with the upwelling areas immediately to the north and south. While silicate-rich waters are potentially available below the mixed layer (thanks to the nearby Angola Dome), upwelling is seasonal and comparatively weak and opal accumulation is very modest for this coastal environment. Organic matter averages 2.5 wt% at Site 1078 and 4 wt% at Site 1079 (where there is less dilution by terrigenous matter). Sediments at Site 1078 (448 m) consist of gray silty clay with varying amounts of nannofossils and foraminifers. In parts of the section, very high sedimentation rates (up to 60 cm/k.y.) were found; much of the material deposited this rapidly may have been delivered by coastal erosion. Dolomite concretions and laminated intervals are present in places, presumably indicating sporadic expansion of anoxic conditions. Site 1079, with sedimentation rates ~60%

lower than those of Site 1078, has uniform olive-gray silty clays with varying amounts of nannofossils and foraminifers.

Site 1080 was drilled off the Kunene River (southern Angola). It is situated near the northernmost coastal upwelling cell of the Namibia upwelling system. Sediments consist of diatom-bearing and diatom-rich silty clays that are accumulating at a rate near 10 cm/k.y. The late Quaternary section is greatly attenuated. Drilling was terminated after a dolomite layer was encountered, slowing the advance of the bit to unacceptable rates. No further reference will be made to this site.

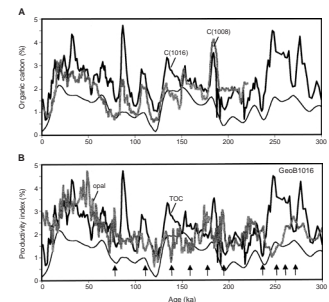
### Background: Quaternary Productivity Fluctuations

The two Lobito sites terminate in the late Quaternary. From the study of core GeoB1016 (11°46.2'S, 11°40.9'E; 4411 m water depth) and comparison with core GeoB1008 (discussed above), it appears that productivity fluctuations off Mid-Angola are similar to those off the Congo (Schneider et al., 1996). In contrast, the rate of opal deposition is some five times lower (Schneider et al., 1997) (Fig. F8). Not only is the overall deposition of organic carbon similar in the two areas, but the patterns match in some detail when correlated using oxygen isotope stratigraphy for guidance (Fig. F18). Thus, it is likely that forcing in the two regions is the same; that is, in both areas high productivity results from strong trade winds (Schneider et al., 1997). A remarkable feature of both patterns (and of many productivity records in general) is the spiky nature of the record. Fluctuations are by no means sinusoidal, but resemble the shape of a chain hung from a number of nails in series—a sequence of catenaries. This morphology suggests a response to narrow optimum conditions, as will be discussed below.

As in core GeoB1008 off the Congo, the opal record does not follow the organic matter record (TOC) very closely in core GeoB1016 (Fig. F18B). While the overall trends coincide, there is actually a marked anticorrelation on the timescale of precession and shorter. This supports our hypothesis that the silicate content of thermocline waters was lower in this region during glacial periods. Since the ratio of silicate to phosphate is positively correlated with the abundance of nutrients in the modern ocean, a high opal to TOC ratio suggests high thermocline fertility and vice versa. A high TOC content accompanied by low opal content (e.g., near 80 k.y. ago and near 250 k.y. ago) suggests strong upwelling from a silicate-impoverished thermocline (Berger and Lange, 1998).

The organic carbon content of core GeoB1016 is readily modeled by combining a standard oxygen isotope curve describing sea level change (in this case OJsox96) with the amount of irradiation in July at 15°N (from Berger and Loutre, 1991). Upwelling tends to be high when glacial conditions prevail and when summer irradiation at 15°N is at a minimum (Fig. F18C). Actually, during maximum glacial conditions, the response to irradiation seems somewhat diminished. The same model does not work at all for the opal abundance (Fig. F18D). In fact, the opal record seems to chart a compromise between strengthened upwelling during glacial periods combined with a greater availability of silicate during periods of intensified monsoon (low TOC times on the precessional timescale).

**F18.** Organic matter and opal fluctuations off Mid-Angola, p. 74.



## Clues to Changing Productivity at Sites 1078 and 1079

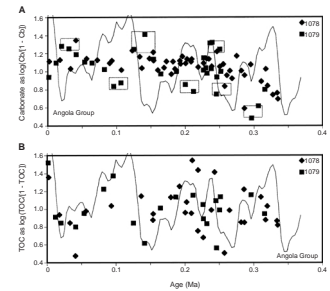
The patterns of carbonate content of the Lobito sites presumably are correlated with productivity, in that a high supply of organic matter will lead to dissolution and a low supply to preservation of carbonate, as discussed above. High values at the sites (Fig. F19) occur late during glacial periods near and within terminations (three boxes: Stage 2, 5–6 transition, and 8–7 transition). High preservation of carbonate during termination intervals is well known from off northwest Africa and elsewhere (“deglacial preservation spike”). It may be a global signal indicating reduced productivity from increased stratification and density contrast between freshened wind-mixed upper water masses and underlying cold and saline masses inherited from ice-age conditions (a scenario envisaged by Worthington, 1968). Low carbonate values are situated within interglacials (near 0.1, 0.2, and 0.4 Ma), indicating a tie-in to 100-k.y. cycles. More detailed work will be necessary to assess the usefulness of the carbonate stratigraphy in this area where dilution from terrigenous materials should play a strong role.

Organic matter content at the Lobito sites is confusing, given the expectations from core Geob1016 (farther offshore) that TOC is high during glacial periods and low during interglacials. Again, dilution effects may be very important at these sites, given the apparent high variation in sedimentation rate and the proximity to an actively eroding coast (Berger, Wefer, Richter, et al., 1998).

Pérez et al., [Chap. 19](#) (this volume) have studied benthic foraminifers at Site 1079 to document the course of changing productivity independently from dilution effects. From biostratigraphy, it appears that there is a sudden change in sedimentation rate between 200 and 400 k.y. ago; thus, there are less than two full glacial–interglacial cycles for reliable documentation. The oxygen isotope stratigraphy is based on *Globobulimina* spp. and reaches back to ~240 ka. The abundance of benthic foraminifers as well as the benthic foraminifer accumulation rate (BFAR) index (Herguera and Berger, 1991) suggest high productivity during glacials and somewhat lower values for Stages 1, 4 and 5, especially for Substage 5e. The fact that planktonic foraminifers show a similar pattern suggests that benthic and planktonic species may be influenced by the same factors, that is, dilution and dissolution. In fact, the fragmentation is at a minimum during glacial periods, supporting this suggestion. A strong carbonate maximum, as well as a sand percent maximum, is associated with late Stage 6 and the 6–5 transition, supporting the pattern read from Fig. F19 above.

Comparing core Geob1016 and Site 1079, Pérez et al., [Chap. 19](#) (this volume) find an excellent correlation between BFAR at Site 1079 and percent organic matter in core Geob1016, supporting the notion that BFAR represents productivity—even though the planktonic foraminifers show similar patterns. Further confirmation comes from the foraminiferal epifauna, which indicates low productivity for high values of abundance. The maxima are found at the major transitions, 6–5 and 2–1, suggesting low productivity during deglaciation. Other high values are seen in Stages 7 and 5 (Pérez et al., [Chap. 19](#), this volume). Organic matter stratigraphy in core Geob1016 and the sequence of *Bolivina pseudopunctata* at Site 1079 run parallel, indicating that *B. pseudopunctata* is a productivity proxy, as the most abundant species. *Bolivina dilatata*, the second most abundant species, tends to show an inverse pattern, presumably because of the forced negative correlation within percentage space.

F19. Carbonate and organic carbon at Sites 1078 and 1079, p. 76.



The balance of the evidence gathered by Pérez et al., [Chap. 19](#) (this volume) supports the standard productivity pattern: high values for glacial periods and low values for interglacials, with BFAR and benthic foraminifers (BF)/g being the most reliable productivity indices. The spectrum of benthic foraminifer abundance at Site 1079 (Fig. [F20](#)), which presumably reflects the spectrum of productivity, shows strong peaks near 100 and 35 k.y. and also power at the precessional lines (24 and 19 k.y.), but very little in the vicinity of obliquity variation (41 k.y.).

How was the power from obliquity moved into power at 35 and 53 k.y.? Power can be moved in various ways, including interference processes and transfer of energy between harmonics. The whole-number harmonics of 100, downward, are 50, 33, 25, and 20, which correspond closely to the power distribution seen. The difference tones between obliquity (41 k.y.) and the main cycle (100 k.y.) is 69.5 k.y. One-half of this period is close to the one seen at 35 k.y. Thus, it is entirely reasonable to expect that energy from both the 100-k.y. cycle and the obliquity-driven cycle are contained in the 35-k.y. cycle. Of course, such reasoning does not address the issue of mechanism; it only asserts that the concept of astronomical forcing need not be abandoned just because one of the important lines (here, 41 k.y.) is missing.

## WALVIS GROUP (SITES 1081, 1082, AND 1083)

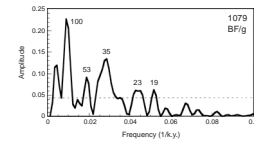
### General Aspects

The Walvis group consists of the three Leg 175 sites on Walvis Ridge and in Walvis Bay, which join two sites drilled earlier in this area, Deep Sea Drilling Project (DSDP) Sites 362 and 532 (Legs 50 and 75). The DSDP sites (with water depths near 1300 m) are seaward of the coastal upwelling regions but contain an upwelling record brought by the Namibia Current in eddies and filaments. Glacial–interglacial cycles are represented as cycles of carbonate dissolution, productivity, and terrigenous sediment supply. Site 1081 (at 760 m water depth) has gray clays with varying amounts of diatoms, nannofossils, foraminifers, and radiolarians. Authigenic minerals such as glauconite, pyrite, and dolomite are present. Sedimentation rates vary between 70 and 150 m/m.y. Site 1082 (at 1290 m water depth) has well-developed cyclic sedimentation. Sediments are composed of green clays with varying amounts of diatoms, nannofossils, foraminifers, and radiolarians. Site 1083 (at 2190 m water depth) has hemipelagic sediments consisting of clayey nannofossil ooze. Sedimentation rates vary between 60 and 150 m/m.y. Productivity changes are reflected in dark–light color cycles throughout the drilled sequence.

### Quaternary Glacial–Interglacial Productivity Cycles: The Walvis Paradox

The Walvis Paradox arises from the observation, first made on Walvis Ridge, that glacial-age sediments contain less opal than interglacial ones (Diester-Haass, 1985a, 1985b). This is precisely opposite to the expected pattern if it is assumed that productivity is at a maximum during glacial times, as we have seen is the case north of Walvis Ridge. To com-

**F20.** Productivity cycles at Site 1079 in the latest Quaternary, p. 77.



licate matters, there is actually evidence that productivity was in reality higher during glacial periods in the vicinity of Walvis Ridge. The evidence consists of cold-water foraminifers (*Neogloboquadrina pachyderma* [sin]) being more abundant during glacial periods within the last 500 k.y., at Site 532 (Oberhänsli, 1991). It seems then that at the Walvis Ridge, the intensity of upwelling is completely decoupled from the deposition of opal—or even more astounding, the least amount of opal is being deposited during the very times when upwelling is most intense. As suggested by Hay and Brock (1992), this conundrum calls for a situation where subsurface waters are impoverished in silicate during glacials in this region.

Increased upwelling results in the deposition of fewer diatoms—this is the Walvis Paradox.

Can we be reasonably sure that productivity was indeed high during times of reduced diatom deposition? If so, the Walvis Paradox will point to fundamental changes in the nutrient chemistry of the eastern Atlantic between glacial and interglacial times.

It is readily established that the organic matter deposition on Walvis Ridge follows the general pattern of increased organic sedimentation during glacial periods (Fig. F21). Core GeoB1028 (20°06.2'S, 09°11.1'E; 2215 m water depth) is situated on Walvis Ridge close to DSDP Site 531, west of Site 532. The stratigraphy of organic matter can be modeled in the fashion exemplified above for core GeoB1016 off Angola (Fig. F18C). Again, a globally valid oxygen isotope standard (806sox, parent to OJsox96, used above) is combined with insolation in July at 15°N in an appropriate fashion to estimate the TOC. In the present case, the formula used is

$$\text{TOC} = \text{d18}^a \times \text{ins}^{(1-a)}, \quad (3)$$

where

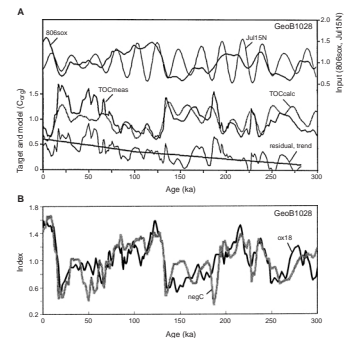
TOC = the organic matter abundance,  
 d18 =  $\delta^{18}\text{O}$ ,  
 ins = insolation at 15°N in summer,  
 a = 0.67,

and all variables are standardized to mean = 1 and deviation = 0.25. When the overall trend is removed, the estimate yields  $r^2 = 0.65$  (see Fig. F21A).

Direct evidence for an excellent fit with glacial–interglacial fluctuations is given by the match of the TOC with the oxygen isotope stratigraphy within the core itself (Fig. F21B). The two records are precisely in phase at the terminations. At the warm peaks (low TOC) and the cold peaks (high TOC) there is some indication of a lead of the TOC; that is, warming and cooling are as important as the state itself in determining productivity. This phase relationship suggests that the same process producing warming and cooling (the orbitally driven changes in insolation) strongly affect productivity. Insolation drives seasonal winds. The interplay between monsoon and trade winds (see above) is one available mechanism; a shift in mid- and high-latitude seasonal fronts is another.

It has been suggested (e.g., Diester-Haass et al., 1992) that redeposition of organic matter from shelves during glacial periods when sea level was lowered could have simulated increased productivity within

**F21.** Match of total organic matter with glacial–interglacial climate fluctuations, p. 78.



the downslope sediments now enriched in organic carbon. If this were so, one would not expect that the benthic foraminifer content should be similarly enriched within glacial sections. In fact, the benthic foraminifer abundance does follow the oxygen isotope record rather closely (Fig. F22B). Thus, it appears that the TOC represents mostly in situ supply of organic matter and, hence, the productivity of overlying waters.

Weinheimer (Chap. 3, this volume) has studied the uppermost section of Site 1082 in some detail with regard to radiolarian content. From the sedimentation rate for this site (see Fig. F10), her “warm-water” radiolarian curve can be interpreted to reach the last glacial maximum at 3 mbsf, the Stage 5–4 transition at 7 mbsf, and Substage 5e near 12 mbsf at the end of her series. The observation relevant to the discussion of the Walvis Paradox is that “intermediate-water” radiolarians, which presumably indicate upwelling, are abundant throughout the section comprising Stages 4 to 2. Moreover, the intermediate forms become abundant even before the transition into Stage 4, implying that upwelling starts at the end of the warm period rather than within the transition. This is wholly in agreement with the notion that insolation is just as important as the overall glacial–interglacial climate state in driving the upwelling system.

### Pre-Quaternary Glacial–Interglacial Productivity Cycles and the Post-Gauss Cooling Step

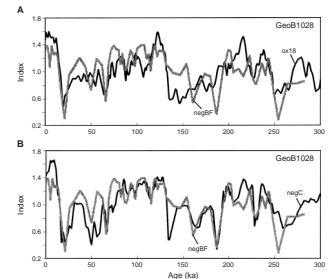
Do these relationships between climate state and productivity apply to pre-Quaternary sediments as well?

Apparently so. Regarding opal, this was already indicated by work on DSDP Site 532 (Diester-Haass, 1985a, 1985b; Diester-Haass et al., 1992). Intriguingly, Diester-Haass et al. (1990) found that the phase between climate state and productivity in the Miocene was the reverse of that found for the Quaternary and Pliocene. In the older sediments, high productivity paralleled opal deposition, assuming that low carbonate content, low sand content, and high benthic/planktonic foraminifer ratios indicate high productivity. This seems reasonable, especially since the organic matter content is high in the several cases where this was checked against the carbonate, sand, and benthic/planktonic (B/P) ratio indices (Diester-Haass et al., 1990).

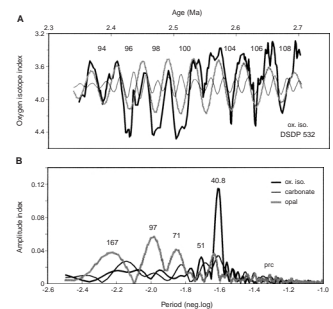
Sancetta et al. (1992) made a detailed study of the section between 2.7 and 2.35 Ma at Site 532 in an interval containing major early glacial excursions (Stages 96, 98, and 100) and displaying a major cooling step toward Northern Hemisphere glaciation (near 2.53 Ma) (see Fig. F23). This step is identical to the “intensification of Northern Hemisphere glaciation” event or “iNH” of some authors. In what follows, we refer to this abrupt increase in excursion to heavy values as the “post-Gauss cooling step,” to avoid direct implications for “Northern Hemisphere” or “glaciation,” for which Leg 175 has no evidence.

The cold–warm cycles in the oxygen isotopes (*Uvigerina*) in the entire interval are wholly dominated by obliquity-related cycles (Fig. F23A, F23B). Although precessional information plays a role (Fig. F23A), it is unimportant as far as spectral power (Fig. F23B) (as previously noted by Sancetta et al., 1992). Extracting the obliquity-related cycles from the Fourier matrix (Fig. F24), it is seen that carbonate content (Fig. F24A) and opal content (Fig. F24B) are close to being in phase with the oxygen isotopes, such that peaks in either coincide with warm periods. However, in the high-amplitude portion of the record after the post-Gauss shift, carbonate tends to lead the oxygen isotopes and opal tends

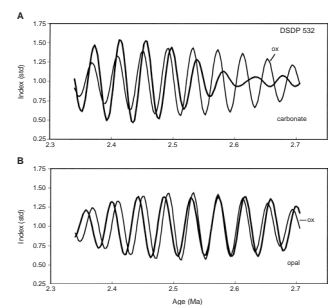
F22. Benthic foraminifers and TOC on Walvis Ridge, p. 79.



F23. Glacial–interglacial cycles in the late Pliocene, p. 80.



F24. Oxygen isotopes and carbonate and opal content, Site 532, p. 81.



to lag. We interpret this to mean that low productivity (high carbonate) is shifted toward warming, whereas high opal productivity is shifted toward cooling, a phase relationship familiar from the Quaternary (see above).

The spectrum of the opal record shows power at periods other than 41 k.y. (Fig. F24B). The relevant peaks are at 167, 97, and 71 k.y. The peak at 71 k.y. derives its power from interaction of precession and obliquity, as the difference tone between 96 k.y. (precession modulation by eccentricity) and 41 k.y. (obliquity) is 71 k.y. The sum tone between 71 and 125 k.y. (the second eccentricity period modulating precession) yields 164 k.y. The 51-k.y. period is but little above the noise level; it crops up when beating obliquity (41 k.y.) with the main precessional peak (23 k.y.).

The particular mixture of the interference tones in the opal record is of considerable interest. It is very similar to the mixture seen for the deepwater carbon isotope record of the interval in question in the Atlantic Ocean on Ceara Rise (Bickert et al., 1997) (fig. 6: 2.1–2.6 Ma). The peaks of the spectrum in this instance (Sites 925 and 927) are 166, 69, 41, 33, and 23 k.y. Neither the oxygen isotopes of any of the intervals studied in that paper nor the carbon isotopes of any other interval but the one between 2.6 and 2.1 Ma show this mixture of periods. We take this as evidence that the opal record on Walvis Ridge is somehow related to the deep circulation of the Atlantic Ocean, in addition to or in preference to the climatic agents forcing upwelling off Namibia. The message from this evidence, we think, is that the nutrient content of upwelled waters changes through time in this region (supporting suggestions by Hay and Brock, 1992; Berger et al., 1998a; Lange et al., 1999; and Ettwein et al., Chap. 18, this volume).

The change must comprise large areas off southwestern Africa if it is tied to deep-sea circulation. In particular, we propose that the silicate content of glacial-age subsurface waters decreases much more in proportion than phosphate and nitrate and that this discrepancy is at the root of the Walvis Paradox (cf. Berger et al., 1998a; Lange et al., 1999).

A detailed study of glacial–interglacial cycles in the late Pliocene is presented by Ettwein et al. (Chap. 18, this volume) based on material from Site 1083. Their data (Ettwein et al., Chap. 18, this volume, fig. F2) suggest a change in the response of the upwelling system (as seen in diatom deposition) at the time of the post-Gauss cooling step (2.54 Ma). Regarding organic matter, the maximum before the shift is broadly straddling a cool period (Stage 104), with the subsequent three stages too warm for high TOC values. The highest values appear at the post-Gauss cooling step itself, centered between 2.53 and 2.54 Ma. Also, the subsequent maxima are centered on cooling events, while both warm and cold stages have smaller TOC values. Thus, the system is most productive for an optimum condition that is intermediate between warm and cold (but not on the warming side) whenever the warming goes through a substantial range. Since there is no substantial warming before the post-Gauss shift in this sequence, the rule only applies after the shift.

Regarding the diatom abundance—plotted by Ettwein et al. (Chap. 18, this volume) as endemic Antarctic species and *Chaetoceros* spores—it is noted that the endemic Antarctic species become less abundant after the shift, avoiding Stage 100, but are otherwise without a clear tie-in to warm and cold stages, while before the shift there is a certain preference for warm stages. The *Chaetoceros* spores, like TOC, tend to be abundant at the cooling events but also favor the mild cold stages before the shift.

They avoid the maximum glacial states in Stages 96 and 100. From inspection, there seems to be a negative correlation between endemic Antarctic species and *Chaetoceros* before the shift and a positive one after the shift. This suggests that after the shift both become strongly dependent on the same factor, that is, the availability of silicate in subsurface waters. Ettwein et al. reach a similar conclusion regarding the importance of the supply of silicate in attempting to explain the patterns of diatom deposition.

The various lines of evidence inherent in all the studies summarized here allow the conclusion that productivity is a function of wind-driven upwelling on Walvis Ridge and that the opal content of the sediments reflects silicate content in subsurface waters more than it reflects intensity of upwelling, at least after the post-Gauss cooling step. The same is apparently true for the early Quaternary off southern Namibia (Anderson et al., [Chap. 21](#), this volume). This conclusion will be important in interpreting the subject of the late Pliocene Diatom Maximum off Namibia, also referred to as the “early Matuyama Diatom Maximum” (Lange et al., 1999). To this subject we turn next.

### **Pliocene–Pleistocene Diatom Deposition: The Namibia Opal Paradox**

The Namibia Opal Paradox is analogous to the Walvis Paradox, which derives from the contrasting views on glacial–interglacial productivity patterns held by geologists working on the record of Site 532. Diester-Haass (1985a, 1985b) found that opal deposition was higher during interglacial periods than during glacial ones and argued for lowered glacial productivity. Oberhänsli (1991) found that upwelling increased during glacial periods within the Quaternary. At first glance, the two findings seem incompatible. However, they are resolved if it is assumed that the fertility of the thermocline decreases during glacial periods, especially with regard to silicate.

On a scale of several million years, according to the data gathered by Leg 175 scientists, we again see a puzzling pattern. With overall cooling in the late Pliocene, diatom deposition increases off Namibia (unsurprisingly), but with additional cooling after 2 Ma, the abundance of diatoms decreases again, despite indications for strong upwelling. It is as though the cold water supplied by upwelling is impoverished in the silicate necessary to make diatom shells. On the whole then, we are tentatively equating glacial (silica poor) conditions with the late Quaternary and the late Pliocene with interglacial (silica rich) conditions.

The Namibia Opal Paradox was discovered not just by mapping maximum diatom deposition during the late Pliocene (which had been done before for the Walvis Ridge by Leg 75 scientists; see Hay, Sibuet, et al., 1984). Instead, several additional ingredients define this important discovery by Leg 175 scientists:

1. The abundance patterns are similar all along Namibia, with a well-defined broad maximum well before the Pliocene/Pleistocene boundary, centered between the Gauss and the Olduvai Chrons;
2. The composition of the diatom flora is quite different for the periods before, during, and after the time of maximum deposition; and
3. The flora allows the statement that strong frontal systems dominated the time of maximum deposition, but strong coastal up-

welling reigned after the Gauss/Olduvai maximum had been left behind, all through the Quaternary (Fig. F25).

It is the study of the species composition of the diatom assemblages at several sites along Namibia that lets the paradox emerge. We spell this out to emphasize the importance of diatom paleoecology in the context of upwelling dynamics. Studies on upwelling without reference to the types of diatoms in the sediments are at a disadvantage, as far as the reconstruction of upwelling dynamics.

The question is, can we assume that productivity was higher in the Quaternary than during the Gauss-to-Olduvai diatom maximum because of the signs for strong coastal upwelling? Or was the productivity much the same since the end of the Gauss Chron, and only the silicate content of subsurface water changed? Or else was the productivity, in fact, lower in the Quaternary but insufficiently so to explain the drop in diatom abundance?

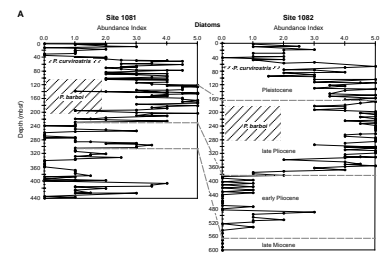
Answers to these central questions are not readily available. The data at hand may fall short of providing the necessary information at this time. In principle, the timescale may be sufficiently stable for the last 3 m.y. to allow the use of mass accumulation rates in helping to unravel the pattern. Of course in practice, the age models for any one site depend on the quality of the stratigraphic record available for dating. Fortunately, for Site 1084 the age model seems to be excellent (see below), and the sedimentation rates apparently do not change much in going from the Namibia opal maximum to the Quaternary (Fig. F11). Thus, plotting mass accumulation rates (Lange et al., 1999; Giraudeau et al., 2001) brings refinement but does not change the argument in fundamental ways. In what follows, we discuss the question of changing productivity in terms of facies and content rather than converting to mass accumulation rates.

As one result of this exercise, we shall reaffirm the notion that the various records within the Namibia upwelling system are closely related and subject to similar dynamics. This does not preclude local variations, but it puts them in context as variations on the same theme. In fact, the present-day geographic setting for the Walvis group of Leg 175 (Fig. F1) suggests that we should expect their records to reflect changes in a system, albeit in the manner appropriate to local conditions.

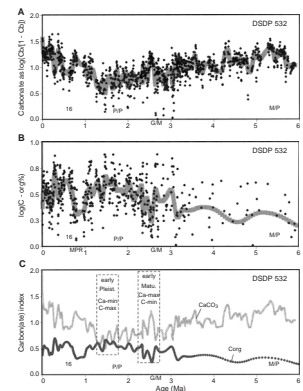
### Pliocene–Pleistocene Productivity Record of the Namibia Upwelling System

The long-term trend in carbonate content of the record at Site 532 (Gardner et al., 1984) suggests a general increase in productivity on Walvis Ridge throughout the Pliocene, culminating in the early Quaternary. After this, increasing carbonate values point to a general decrease in productivity in that region (Fig. F26). Pulses of high productivity (thought to coincide with minimum carbonate content) occur between 3 and 1.2 Ma, but rarely before or after that interval. Within this pulsed production interval, a time of high carbonate values just after the Gauss/Matuyama reversal stands out (Fig. F26A). The record of organic carbon deposition shows a large amount of scatter (Fig. F26B; note log transform). In general, however, it supports the tentative conclusions based on the carbonate record: a general increase of productivity into the early Quaternary and a drop after 1.2 Ma or so. This apparent drop, however, seems less pronounced in the organic carbon than suggested by the increase in carbonate.

F25. Discovery of the Namibia Opal Paradox, p. 82.



F26. Carbonate and organic carbon stratigraphy and carbonate index, Site 532, p. 84.



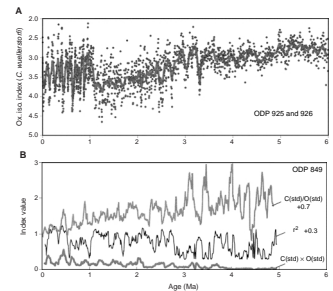
On the scale of 400 k.y. or so, we find substantial excursions in both carbonate and organic carbon, in addition to the overall trend described (Fig. 26C). Three events stand out (two of these are marked on the graph). They are (1) a low-productivity period lasting roughly 250 k.y. just after the Gauss/Matuyama reversal (“early Matuyama productivity minimum”), (2) a high-productivity period centered around 1.4 Ma (“early Pleistocene productivity maximum”), and (3) a distinct productivity minimum in the interval between 1 Ma and Stage 16, that is, roughly between the mid-Pleistocene climate shift and the onset of 100-k.y. cycles. Another important feature is the rather sudden onset of elevated productivity near 3 Ma.

The overall productivity pattern reflected in the record of Site 532 (Fig. F26) must be seen against the background of major changes in climate during the Pliocene–Pleistocene, as reflected, for example, in the oxygen isotope pattern of benthic foraminifers at Sites 925 and 926 on Ceara Rise (Bickert et al., 1997, and unpublished data kindly provided by Torsten Bickert for ages >2.6 Ma) (Fig. F27). The pattern observed is a result of global changes of water chemistry from ice-mass buildup and decay and from local changes in temperature, tied to vertical movements in the boundary between North Atlantic Deep Water and Antarctic Bottom Water at the depth of the sites (3.3 to 4.3 km). Maximum long-period excursions are seen to occur at intermediate stages of overall cooling in the 1-m.y. intervals centered on 3 and 0.5 Ma. The generally low-productivity situation before 3 Ma is well represented by the absence of “cold” excursions, that is, by the narrow range of values fluctuating on the “warm” side of the  $\delta^{18}\text{O}$  record.

After the first strong cooling in the late Pliocene (near 3.2 Ma), the deepwater system responds to further cooling and orbital forcing by creating long-wave oscillations related to eccentricity (Fig. F27A). The same kind of thing (although with more regular cycles) is seen again after 1 Ma. Within the period from the end of the Gauss to 1 Ma, however, such fluctuations are subdued, presumably because the 41-k.y. cycle becomes dominant. In a broad brush scenario one might state the hypothesis thus: in the warm part of the Pliocene, productivity is low and cyclicity is precession forced. In the transition stage (3.3 to 2.3 Ma), productivity is increased and large, long-wave fluctuations feed off the energy delivered by the interference of obliquity and precession forcing. Within the first half of the Quaternary (2 to 1 Ma), precessional effects are subdued, which removes energy from long waves (since they depend on eccentricity variation, which expresses itself through precession). In the second half of the Quaternary, interference patterns re-emerge, as precessional effects reassert themselves.

Additional ideas for how the system changed can be gleaned by comparing the deepwater stratigraphy of oxygen and carbon isotopes (Fig. 27B). The data are from the eastern equatorial Pacific (Site 849) (Mix et al., 1995). All three series represent comparisons of the two isotope stratigraphies, one is the ratio of variability over a 100-k.y. window, another shows the correlation ( $r^2$ ), and the third shows the product of variability. We see that there is a fundamental transition from a world dominated by variability in carbon isotopes to one dominated by that of oxygen isotopes, with the most striking change happening just before 3 Ma. We might refer to this as the transition from a “carbon-dominated system” to an “ice-dominated system” in the present context (within the Pliocene–Pleistocene sequence). We also note that the correlation between the two responses is quite poor at times before 2.8 Ma but improves overall after that. Within the ice world, correlation is

F27. Characterization of climate regimes as seen in deep-ocean sediments, p. 85.



worst during the first half of the Pleistocene, when obliquity dominates fluctuations. Presumably, carbon is more tied to precession and eccentricity, since we find 100-k.y. fluctuations well before these occur in the oxygen isotopes (Schmidt et al., 1993). As far as the sensitivity of the system to outside forcing, it increases all the time, on average, as shown by the product in the variability of oxygen and carbon isotopes (dark gray line in Fig. F27). Comparing the C/O variation ratio with  $r^2$ , one notes that there is an inverse correlation before 2.2 Ma and a positive correlation after that.

From the foregoing discussion of the data in Figures F26 and F27, we conclude that there are three major regime shifts: the first near 3.2 Ma (increase of carbon-independent oxygen isotope variations; increase in production), near 2.8 Ma (increased coherence between carbon and oxygen isotopes whenever carbon variability is relatively low; decrease of production), and near 2.2 Ma (increased coherence between carbon and oxygen isotopes whenever carbon variability is relatively high; increase in production). What we see as an overall trend is an increasing entrainment of the carbon system (including NADW production, which is reflected in carbon isotopes in the deep Pacific) by the ice-dominated system. The overall result in terms of Namibian production is an increase, albeit with interesting (and puzzling) minima, in the early Matuyama and the late Matuyama.

The productivity-related record of Sites 1081, 1082, and 1083 presents the same elements as those seen at Site 532 in the data of Gardner et al. (1984). Again, carbonate is at a maximum near the Miocene/Pliocene boundary (Figs. F26B, F28A). There is then a more or less gradual drop to low values between 3 and 2.5 Ma, a period of major cooling steps (see Maslin et al., 1998, for review). The following period, between the end of the Gauss and Olduvai Chrons and crucial for the Namibia opal maximum, has both high and low carbonate values, presumably reflecting large-scale climate excursions. The absolute minimum of carbonate content is then reached between 2 and 1.5 Ma (centered on 1.5 Ma at Site 532), followed by a rise toward generally higher values, especially after 1 Ma. A minimum within that interval of the second half of the Quaternary appears near Stages 16 and 15, as it does at Site 532.

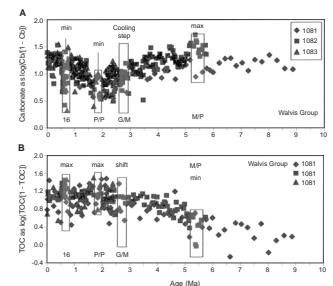
Thus, we are satisfied that Sites 532, 1081, 1082, and 1083 show the same general carbonate pattern and may be considered as telling more or less the same story as concerns large-scale patterns of productivity. The distribution of organic matter (Fig. F28B) confirms this impression from comparison of the Leg 175 Walvis group results with those from Site 532. Inspection also confirms the strong tendency for negative correlation between carbonate and organic carbon already noted (see also Gardner et al., 1984). High organic matter and low carbonate, that is high productivity, dominate between 3 and 1 Ma, with the peak of productivity offset toward the younger part of the interval, to ~1.5 Ma. This is not the same as the pattern for the opal abundance.

## LÜDERITZ SITE (SITE 1084)

### General Aspects

In many ways, Site 1084 may be considered the “flagship” site of Leg 175. It has the highest content of organic matter and the greatest number of diatom mat deposits. Its interstitial water chemistry provides evidence for intense diagenetic activity driven by redox reactions. The

**F28.** Overall patterns of carbon sedimentation at the Walvis group sites, p. 86.



site's sediments showed intense sulfate reduction in the upper few meters and had extremely high ammonia values. Also, an unusual amount of gas was produced by the sediment on being depressurized and an offensive odor emanated from much of the section. There was no doubt about the record having a high-productivity signal.

Site 1084 was drilled not far from Lüderitz Bay, a major upwelling center. The sediment sequence consists of clay-rich nannofossil diatom ooze, diatomaceous nannofossil ooze, and clay-rich nannofossil ooze. Conspicuous decimeter-thick intervals of dark organic-rich clay layers are present between 120 and 510 mbsf and are characterized by reduced carbonate content. Diatoms are abundant in these layers, with *Chaetoceros* resting spores dominant. These spores may be taken as upwelling indicators (Lange et al., 1999). The close proximity of Site 1084 to the Lüderitz upwelling cell results in well-expressed cycles of organic carbon content and diatom and coccolith abundance, as a consequence of cyclic changes in productivity of the type described for the late Quaternary record in this area (Little et al., 1997).

The record of Site 1084, as concerns the important issue of the course of opal deposition, is not fundamentally different from the record of the Walvis group sites. In fact, the diatom data are readily merged when considering general patterns as derived from smear slide data (Fig. F29). Peak values for diatom abundance agree well between Sites 1081 and 1084; they occur between ~ 2.7 and 2.1 Ma; the most persistent peak is offset to the younger part of this interval, between 2.2 and 2.3 Ma. The rise from low values in the early Pliocene to high values in the late Pliocene is extremely rapid; it takes place at 3.2 Ma. For the first part of the high opal condition, oceanic diatom types still dominate. Then, increasingly, cold-water diatoms and spores become important. Finally, *Chaetoceros* spores and other upwelling indicators dominate from ~2.1 Ma.

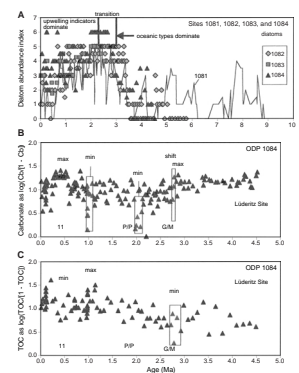
The shift to high-productivity conditions near 3 Ma is notable in the carbonate data (Fig. F29B), and another shift to lower productivity occurs just after 1 Ma (following an interval with two unusually low values). Extremely low values of carbonate occur between 2.2 and 1.9 Ma, just after maximum diatom supply. This suggests that maximum export of organic matter followed maximum export of diatoms. The relatively low values of organic matter between 3 and 2.5 Ma are somewhat surprising. The Walvis group as a whole shows high values for this interval. The small number of points, which invites the possibility of aliased sampling overemphasizing one or the other deviation from the mean, makes interpretation difficult.

On the whole, the data from Site 1084 agree with those of the other sites, with maximum opal deposition near 2.2 to 2.3 Ma embedded in an interval of generally increased background productivity between 3 and 1 Ma. A secondary opal maximum near 1 Ma seems associated with a productivity peak (as seen in the TOC). We infer that on timescales of long periods (0.2 m.y. or more), opal deposition and organic productivity are positively correlated, despite the fact that they are anticorrelated on the scale of periods of 0.1 m.y. or less.

### Productivity Record of Site 1084: Evidence from Benthic Foraminifers

When using carbonate as a productivity indicator—by assuming that dissolution intensity is a function of the supply of organic matter—one runs the risk of confusing dilution with dissolution. Although this is

F29. Diatom abundance, carbonate, and organic carbon content, Site 1084, p. 87.

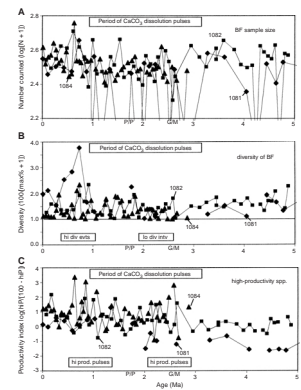


not the only risk (the other one refers to the changing undersaturation of deep water), it may be important. It is also readily diminished by noting the preservation of calcareous fossils. No systematic studies of preservation stratigraphy are available as yet, but we can make use of the number of benthic foraminifers counted by the specialist on board, Otto Hermelin. Hermelin desired to obtain a representative estimate of the proportion of the more important species present. For this purpose, one needs to count ~300 specimens. Thus, when foraminifers were plentiful, Hermelin counted this number, or even more. But when his samples did not contain sufficient tests, he counted whatever was available. The list of numbers counted (which he provided) is therefore a measure of the preservation of benthic foraminifers. In particular, periods of low numbers counted are periods of low availability and represent dissolution events.

When plotting Hermelin's counts, it becomes apparent that dissolution events are greatly concentrated between 3 and 1 Ma at Site 1084 (and also at Site 1081) (Fig. 30A). This is precisely the interval previously identified as a high-production period. The diversity of benthic foraminifers is another potential measure of productivity. As in most situations in different types of ecosystems, a high supply of food suppresses diversity and encourages rapidly growing opportunists. As a matter of observation, the number of species in the open ocean environment tends to be much larger than the number of species living under high-productivity regions at the margins of the ocean (Berger et al., 1998a). Diversity values for Hermelin's samples (Shipboard Scientific Party, 1998g, 1998j) were calculated as the logarithm of the inverse of the maximum percentage in a given sample. (The percentage was augmented by one point.) Results show low diversity values between 3 and 1 Ma, with a minimum near 2.2 Ma, rather close to the peak of the diatom deposition (Fig. F30B). Diversities at Site 1084 are especially low, as here productivity is highest. Poor preservation can interfere with this index to some extent. If there are only a few specimens, the most abundant species is bound to have a relatively high number.

Species belonging to the genera or groups *Bolivina*, *Bulimina*, *Globobulimina*, and *Praeglobobulimina* may be combined to yield yet another index for productivity (Fig. F30B). Maximum values throughout belong to Site 1084, which is situated in the most productive region of the sites drilled off Namibia. Unusually high values are concentrated between 2.5 and 2 Ma (in the Namibia opal maximum) and around and just after 1 Ma. The values after 1 Ma are not in agreement with the scenario of high productivity from 3 to 1 Ma, with lower values following. Interestingly, some of the lowest values of the *Bolivina*-*Bulimina* ("BoBu") index also are situated within the Namibia opal maximum itself. This means that the opal maximum is a time of maximum range of fluctuation between high and low productivity. Overall, ignoring the spikes, there is actually little change in the typical value from 2.5 Ma to present. This suggests that the opal maximum represents a period of transition between the pre-late Pliocene low-production time and a subsequent (Quaternary) high-production time, with the transition expressed as a flipping back and forth between the old and the new situation.

**F30.** Productivity indices based on benthic foraminifers at Site 1084 and Walvis group sites, p. 88.



### Early Matuyama Diatom Maximum: Search for Mechanisms

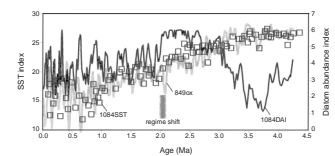
The origin of the early Matuyama Diatom Maximum, between the end of the Gauss and the beginning of the Olduvai Chrons, is complex. It involves seasonal mixing and background supply of silicate within the thermocline in an upwelling environment, as well as frontal zone activity of varying degrees of relative importance and with the participation of various water masses. In preparation for numerical modeling of such a system, it is useful to take account of the patterns emerging from available data. The basis for discussion is the “diatom abundance index” (DAI) used in shipboard work and in subsequent more detailed work on the diatom content of Site 1084 and neighboring sites (Lange et al., 1999; Pérez et al., [Chap. 4](#), this volume). It has a pattern similar to the logarithm of percent opal, except that it has an upper limit of value 6 (“extremely abundant”). The stratigraphy of the DAI (edited and smoothed) shows the familiar ramping up, with superposed long-wave cycles, to the Namibia opal maximum between 2.6 and 2.1 Ma (Fig. [F31](#)). Opal content (Pérez et al., [Chap. 4](#), this volume) shows that, in fact, the maximum is not at the center of the plateau, but shifted to the younger side, near 2.2 Ma.

The optimum temperature of surface waters at Site 1084, which prevailed during maximum opal deposition between 2.3 and 2.2 Ma, can be read from the alkenone-based temperature curve of Marlow et al. (2000). It is 22.5°C, considerably warmer than typical present temperatures, which fluctuate around a mean of 18°C or so, using the maximum for late Pleistocene values recorded in the alkenones (cf. Tchernia, 1980). The value of 22.5°C is beyond three standard deviations from the mean for the last 0.5 m.y., according to the data of Marlow et al. (2000); that is, a spike of opal deposition as high as during the Namibia optimum (if tied to temperature) might be expected once or twice in the last million years, given the sampling density of the DAI determinations (Fig. [F31](#)). (The sea-surface temperature (SST) series shown in Fig. [F31](#), marked 1084SST, is based on data kindly supplied by J. Marlow. The points are generalized from the original data by arbitrarily reassigning positions of sampling points by up to 15 k.y., for more even spacing, and by eliminating points with neighbors at 10 k.y. or less.)

To make the relationship to temperature more precise, we have used the  $\delta^{18}\text{O}$  record of benthic foraminifers at Site 849 in the eastern equatorial Pacific (Mix et al., 1995), reversed the sign, and set the series to the mean and standard deviation of the alkenone data. We then resampled the smoothed curve (40-k.y. boxcar) for the (adjusted) sampling positions of the diatom index. (The adjustment results from smoothing both age and DAI values with the same three-point boxcar.) The resulting curve, labeled “849ox” describes the alkenone data very well over much of the record. Exceptions occur between 2.6 and 2 Ma where the alkenone data seem to scatter in the upper part and above the range defined by the  $\delta^{18}\text{O}$  series. This period of anomalously warm surface water (relative to general trends) is also the period of the Namibia diatom maximum.

It is evident from the history documented in the series plotted (Fig. [F31](#)) that the warm waters of the early Pliocene are unfavorable for diatom growth. On entering the “high-productivity interval” between 3 and 1 Ma, identified above, the diatom supply suddenly increases; that is, diatom supply simply follows productivity at this point. The 3-Ma productivity increase is marked by a cooling step, as seen in the deep-

**F31.** Diatom abundance vs. alkenone-derived temperature series, p. 89.



water data. The next two global cooling steps are near 2.75 and 2.55 Ma; they result in further increases of diatom supply (and presumably overall productivity). (A strong admixture of allochthonous material makes interpretation difficult.) Near 2.1 Ma, with another marked cooling step, there is a regime shift. No longer does the Namibia upwelling system respond with increased diatom supply to an increase in cooling and production. At the cooling step between 2.1 and 2.0 Ma, there is a distinct reduction of opal accumulation. The reduction persists over the rest of the record, throughout the Quaternary. Thus, the 2-Ma cooling step produces an overall regime shift in the system: the response to forcing changes in fundamental ways (as pointed out above when discussing Fig. F27). We can only guess at this point what this change of response might be, but it resulted in the separation of diatom productivity from general productivity. Thick organic-rich layers occur well before and after the shift, from the post-Gauss cooling step (2.55 Ma) to the Brunhes/Matuyama boundary (0.78 Ma), with maxima at 1.1 to 1.2, near 1.45, 1.7, 1.9, and 2.4 to 2.5 Ma. Organic matter content does not seem to decrease after 2 Ma (Fig. F29) and neither does the abundance of benthic foraminifer indicators of high productivity such as *Bolivina* and *Bulimina* (Fig. F30).

We interpret these data to mean that cooling increases upwelling and productivity but at the same time decreases nutrient content in the upper thermocline, especially silicate. It is precisely the same dynamics as postulated in attempting to resolve the Walvis Paradox (Berger et al., 1998a; Lange et al., 1999). We also note that the discrepancy between expected and observed surface temperatures mentioned above (during the diatom maximum in Fig. F31) suggests frontal development, with increased temperature gradients.

This simple conceptual model—cooling increases mixing but decreases thermocline fertility—can produce a pattern of productivity history that is appealingly similar to the one observed (Fig. F32). To fit the DAI index (here represented with a mean of unity and a standard deviation of 0.14), we used two factors. One is the system state (labeled “ $x$ ”) as proxied by the  $\delta^{18}\text{O}$  values of benthic foraminifers at Site 849, eastern equatorial Pacific. We assume that upwelling increases with  $x$  (downward), as marked on the graph. At the same time, the sea-surface temperature decreases (as shown on the y-axis) in the fashion prescribed by regression on the alkenone results (Marlow et al., 2000). The other factor is the “distance from optimum conditions,” defined as

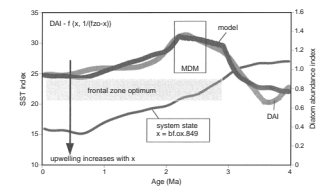
$$\text{abs}[1/(fzo-x)],$$

where  $fzo$  (for “frontal zone optimum”) has the values corresponding to  $x$  within the frontal zone (plus 0.5 to avoid dividing by zero),  $x$  is the  $\delta^{18}\text{O}$  value as before, and the difference is the distance to the nearest frontal zone value. (Thus, within the frontal zone optimum, the “distance from optimum” factor =  $1/0.5$ ). The series labeled “model” results from adding the two factors:

$$\text{DAI est} = f\{x, 1/(fzo-x)\} = a \times \delta^{18}\text{O} + b \times 1/(0.5 + \text{abs}[\text{distance from optimum}]) + c, \quad (4)$$

where  $a$ ,  $b$ , and  $c$  are set for best fit. Distance from optimum turns out to be the more powerful of the two variables, with twice the weighting.

**F32.** Conceptual model of the Matuyama Diatom Maximum between 2.6 and 2.1 Ma, p. 90.



The nature of the residual DAI, after subtracting the smoothed version shown in Fig. F32, is of some interest. It has considerable variation at the scale of 0.4 m.y., the period of modulation of eccentricity amplitude, which in turn modulates precession. The smoothed residual fits quite well with the seasonal contrast potential from orbital parameters (as given by Berger and Loutre, 1991); that is, diatom productivity is high during times when climatic fluctuations are large (Berger and Wefer, in press). The effect is dominated by precession. After 1 Ma the fit deteriorates, presumably as a result of increased decoupling between organic productivity and diatom productivity. A similar residual, based on opal determinations (see Pérez et al., Chap. 4, this volume), shows striking parallelism with the benthic carbon isotope record from Site 849 (in the eastern equatorial Pacific) (Mix et al., 1995). This may be interpreted as another clue to the link of silicate supply in thermocline waters of the eastern South Atlantic to deep circulation.

The same processes enriching Pacific deep waters with  $^{12}\text{C}$  enrich the upper intermediate waters of the South Atlantic with silicate (Berger et al., in press). We take this as confirmation of our hypothesis that the delivery of silicate from NADW is crucial in explaining optimum diatom production in the Southern Ocean (Berger and Wefer, 1991). Delivery of thermocline water from the Southern Ocean, then, would seem to provide a link to this global system and a starting point for the exploration of mechanisms producing the MDM. A strong 0.4-m.y. cycle, in addition, suggests the possible influence of chemical weathering on land as a factor modulating silica supply. In this respect, the studies of Lin and Chen (in press) on the Ge/Si ratio in diatomaceous shells are of special interest.

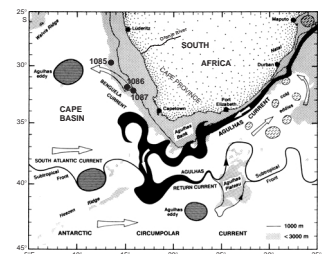
## CAPE BASIN GROUP (SITES 1085, 1086, AND 1087)

### General Aspects

The Cape Basin group comprises Sites 1085, 1086, and 1087. They were drilled off South Africa, south of the Oranje River, just north of the Cape of Good Hope. They are situated south of the "Lüderitz boundary," in the so-called "Southern Benguela Region" (Giraudeau, 1993; Dingle 1995). The sites are some 2000 km south of the port of Benguela in Angola and well south of the Namibia upwelling system; they are part of a system including incursions from the South Atlantic Current and eddies from the Agulhas Retroflexion. Upwelling is much less prominent than off Namibia. This environment might be reasonably referred to as the "Cape Region," since it is part of the Cape Basin and off the Cape Province of South Africa (Fig. F33).

The prevailing facies in the three cores, despite their proximity to the continent, is nannofossil ooze, a pelagic deposit. Diatoms, radiolarians, and other opaline fossils generally are rare or absent, further demonstrating the lack of a strong upwelling signal. (However, diatoms were indeed present in the early Matuyama at all Cape sites, indicating that the early Matuyama Diatom Maximum extends to these sites as well.) At Site 1086, which is quite shallow (780 m), there is a strong showing of foraminifers, especially toward the top portion of the section, which seems strongly winnowed (much of the late Quaternary is missing altogether). The overall rate of deposition is near 3 cm/k.y., but sedimentation rates tend to decrease in the upper Pliocene and in the Pleistocene.

F33. Location of the Cape group sites, p. 91.



At Site 1085, the calcareous ooze is clay rich and olive in color, as appropriate for a strong hemipelagic influence. The site is on the southern rim of the Oranje River Fan; its sedimentation rate is near 5 cm/k.y., intermediate between hemipelagic and pelagic deposits. Site 1087, at slightly shallower depth than Site 1085 (1380 vs. 1710 m), has similar facies, similar sedimentation rates, and similar olive hues, at least in the late Neogene section.

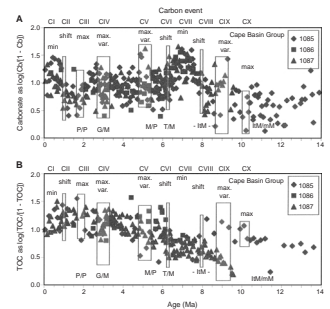
### Carbonate and Organic Carbon Record

An important question is whether the Cape group shows roughly the same patterns, as far as carbonate deposition and organic matter deposition, as the group of cores off Namibia or whether there are striking differences. If similar, we may take this as a hint that wind forcing (productivity) and nutrient supply (thermocline fertility) act similarly all along the coast of southwestern Africa. If different, we might discover that local mechanisms of control on production of sediment are much more important than the concept “Benguela Current System” would imply.

The carbonate records of the three Cape sites are sufficiently similar to allow the recognition of general patterns (Fig. F34). Carbonate is plotted as the log of the ratio of carbonate to noncarbonate to avoid the deceptive nonlinearity of values above 80% as they approach the limit. A value of unity corresponds to  $C_b/(1-C_b) = 10$ ; that is,  $C_b = 10/11 = \sim 91\%$ . After a start with very low carbonate values near the late Miocene/middle Miocene boundary and in the earliest late Miocene (Carbonate Event CX, well known as a CCD excursion upward in the South Atlantic), there follows a period of high variability within the late Miocene. At  $\sim 8$  Ma, there is a distinct and quite abrupt rise to a new regime of high carbonate values (Carbonate Event CVIII; marked “shift” in Fig. F34). Maximum carbonate values are attained near 7 Ma, within the late Miocene (CVII), followed by a shift downward near 6.25 Ma (CVI). A highly variable regime follows, apparently with maximum variability around 5 Ma (CV). The productivity shift seen off Namibia is here marked by maximum variability in the carbonate content (CIV). Low values prevail in the early Pleistocene, especially in the earliest part of the epoch (CIII). A shift to higher values occurs almost precisely at 1 Ma (CI). The sequence of events is not fundamentally different from that seen in the Walvis group (Fig. F28) back to 6 Ma.

The organic carbon record (Fig. F34B) poses no surprises in that it fluctuates counter to the carbonate values: carbonate maxima correspond to organic minima and vice versa. Also, the position of shifts is fairly congruent: a drop near 8 Ma (at Site 1085), a rise at 6.25 Ma (at Sites 1086 and 1087), and a drop near 1 Ma—all superposed on a general rise in organic matter content after 10 Ma (in good agreement with Siesser, 1980). However, the resolution here achieved through stacking of the cores (albeit still highly unsatisfactory) allows the statement that productivity increased in steps and that the step just before 6 Ma (CVI) and the one at 3 Ma (CIV) were the most important, with both steps followed by increased variability. Regarding the time after 3 Ma, there is a “pulling down” of values by Site 1086, presumably as a result of increased winnowing. On the whole, the Cape group record can be reconciled with that of the Walvis group, or more cautiously, differences cannot be demonstrated given the spotty data, while the overall trends seem similar.

F34. Carbon record of the Cape group sites, p. 92.



The paleoproductivity of the late Miocene is explored by Diester-Haass et al. (Chap. 1, this volume) using materials from Site 1085. A general increase in carbonate deposition at this site is well documented, beginning near 7 Ma. This trend and associated long-term cycles in carbonate preservation likely affect the various productivity proxies based on calcareous fossil abundance.

### Productivity Record of Site 1086: Preliminary Results

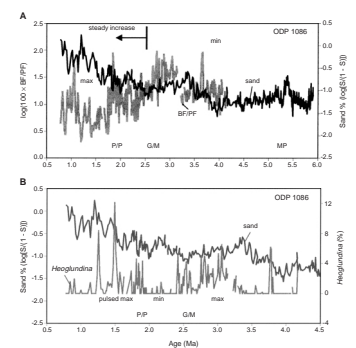
The question regarding the similarity of productivity patterns recorded at the Cape group sites and at the Walvis group sites is unresolved. It is unlikely that it can be answered convincingly on the basis of the available data, for which sample spacing invites severe errors from aliasing (that is, sampling cyclic sediments in ways that prevent random representation of conditions). To escape from this conundrum, high-resolution sampling is needed. Such sampling was done for Site 1086 for the section corresponding to the last 4 m.y. As mentioned above, the late Quaternary record is missing from Site 1086, presumably owing to winnowing, as suggested by the high content of sand in the uppermost cores (Fig. F35).

To obtain diatom-independent information on productivity (for the purpose of assessing the circumstances of the Namibia opal acme), we turn to the faunal composition of benthic foraminifers. Foraminifers are the main component of the sand fraction. Whatever biological processes affect foraminifers also affect the sand content, and whatever physical processes affect the sand fraction also affect foraminiferal abundance and composition. The foraminifer data reported on in this section are part of a larger set of counts by Susan Burke, at SIO. A more comprehensive account of these results is in preparation for publication in the SIO Reference Series.

The sand content at Site 1086 is usually below 9% in the late Miocene and early Pliocene (index of  $<-1$  for the sand% index) (Fig. F35). It rises above background at  $\sim 3.5$  Ma, reaches a maximum between 3.3 and 3.4 Ma, drops slightly toward 2.5 Ma, and rises after that to rather high values near 50% (for which the log index is 0). Assuming that the BF/PF ratio (and therefore its logarithm) is a proxy for productivity (shaded line in Fig. F35A), we can ascribe the decrease in sand content between 3.2 and 2.5 Ma—against a background of generally elevated values and a rising trend—to depression of sand content by dissolution of foraminifers. If planktonic foraminifers are (on the whole) more easily dissolved than benthic ones (as seems likely) (Parker and Berger, 1971), the BF/PF index would be enhanced by this effect through dissolution of carbonate by the carbonic acid evolved from the combustion of organic matter. High productivity, then, seems indicated for the intervals between 3.2 and 2.5 Ma and very low productivity for the interval between 1.8 and 1.2 Ma. This appears to conflict with the patterns for the Walvis group, reported above. A period of high productivity between 3 and 1 Ma was suggested for that group, with values peaking in the early Pleistocene.

We suggest this discrepancy in the apparent productivity patterns may be owing to the winnowing effect: winnowing removes organic carbon and moves it downslope. Clearly, sediments in the late Pleistocene at this site have no carbon at all, simply because there are no sediments left behind. Because of apparent strong winnowing in the entire Quaternary, useful data regarding the export production of or-

**F35.** Sand content at Site 1086 compared with BF/PF and *Hoeglundina elegans*, p. 93.



ganic carbon (or of diatoms) are unlikely to emerge, even from detailed studies. This is true because winnowing affects the very surface of the sediment and thereby also the living conditions of benthic foraminifers, which will simply record that there is little organic matter around in this region of strong currents.

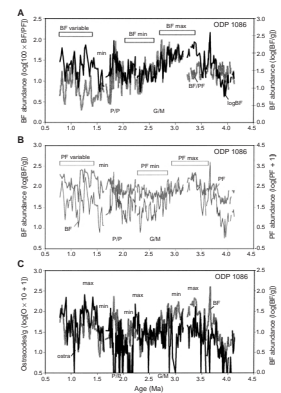
Additional clues to the presence of organic matter at the interface, at least sporadically, can be found in the abundance of *Hoeglundina elegans*, a benthic foraminifer with an aragonitic shell (Fig. F35B). Interestingly, it is actually quite abundant (in proportion to its own record, that is) within the interval between 3.2 and 2.5 Ma, which the BF/PF ratio indicated as a time of high production. In contrast, it goes to zero between 2.4 and 2 Ma during the very time of the MDM off Namibia. Throughout the rest of the section (all the Quaternary present), *Hoeglundina* comes and goes, but it has pulsed maxima around 1.5 Ma. It seems to us that these particular data are compatible with maximum productivity during the Namibia opal maximum off the Cape Province and rather low productivity before and after. We then have two possibilities from reading these high-resolution records: (1) high productivity between 3.2 and 2.5 Ma (early in the Namibia opal maximum) or (2) high productivity between 2.4 and 2 Ma (late in the Namibia opal maximum and congruent with its center).

A useful index of productivity is the accumulation rate of benthic foraminifers (Herguera and Berger, 1991), which reduces to BF/g for sections without variations in sedimentation rates. The use of mass accumulation rates (rather than content) has one drawback: after multiplication with a series of instantaneous sedimentation rates, all indices in a sequence tend to look similar whether the rates are correct or not. Thus, for qualitative characterization, the use of indices based on ratios is much safer than the conversion to mass accumulation rates. Comparing the index for benthic foraminifer abundance (BF/g) with the BF/PF ratio (Fig. F36), we find that the two track quite nicely over much of the record, with the exception of the early part of the Pleistocene. Here, planktonic foraminifers are unusually well preserved and depress the BF/PF ratio even though benthic foraminifers are quite abundant. Of course, since they are components of the sand, they increase with sand content and hence with winnowing. Correcting by this effect, we would see that productivity is in fact low within the Pleistocene and presumably for the reason given: intense winnowing. That winnowing is a source of confusion is also suggested by the fact that benthic foraminifers seem more affected by changes in the Pleistocene than planktonic forms (Fig. F36B). Strong winnowing removes their food. But for this fact, they might just follow sand content as do the planktonic species.

The abundance of ostracodes follows rather closely that of benthic foraminifers (Fig. F36C), presumably as a result of the fact that ostracodes likewise are a component of the sand and are subject to similar effects from removal of nourishment through winnowing.

Different species of benthic foraminifers prefer different environments (Lutze, 1980; Hermelin, 1992; Burke et al., 1993; Loubere, 1994; Fariduddin and Loubere, 1997). Such preferences can be used to construct productivity indices. A good assumption is that benthic foraminifers that are abundant on upper-slope environments in areas of high productivity but rare in the deep sea make excellent markers of high organic carbon supply to the seafloor. Thus, the more abundant species at Lüderitz Site 1084 that are also less abundant in the pelagic environment (e.g., Site 1087) would qualify as productivity indicators.

F36. Comparison of BF, PF, and ostracodes, Site 1086, p. 94.

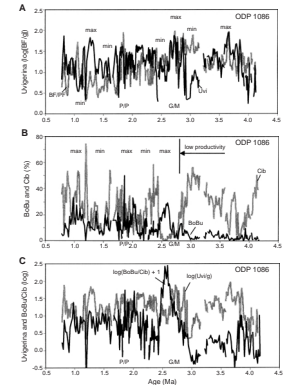


One of the more abundant species indicating elevated productivity in a pelagic setting is the genus *Uvigerina*. (It has also been used to indicate reduced oxygen supply) (Burke et al., 1993.) *Uvigerina* follows the pattern of BF/PF rather closely, except at two intervals in the record (Fig. F37A). The two exceptions are in the early Pleistocene and between 3.2 and 2.9 Ma. In the early Pleistocene, the abundance of *Uvigerina* suggests that this interval was not one of unusually low productivity, which should have reduced abundance. A minimum does persist near 1.5 Ma, however. The discrepancy near 3 Ma is unexplained. Low *Uvigerina* content is supported by high values of *Cibicides*, an open-ocean form, indicating reduced supply of organic matter. However, both indices are contradicted by the rather high BF/PF values and the BF/g maximum centered near 3 Ma (Fig. F36). One possibility is that winnowing during this period (~3 Ma) is responsible for the high values for BF/PF and BF/g and that they say nothing about productivity in this particular setting. Additional checks will be necessary to confirm that this anomaly is real.

Two genera that are very much at home in high-production regions are *Bolivina* and *Bulimina*, while species of the genus *Cibicides* (or *Cibicides* or *Planulina*) are generally taken to be adapted for the pelagic realm (where they record bottom-water properties in their shells). A comparison of the percentages of these forms at Site 1086 is instructive (Fig. 37B). On the whole, *Bolivina* and *Bulimina* are low where *Cibicides* has high abundance, and vice versa. The most impressive shift in abundance is near 3 Ma, where *Cibicides* suddenly drops to very low values, within 200 k.y. or so, and *Bolivina* and *Bulimina* begin their increase to an overall greater presence within the section. Starting at the Pliocene/Pleistocene boundary, the two groups show positive correlation in places. We interpret this as an expansion of the range of productivity on scales too small to see in these data. When times of high productivity alternate with times of low production, both groups can thrive apparently simultaneously (since each sample is a mixture comprising many centuries). A low-productivity interval centered on the early Pleistocene seems supported by these indices.

If *Bolivina* and *Bulimina* respond to high production and *Cibicides* spp. to low, a ratio between the two should be especially sensitive to productivity variation (Fig. F37B). A plot of this index (log scale) confirms that the biggest step in the last 4 m.y. is the one from low productivity before 3 Ma to high productivity beginning at ~2.7 Ma and persisting since. An impressive peak is seen centered on 2.6 Ma, and a precipitous drop to modest values occurs at 2.5 Ma. The reduced ratio persists to ~2.1 Ma. In essence, the reduced productivity (within the generally elevated background) is congruent with the Namibia opal maximum to the north. The discrepancy is intriguing. Either the mixed layer thickened in this region (for example, by pulling in Agulhas waters around the Cape, with increased winds) or the nature of the food changed unfavorably for the *Bolivina* and *Bulimina* group. We think the first alternative is more likely. On the whole, the index offers no evidence for reduced production within the Pleistocene, either around 1.5 Ma or as a trend. Taken together, the abundance patterns of *Uvigerina* and of *Bolivina* and *Bulimina* vs. *Cibicides* suggest that there was one big change in productivity near 3 Ma and that high production of organic matter persisted ever since, possibly with an increased range of fluctuation. It is noted that the BoBu/Cib index backs up the reality of the strangely low values of *Uvigerina* around 3 Ma, to a degree.

F37. Productivity reconstruction from benthic foraminifers, p. 95.



In summary, the detailed data gathered for Site 1086 suggest that there are two regimes of productivity in the Cape Province region south of the Oranje River: a time of low production in the early Pliocene ending near 3 Ma and a time of high production since, with a peak centered on 2.6 Ma and a minimum lasting from 2.5 to 2.1 Ma. It appears therefore, that the Namibia opal maximum was inaugurated by upwelling both off Namibia and off the Cape Province but that the southern upwelling shut down again while the Namibian upwelling system kept ramping up. We propose that the increased frontal activity off Namibia during the early Matuyama was accompanied by increased import of warm water into the Cape Province region, presumably Agulhas eddy water and water from a strengthened South Atlantic Current. Such input must have been pulsed and alternating with Southern Ocean input to account for the occurrence of Antarctic diatom species in the sediment. The development of fronts (convergences) between nutrient-rich cold and nutrient-poor warm water masses is known to result in intense pulses of diatom sedimentation in the eastern equatorial Pacific in the Neogene (Kemp and Baldauf, 1993).

### Notes on the Agulhas Eddy Effect

The contribution of warm water from the Indian Ocean to the Benguela Current in the form of numerous large eddies rounding the Cape (Fig. F33) has been well appreciated for some time. Estimates of the flow of water vary greatly; in recent years values between 6 and 8 sverdrup have been suggested (see reviews by Lutjeharms, 1996; Shannon and Nelson, 1996). If this is so, the Agulhas source contributes substantially to the water volume of the Benguela Current and to the heat transported northward by this current.

The history of the contribution of warm water from Agulhas eddies to the great current off Namibia is of central importance in understanding the history of productivity of the coastal ocean off southwestern Africa. It may be surmised from first principles that this contribution goes through an optimum when conditions are "just right," and it may also be assumed that conditions are not precisely at optimum right now, by happenstance. The strength of the Agulhas Current, a western boundary current like the Gulf Stream and the Brazil Current, depends on the wind field and hence on the temperature gradient in the Southern Hemisphere. This gradient is increased within the Neogene cooling trend. Thus, overall cooling (in high latitudes) and increased winds should drive more warm water southward along the shores of eastern Africa. In contrast, a strengthening of westerly winds driving the South Atlantic Current, and especially a northward motion of the polar and subpolar frontal systems, should make it more difficult for the Agulhas waters to penetrate into the Cape Basin against the prevailing current. The optimum delivery of warm water around the Cape, presumably, will occur when strong seasonal contrast allows appropriate phase shifts in driving and opposing wind forcing. Strong seasonal contrast also stimulates diatom production (as shown by the analysis of cycles contained in the diatom record of Site 1084) (Berger and Wefer, 2001), so that one would expect, under this hypothesis of an Agulhas optimum, that maximum diatom production coincides with maximum delivery of warm eddies.

How can this hypothesis be tested? First, we should find that strong winds deliver warm water to high latitudes on the eastern side of Africa, even during glacial periods. This is indeed the case, judging from the ar-

guments presented by Winter and Martin (1990), based on the study of cores taken off the eastern and southern coasts of South Africa. Winter and Martin suggest from isotopic evidence and nannofossil content that the Agulhas Current did not shift much laterally and that “it did not cool off appreciably during the LGM at least between latitudes 27° and 34°S” (Winter and Martin, 1990, p. 484). They conclude “if the Agulhas Current continued to retrofect in glacial times, then the Holocene resurgence of the Agulhas Current could be obviated and this mechanism would not be necessarily responsible for reseeded the planktonic foraminifer *Globorotalia menardii* into the Atlantic, nor for pulses in North Atlantic Deep Water production (Berger and Vincent, 1986)” (Winter and Martin, 1990, p. 485). We suggest in response that eddy delivery to the South Atlantic does not readily follow from maintaining the strength of the Agulhas Current through glacial–interglacial cycles. Presumably, the West Wind Drift south of the Cape is greatly strengthened during glacials as the polar front moves northward following sea ice expansion. Thus, access of Agulhas waters is likely to be more difficult under these conditions and perhaps denied entirely. The long absence of *G. menardii* within the Caribbean and central Atlantic, at times within the late Pleistocene, in cases through times when conditions would seem favorable (see Imbrie et al., 1973), suggests that reseeded from the Indian Ocean (which is the obvious source) is not a common and automatic process.

The complexity of hydrographic conditions along the shores of the Cape Province—presumably influenced by processes associated with eddy delivery through the Cape valve—is well illustrated by the results of the study by Pierre et al. (Chap. 12, this volume). They generated a stable isotope record for the last 500,000 yr at Site 1087. They find (abstract of their contribution) that “oxygen and carbon isotopic gradients between surface and deep waters display long-term changes superimposed to rapid and high-frequency fluctuations which do not follow the regular (glacial–interglacial) pattern.” In the oxygen isotope record (*Cibicides wuellerstorfi*), unusually large warm peaks are associated with Stage 11 and Substage 5e, and also with the present, indicating strong warming of thermocline waters (Site 1087 is at 1370 m water depth) during these periods. In a companion paper on the same section, Giraudeau et al. (Chap. 7, this volume) suggest that delivery of warm waters from the Indian Ocean continued throughout the last 460 k.y. based on the presence of the warm-water foraminifer *G. menardii* at Site 1087. They propose that interocean exchange was most effective at glacial terminations.

## SUMMARY AND CONCLUSIONS

### Geographic Patterns of Upwelling

Upwelling along the western coast of Africa south of the equator may be partitioned into three major areas, each having its own dynamics: (1) the eastern equatorial region comprising the Congo Fan and the area of Mid-Angola; (2) the Namibia upwelling system, extending from the Walvis Ridge to Lüderitz; and (3) the Cape Province region, where upwelling is subdued. The eastern equatorial region has very nutrient-rich thermocline waters, fed by subsurface eastward flow near the equator and by the Angola dome. An extensive oxygen minimum is present throughout the coastal ocean off Angola, which does not, however,

have the highest productivity of the region. The thermocline waters of the Namibia upwelling system have but a modestly high nutrient content compared with waters off Angola, and concentrations decrease rapidly going southward from the Walvis Ridge. In essence, the pattern suggests diffusion of nutrients southward, from the Angola maximum, and erosion of poleward-flowing nutrient-rich waters by the Benguela Current as it sweeps past Namibia. The mobility of the phosphate seems somewhat greater than that of silicate in the southward migration (Fig. F4). Thus, the export production at the southern margin of the Namibian system is expected to contain a lower Si-to-C ratio than that in the north near Walvis Bay. The Cape Province upwelling region has relatively low phosphate and silicate values in subsurface waters and is correspondingly less productive.

The highest productivity is reached off Namibia between 20° and 25°S. Here, there is an optimum situation regarding the product of rate of upwelling and nutrient content of upwelled waters. Trade winds are strong, offshore transport is vigorous, and the cold water from below is high in both phosphate and silicate.

It is the product of upwelling and nutrient content that determines productivity, not just the rate of upwelling. Changes in any one of the upwelling regions, therefore, can be produced either by changes in wind strength (or direction) or by changes in the nutrient content of the thermocline “thermocline fertility”), or both.

### Quaternary Cycles and the Walvis Paradox

In the deep-sea deposits of the eastern equatorial region, carbonate content is high for interglacial periods, while opal content is high for glacial intervals. The two components are precisely 180° out of phase, with opal expanding into the noncarbonate space during glacials. Regarding opal, the pattern in the sediments of the Congo Fan region is quite similar to that of the deep sea. (The carbonate pattern is not.) In addition, opal tends to follow organic carbon quite closely, with the proviso that organic carbon has a strong precessional component, while opal does not, instead reflecting general climate change (that is, a general oxygen isotope curve). Despite relatively low opal content, sediments off Angola show the same patterns as those off the Congo; thus, they are part of the same regime. The organic matter content is quite readily modeled as a combination of a global oxygen isotope curve and insolation forcing at low latitudes (15°N, almost all precessional forcing). The same model does not work for opal. Apparently, orbital forcing from high and low latitudes interacts nonlinearly for the silicate (high-latitude processes perhaps being responsible for thermocline fertility, low latitude for wind forcing). The result is a record that is difficult to model and whose spectrum shows lines well off the orbital ones.

On Walvis Ridge, as in the Congo-Angola region, the organic matter record can be modeled using a global oxygen isotope curve and combining it with precessional forcing. Glacial periods and periods of low summer insolation in the Northern Hemisphere are favorable for high export production. In contrast, interglacial periods are favorable for opal deposition. Thus, in moving from Angola to Walvis Ridge, the sign of the opal record reverses with respect to organic matter. The patterns suggest that silicate within the thermocline decreases off Congo and Angola during glacial times, but this decrease is insufficient to result in a reversal of patterns relative to organic matter. On Walvis Ridge, however, the decrease in silicate is sufficient to produce the reversal. The re-

versed phase (opal abundant during interglacials) persists throughout the entire Pleistocene, not just on Walvis Ridge but all the way to the Oranje River and off the Cape Province (Site 1085) (Anderson et al., **Chap. 21**, this volume).

It appears that glacial conditions led to a reduction of silicate in the thermocline all along the eastern margin of the South Atlantic, with the reduction weak in the eastern equatorial region but strong from the Walvis Ridge on southward. The situation is reminiscent of the North Pacific (Berger et al., 1997) and the west equatorial Pacific (Berger and Lange, 1998) but with the east equatorial Pacific being exempt, presumably because of silicate imported by the equatorial undercurrent.

The patterns suggest that the upper thermocline of the entire ocean was depleted in silicate relative to now during glacial periods. Presumably, stronger wind-driven mixing exposed silicate more readily to sunlight, which led to precipitation and removal. Increased supply of eolian dust may have helped the process. The lack of shelves further prevented trapping of opal at shallow depths, from where silicate can reenter the thermocline upon dissolution. In this scenario, the Walvis Paradox is not a local phenomenon but one with global implications.

The hypothesis of global thermocline depletion with silicate during glacial intervals does not preclude a regional increase in places where this is appropriate, as, for example, in the North Atlantic, which normally loses silicate through vigorous NADW production. The Walvis Hypothesis simply states that silicate is diminished in the global thermocline on average whenever winds become strong enough to shorten the residence time of silicate in upper waters substantially.

### **Pliocene–Pleistocene Climate Steps and Namibia Opal Acme**

A central discovery of Leg 175 was the documentation of a late Pliocene opal maximum for the entire Namibia upwelling system. The maximum is centered on the period between the end of the Gauss Chron and the beginning of the Olduvai Chron. A rather sharp increase in both organic matter deposition and opal deposition occurs near 3 Ma in the middle of the Gauss Chron, in association with a series of major cooling steps. This association is also reflected in high P/Al and Ba/Al ratios at Site 1085 off the Oranje River (Murray et al., in press). As concerns organic matter, high production persists at least to 1 Ma, when there are large changes in variability, heralding subsequent pulsed production periods. From 3 to 2 Ma, organic matter and opal deposition run more or less parallel, but after 2 Ma opal goes out of phase with organic matter. Apparently, this is the point when silicate becomes strongly limiting to opal production. In contrast, carbon cannot become limiting, and phosphate (which is equally important to opal and organic matter production) remains sufficiently available to maintain high production, aided by increased mixing.

Maximum (carbon) productivity off Namibia is reached after the opal acme within the early Pleistocene. After that time, the quality of the upwelled water may have deteriorated further, for example, by increased erosion (by the Benguela Current) of poleward-moving waters bringing nutrients from the region off Angola and from the northern Namibia upwelling area. However, increased mixing of ever deeper waters during the high-amplitude glacials of the late Pleistocene tended to counteract the drop in thermocline fertility. The fact that (carbon) productivity stayed high from 3 to 1 Ma is also reflected in increased dissolution of

carbonate in this interval off Namibia and in a number of productivity-related indices. NADW production is thought to be important in the delivery of silicate to the Antarctic circumpolar water body, which ultimately provides a source for silicate for intermediate waters. It was previously suggested that an Antarctic opal maximum is tied to optimum conditions for NADW production (Berger and Wefer, 1991). The hypothesis is based on the notion of silicate enrichment of Antarctic waters by import of NADW (called "firehose concept" by Boyle and Rosenthal, 1996).

The early Matuyama Diatom Maximum, or Namibia opal acme (NOA), owes its existence and position to sharply increased mixing and upwelling beginning around 3 Ma, owing to global cooling. The thermocline waters delivering upwelled waters were fed by an Antarctic system exceedingly rich in silicate, a condition inherited from a warm ocean and sustained by increased NADW production. As the ocean cooled, silicate content in the entire ocean dropped because of increased mixing and precipitation (in part from increased dust supply to the sea surface) and because opal dissolves more slowly in cold waters than in warm (for a number of reasons). The large-scale frontal activity that characterized the NOA retreated poleward with the spin-up of the Circumpolar Current. The result of diminished silicate supply and decreased frontal activity was a precipitous drop in opal supply to the seafloor ~2 m.y. ago off Namibia.

### **General Considerations: A Paradigm for Silicate Deposition**

The above-stated hypothesis concerning the origin of the Namibia opal acme is not fundamentally different from the Walvis Hypothesis, stating that glacial conditions result in removal of silicate from the thermocline. By making use of the Monterey Hypothesis (Vincent and Berger, 1985), which states that increased upwelling produces a drop in atmospheric carbon dioxide, we can produce another corollary: whenever silicate becomes severely limiting for diatom production in most of the ocean, and especially in places of upwelling, the carbon dioxide content of the atmosphere has already been lowered. From this corollary, we deduce that there was a reduced level in  $p\text{CO}_2$  at ~2 Ma, with a sharp drop taking place between 3 and 2 Ma. (Since cooling produces upwelling and upwelling reduces  $p\text{CO}_2$ , this is a positive feedback on climate change.).

Moore (1969) argued some time ago that the thinning of radiolarian shells in the Cenozoic has to do with the fact that diatoms remove silicate from the ocean. He saw the process in terms of evolution. The view here taken, in accord with the Walvis Hypothesis, is that a cooling ocean automatically results in a decrease of silicate, provided that diatoms are present (Berger, 1991). The great cooling steps of the Cenozoic are intimately related to the production of diatomaceous deposits (Baron and Baldauf, 1989). Increased mixing from increased wind-driven stirring will favor the growth of diatoms as long as silicate is available to make frustules. Localization of upwelling areas will concentrate the deposits such that remobilization is hindered. Cold water will slow reactions leading to the recycling of silicate (Kamatani, 1982), both in upper waters (slowing removal of organic protective layers on the shells) (Bidle and Azam, 1999) and in deep waters (slowing kinetics of dissolution). The overall preservation ratio (opal accumulation vs. pro-

duction in surface waters) is thought to average near 3% (Tréguer et al., 1995). A small temporary increase in this ratio (say, from cooling) could quickly bring down silicate values, because of the relatively small reservoir of this nutrient. (The many intricacies and difficulties in modeling the Si cycle have recently been reviewed by Nelson et al., 1995; Tréguer et al., 1995; and Ragueneau et al., 2000.)

The geographic distribution of opal and organic matter in the present ocean (Fig. F38) shows the success of processes segregating opal from organic matter. Why should these patterns look different at all?

In a warm ocean, fractionation processes are difficult to visualize. In a cold ocean where production is highly localized in upwelling areas (the largest of which is the Antarctic upwelling ring), fractionation is straightforward. The greater difficulty in recycling silicate, as compared with organic matter and its phosphate, allows opal to become concentrated in regions where organic matter cannot stay because of reoxidation and reworking. Upwelling generates complex interactions between physical and biological processes. High productivity encourages “luxury feeding,” which generates rapidly sinking fecal strings and pellets. Pulsed productivity generates senescence and consequent mass settling of diatoms. Frontal submergence brings diatoms into the dark, forcing their settling. In all these scenarios, the result is rapid removal of silicate from the upper water layer. (Thus, silicate is a crucial component of the biological pump, as emphasized by Dugdale and Wilkerson, 1998.)

In general, a cold ocean is much better at fractionating different types of biogenic sediments from each other than is a warm ocean. The contrast between high- and low-productivity systems is greater in a cold ocean, as is the range in density of water masses. Contrast in productivity and the effects of deep circulation, driven by density contrast, result in contrast in facies. In this very general sense, the Namibia opal acme, and other opal maxima in the latest Neogene in other regions of the ocean, mark the interval when a cooling ocean (tied to a strengthened wind field) selectively removes the excess silicate inherited from a warm ocean. When the excess silicate is removed, the process ceases.

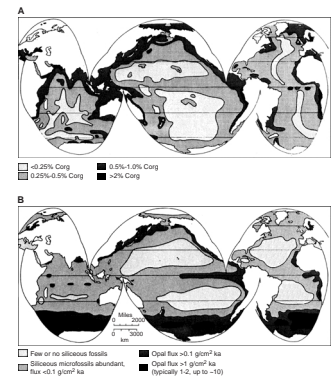
### When Did Upwelling off Southwestern Africa Begin?

The question about the starting time of upwelling has been discussed by a number of authors (e.g., Siesser, 1980; see list in Diester-Haass et al., Chap. 1, this volume). The deposits recovered during Leg 175 suggest shifts to higher production at the Tortonian–Messinian transition (in the late late Miocene, just before 6 Ma) and at 3 Ma, as mentioned. A shift toward overall lower production is indicated for the last million years. The record of the fraction of reactive phosphate at Sites 1082, 1084, and 1085 (Anderson et al., 2001) supports a statement that high-productivity effects begin to show at 6 Ma or later. This does not preclude a gradual ramping up from the middle Miocene into the late Miocene. A choice of a threshold within that interval (say, 10 or 8 Ma) might be possible but would be in need of additional justification beyond the available data.

## ACKNOWLEDGMENTS

We are indebted to a number of Leg 175 scientists for allowing us to inspect their data in advance of publication. Torsten Bickert, Bremen, made unpublished isotope data from Ceara Rise available. Susan Burke,

**F38.** Present-day distribution of organic matter and opal on the seafloor, p. 96



SIO, generated the microfossil data for Site 1086. Lydie Dupont, John Barron, and W.W. Hay reviewed the draft of the manuscript and made valuable suggestions for improvement. In addition, as before, we express our thanks to all who helped prepare for Leg 175 (with special thanks to Volkhard Spiess, who was in charge of seismic surveys) and to all on board who made Leg 175 the record-breaking success it turned out to be.

This research used samples and/or data provided by the Ocean Drilling Program (ODP). ODP is sponsored by the U.S. National Science Foundation (NSF) and participating countries under management of Joint Oceanographic Institutions (JOI), Inc. The work on benthic foraminifers on Site 1086 reported in the section entitled "The Productivity Record of Site 1086: Preliminary Results" was supported by a postcruise JOI-USSSP grant to W.H.B., administered by the Ocean Drilling Program, Texas A&M, College Station, Texas. G. Wefer was supported by the German Research Foundation through SPP DSDP/ODP and the Research Center for Ocean Margins.

## REFERENCES

- Anderson, L.D., Delaney, M.L., and Faul, K.L., 2001. Carbon to phosphorus ratios in sediments: implications for nutrient cycling. *Global Biogeochem. Cycles*, 15:65–79.
- Baldauf, J.G., and Barron, J.A., 1990. Evolution of biosiliceous sedimentation patterns—Eocene through Quaternary: paleoceanographic response to polar cooling. In Bleil, U., and Thiede, J. (Eds.), *Geological History of the Polar Oceans: Arctic Versus Antarctic*: Dordrecht (Kluwer Academic), 575–607.
- Barron, J.A., and Baldauf, J.G., 1989. Tertiary cooling steps and paleoproductivity as reflected by diatoms and biosiliceous sediments. In Berger, W.H., Smetacek, V.S., and Wefer, G. (Eds.), *Productivity of the Oceans: Present and Past*: New York (Wiley-Interscience), 341–354.
- Berger, A., and Loutre, M.F., 1991. Insolation values for the climate of the last 10 million years. *Quat. Sci. Rev.*, 10:297–317.
- Berger, W.H., 1991. Produktivität des Ozeans aus geologischer Sicht: Denkmodelle und Beispiele. *Z. Dtsch. Geol. Ges.*, 142:149–178.
- Berger, W.H., Bickert, T., Yasuda, M.K., and Wefer, G., 1996. Reconstruction of atmospheric CO<sub>2</sub> from the deep-sea record of Ontong Java Plateau: the Milankovitch chron. *Geol. Rundsch.*, 85:466–495.
- Berger, W.H., and Herguera, J.C., 1992. Reading the sedimentary record of the ocean's productivity. In Falkowski, P.G., and Woodhead, A.D. (Eds.), *Primary Productivity and Biogeochemical Cycles in the Sea*: New York (Plenum), 455–486.
- Berger, W.H., Herguera, J.C., Lange, C.B., and Schneider, R., 1994. Paleoproductivity: flux proxies versus nutrient proxies and other problems concerning the Quaternary productivity record. In Zahn, R., Kaminski, M., Labeyrie, L.D., and Pederson, T.F. (Eds.), *Carbon Cycling of the Glacial Ocean: Constraints on the Ocean's Role in Global Change: Quantitative Approaches in Paleoceanography*: Berlin (Springer-Verlag), NATO ASI Ser., 17:385–412.
- Berger, W.H., and Jansen, E., 1994. Mid-Pleistocene climate shift: the Nansen connection. In Johannessen, O.M., Muensch, R.D., and Overland, J.E. (Eds.), *The Role of the Polar Oceans in Shaping the Global Environment*. Geophys. Monogr., Am. Geophys. Union, 85:295–311.
- Berger, W.H., and Lange, C.B., 1998. Silica depletion in the thermocline of the glacial North Pacific: corollaries and implications, 45:1885–1904.
- Berger, W.H., Lange, C.B., and Pérez, M.E., in press. The Early Matuyama diatom maximum off SW Africa: conceptual model. *Mar. Geol.*
- Berger, W.H., Lange, C.B., and Weinheimer, A., 1997. Silica depletion of the thermocline in the eastern North Pacific during glacial conditions: clues from Ocean Drilling Program Site 893, Santa Barbara Basin, California. *Geology*, 25:619–622.
- Berger, W.H., and Vincent, E., 1986. Sporadic shutdown of North Atlantic deep water production during the Glacial-Holocene transition? *Nature*, 324:53–55.
- Berger, W.H., and Wefer, G., 1991. Productivity of the glacial ocean: discussion of the iron hypothesis. *Limnol. Oceanogr.*, 36:1899–1918.
- , 1992. Klimageschichte aus Tiefseesedimenten—Neues vom Ontong-Java-Plateau (Westpazifik). *Die Naturwissenschaften*, 79:541–550.
- , 1996a. Central themes of South Atlantic circulation. In Wefer, G., Berger, W.H., Siedler, G., Webb, D.J. (Eds.) *The South Atlantic: Present and Past Circulation*: Berlin (Springer-Verlag), 1–11.
- , 1996b. Expeditions into the past: paleoceanographic studies in the South Atlantic. In Wefer, G., Berger, W.H., Siedler, G., Webb, D.J. (Eds.), *The South Atlantic: Present and Past Circulation*: Berlin (Springer-Verlag), 363–410.
- , in press. On the reconstruction of upwelling productivity: Namibia upwelling in context. *Mar. Geol.*
- Berger, W.H., Wefer, G., Richter, C., Lange, C.B., Giraudeau, J., Hermelin, O., and Shipboard Scientific Party, 1998a. The Angola-Benguela upwelling system: pale-

- oceanographic synthesis of shipboard results from Leg 175. In Wefer, G., Berger, W.H., and Richter, C., et al., *Proc. ODP, Init. Repts.*, 175: College Station, TX (Ocean Drilling Program), 505–531.
- Berger, W.H., Wefer, G., Richter, C., and Shipboard Scientific Party, 1998b. Color cycles in Quaternary sediments from the Congo Fan region (Site 1075): a statistical analysis. In Wefer, G., Berger, W.H., and Richter, C., et al., *Proc. ODP, Init. Repts.*, 175: College Station, TX (Ocean Drilling Program), 561–567.
- Berggren, W.A., Kent, D.V., Swisher, C.C., III, and Aubry, M.-P., 1995. A revised Cenozoic geochronology and chronostratigraphy. In Berggren, W.A., Kent, D.V., Aubry, M.-P., and Hardenbol, J. (Eds.), *Geochronology, Time Scales and Global Stratigraphic Correlation*. Spec. Publ.—Soc. Econ. Paleontol. Mineral., 54:129–212.
- Bickert, T., Curry, W.B., and Wefer, G., 1997. Late Pliocene to Holocene (2.6–0 Ma) western equatorial Atlantic deep-water circulation: inferences from benthic stable isotopes. In Shackleton, N.J., Curry, W.B., Richter, C., and Bralower, T.J. (Eds.), *Proc. ODP, Sci. Results*, 154: College Station, TX (Ocean Drilling Program), 239–253.
- Bickert, T., and Wefer, G., 1996. Late Quaternary deep-water circulation in the South Atlantic: reconstruction from carbonate dissolution and benthic stable isotopes. In Wefer, G., Berger, W.H., Siedler, G. (Eds.), *The South Atlantic: Present and Past Circulation*: Berlin (Springer-Verlag), 599–620.
- Bidle, K.D., and Azam, F., 1999. Accelerated dissolution of diatom silica by marine bacterial assemblages. *Nature*, 397:508–512.
- Bleil, U., and Shipboard Scientific Party, 1995. Report and preliminary results of SONNE cruise SO 86. *Ber. Fachber. Geowiss., Univ. Bremen*, 51:1–139.
- , 1996. Report and preliminary results of METEOR cruise M34/1, Capetown-Walvis Bay, 3.1.1996–26.1.1996. *Ber. Fachber. Geowiss., Univ. Bremen*, 77:1–129.
- Böhnecke, G., 1936. Temperatur, Salzgehalt und Dichte an der Oberfläche des Atlantischen Ozeans. *Meteor-Werk, Bd. 5, Liefg. 1, mit Atlas*. Berlin.
- Bolli, H.M., Ryan, W.B.F., et al., 1978. *Init. Repts. DSDP*, 40: Washington (U.S. Govt. Printing Office).
- Boyle, E.A., and Rosenthal, Y., 1996. Chemical hydrography of the South Atlantic during the last glacial maximum: Cd vs.  $\delta^{13}\text{C}$ . In Wefer, G., Berger, W.H., Siedler, G., and Webb, D. (Eds.), *The South Atlantic: Present and Past Circulation*: Berlin (Springer-Verlag), 423–443.
- Burke, S.K., Berger, W.H., Coulbourn, W.T., and Vincent, E., 1993. Benthic foraminifera in box core ERDC 112, Ontong Java Plateau. *J. Foraminiferal Res.*, 23:19–39.
- Chapman, P., and Shannon, L.V., 1987. Seasonality in the oxygen minimum layers at the extremities of the Benguela system. In Payne, A.I.L., Gulland, J.A., Brink, K.H. (Eds.), *The Benguela and Comparable Ecosystems*. S. Afr. J. Mar. Sci., 5:85–94.
- Curry, W.B., 1996. Late Quaternary deep circulation in the western equatorial Atlantic. In Wefer, G., Berger, W.H., Siedler, G. (Eds.), *The South Atlantic: Present and Past Circulation*: Berlin (Springer-Verlag), 577–598.
- deMenocal, P.B., Ruddiman, W.F., and Pokras, E.M., 1993. Influence of high- and low-latitude on African terrestrial climate: Pleistocene eolian records from equatorial Atlantic Ocean Drilling Program Site 663. *Paleoceanography*, 8:209–242.
- Diester-Haass, L., 1985a. Late Quaternary sedimentation on the eastern Walvis Ridge, southeast Atlantic (HPC 532 and four piston cores). *Mar. Geol.*, 65:145–189.
- , 1985b. Late Quaternary upwelling history off southwest Africa (DSDP Leg 75, HPC 532). In Hsü, K.J., and Weissert, H.J. (Eds.), *South Atlantic Paleoceanography*: Cambridge (Cambridge Univ. Press), 47–55.
- Diester-Haass, L., Meyers, P.A., and Rothe, P., 1990. Miocene history of the Benguela Current and Antarctic ice volumes; evidence from rhythmic sedimentation and current growth across the Walvis Ridge (Deep Sea Drilling Project Sites 362 and 532) *Paleoceanography*, 5:685–707.
- , 1992. The Benguela Current and associated upwelling on the southwest African margin: a synthesis of the Neogene-Quaternary sedimentary record at DSDP Sites 362 and 352. In Summerhayes, C.P., Prell, W.L., and Emeis, K.C. (Eds.),

- Upwelling Systems: Evolution Since the Early Miocene*. Spec. Publ.—Geol. Soc. London, 64:331–342.
- Dingle, R.V., 1995. Continental shelf upwelling and benthic ostracoda in the Benguela System, southeastern Atlantic Ocean. *Mar. Geol.*, 122:207–225.
- Dugdale, R.C., and Wilkerson, F.P., 1998. Silicate regulation of new production in the equatorial Pacific upwelling. *Nature*, 391:270–273.
- Fariduddin, M., and Loubere, P., 1997. The surface ocean productivity response of deeper water benthic foraminifera in the Atlantic Ocean. *Mar. Micropaleontol.*, 32:289–310.
- Gardner, J.V., Dean, W.E., and Wilson, C.R., 1984. Carbonate and organic-carbon cycles and the history of upwelling at DSDP Site 532, Walvis Ridge, South Atlantic Ocean. In Hay, W.W., Sibuet, J.C., et al., *Init. Repts. DSDP, 75* (Pt. 2): Washington (U.S. Govt. Printing Office), 905–921.
- Giraudeau, J., 1993. Planktonic foraminiferal assemblages in surface sediments from the southwest African continental margin. *Mar. Geol.*, 110:47–62.
- Giraudeau, J., Christensen, B.A., Hermelin, O., Lange, C.B., Motoyama, I., and Shipboard Scientific Party, 1998. Biostratigraphic age models and sedimentation rates along the southwest African margin. In Wefer, G., Berger, W.H., and Richter, C., et al., *Proc. ODP, Init. Repts.*, 175: College Station, TX (Ocean Drilling Program), 543–546.
- Giraudeau, J., Meyers, P.A., and Christensen, B.A., in press. Accumulation of organic and inorganic carbon in Pliocene-Pleistocene sediments along the southwestern African margin. *Mar. Geol.*
- Harrison, K.G., 2000. Role of increased marine silica input on paleo-pCO<sub>2</sub> levels. *Paleoceanography*, 15:292–298.
- Haug, G.H., and Tiedemann, R., 1998. Effect of the formation of the Isthmus of Panama on Atlantic Ocean thermohaline circulation. *Nature*, 393:673–676.
- Hay, W.W., and Brock, J.C., 1992. Temporal variation in intensity of upwelling off southwest Africa. In Summerhayes, C.P., Prell, W.L., and Emeis, K.C. (Eds.), *Upwelling Systems: Evolution Since the Early Miocene*. Spec. Publ.—Geol. Soc. London, 64:463–497.
- Hay, W.W., Sibuet, J.C., et al. (Eds.), 1984. *Init. Repts. DSDP, 75*: Washington (U.S. Govt. Printing Office).
- Herguera, J.C., and Berger, W.H., 1991. Paleoproductivity: glacial to postglacial change in the western equatorial Pacific, from benthic foraminifera. *Geology*, 19:1173–1176.
- , 1994. Glacial to postglacial drop of productivity in the western equatorial Pacific: mixing rate versus nutrient concentrations. *Geology*, 22:629–632.
- Hermelin, J.O.R., 1992. Variations in the benthic foraminiferal fauna of the Arabian Sea: a response to changes in upwelling intensity? In Summerhayes, C.P., Prell, W.L., and Emeis, K.C. (Eds.), *Upwelling Systems: Evolution Since the Early Miocene*. Spec. Publ.—Geol. Soc. London, 64:151–166.
- Herzfeld, U.C., and Berger, W.H., 1993. Ocean productivity and indicator variables: map comparison for Atlantic and World Oceans. *SIO Ref. Ser., Univ. Calif. San Diego*, 93-7:1–75.
- Hsü, K.J., Cita, M.B., and Ryan, W.B.F., 1973a. The origin of the Mediterranean evaporites. In Ryan, W.B.F., Hsü, K.J., et al., *Init. Repts. DSDP, 13* (Pt. 2): Washington (U.S. Govt. Printing Office), 1203–1231.
- Hsü, K.J., Ryan, W.B.F., and Cita, M.B., 1973b. Late Miocene desiccation of the Mediterranean Sea. *Nature*, 242:240–244.
- Hsü, K.J., and Weissert, H.J. (Eds.), 1985. *South Atlantic Paleooceanography*: Cambridge (Cambridge Univ. Press), 1–350.
- Imbrie, J., Donk, J.-V., and Kipp, N.G., 1973. Paleoclimatic investigation of a late Pleistocene Caribbean deep-sea core: comparison of isotopic and faunal methods. *Quat. Res.*, 3:10–38.

- Imbrie, J., Hays, J.D., Martinson, D.G., McIntyre, A., Mix, A.C., Morley, J.J., Pisias, N.G., Prell, W.L., and Shackleton, N.J., 1984. The orbital theory of Pleistocene climate: support from a revised chronology of the marine  $\delta^{18}\text{O}$  record. *In* Berger, A., Imbrie, J., Hays, J., Kukla, G., and Saltzman, B. (Eds.), *Milankovitch and Climate* (Pt. 1), NATO ASI Ser. C, Math Phys. Sci., 126:269–305.
- Jansen, J.H.F., van Weering, T.C.E., Gieles, R., and van Iperen, J., 1984. Middle and late Quaternary oceanography and climatology of the Zaire-Congo fan and the adjacent eastern Angola Basin. *Neth. J. Sea Res.*, 17:201–249.
- Kamatani, A., 1982. Dissolution rates of silica from diatoms decomposing at various temperatures. *Mar. Biol.*, 68:91–98.
- Keller, G., and Barron, J.A., 1983. Paleooceanographic implications of Miocene deep-sea hiatuses. *Geol. Soc. Am. Bull.*, 97:590–613.
- Kemp, A.E.S., and Baldauf, J.G., 1993. Vast Neogene laminated diatom mat deposits from the eastern equatorial Pacific Ocean. *Nature*, 362:141–144.
- Kutzbach, J.E., and Liu, Z., 1997. Response of the African monsoon to orbital forcing and ocean feedbacks in the middle Holocene. *Science*, 278:440–443.
- Lange, C.B., Berger, W.H., Lin, H.-L., Wefer, G., and Shipboard Scientific Party, 1999. The early Matuyama diatom maximum off SW Africa, Benguela Current System (ODP Leg 175). *Mar. Geol.*, 161:93–114.
- Larsen, H.C., Saunders, A.D., Clift, P.D., Beget, J., Wei, W., Spezzaferri, S., and the ODP Leg 152 Scientific Party, 1994. Seven million years of glaciation in Greenland. *Science*, 264:952–955.
- Lin, H.-L., and Chen, C.-J., in press. A late Pliocene diatomaceous Ge/Si record from the southeast Atlantic. *Mar. Geol.*
- Little, M.G., Schneider, R.R., Kroon, D., Price, B., Bickert, T., and Wefer, G., 1997. Rapid paleoceanographic changes in the Benguela Upwelling System for the last 160,000 years as indicated by abundances of planktonic foraminifera. *Palaeogeogr., Palaeoclimatol., Palaeoecol.*, 130:135–161.
- Loubere, P., 1994. Quantitative estimation of surface ocean productivity and bottom water oxygen concentration using benthic foraminifers. *Paleoceanography*, 9:723–737.
- Lourens, L.J., Antonarakou, A., Hilgen, F.J., Van Hoof, A.A.M., Vergnaud-Grazzini, C., and Zachariasse, W.J., 1996. Evaluation of the Plio–Pleistocene astronomical time-scale. *Paleoceanography*, 11:391–413.
- Lutjeharms, J.R.E., 1996. The exchange of water between the South Indian and South Atlantic Oceans. *In* Wefer, G., Berger, W.H., Siedler, G., and Webb, D.J. (Eds.), *The South Atlantic: Present and Past Circulation*: Berlin (Springer-Verlag), 125–162.
- Lutze, G.F., 1980. Depth distribution of benthic foraminifera on the continental margin off NW Africa. *“Meteor” Forschungsergeb. Reihe C*, 32:31–80.
- Marlow, J.R., Lange, C.B., Wefer, G., and Rosell-Mele, A., 2000. Upwelling intensification as part of the Pliocene–Pleistocene climate transition. *Science*, 290:2288–2291.
- Martin, J.H., 1994. Testing the iron hypothesis in the equatorial Pacific Ocean. *Nature*, 371: 123–129.
- Maslin, M.A., Li, X.S., Loutre, M-F., Berger, A., 1998. The contribution of orbital forcing to the progressive intensification of Northern Hemisphere glaciation. *Quat. Sci. Rev.*, 17:411–426.
- Meyers, P.A., and Shipboard Scientific Party, 1998. Microbial gases in sediments from the southwest African margin. *In* Wefer, G., Berger, W.H., and Richter, C., et al., *Proc. ODP, Init. Repts.*, 175: College Station, TX (Ocean Drilling Program), 555–560.
- Miller, K.G., Fairbanks, R.G., and Mountain, G.S., 1987. Tertiary oxygen isotope synthesis, sea-level history, and continental margin erosion. *Paleoceanography*, 2:1–19.
- Mix, A.C., Pisias, N.G., Rugh, W., Wilson, J., Morey, A., and Hagelberg, T.K., 1995. Benthic foraminifer stable isotope record from Site 849 (0–5 Ma): local and global climate changes. *In* Pisias, N.G., Mayer, L.A., Janecek, T.R., Palmer-Julson, A., and van Andel, T.H. (Eds.), *Proc. ODP, Sci. Results*, 138: College Station, TX (Ocean Drilling Program), 371–412.

- Moore, T.C., 1969. Radiolaria: change in skeletal weight and resistance to solution. *Geol. Soc. Am. Bull.*, 80:2103–2108.
- Moore, T.C., Jr., Rabinowitz, P.D., et al., 1984. *Init. Repts. DSDP*, 74: Washington (U.S. Govt. Printing Office).
- Moore, T.C., Rabinowitz, P.D., Borella, P., Boersma, A., Shackleton, N.J., 1984. Introduction and explanatory notes. *In* Moore, T.C., Jr., Rabinowitz, P.D., et al., *Init. Repts., DSDP*, 74: Washington (U.S. Govt. Printing Office), 3–39.
- Murray, R.W., Wigley, R., and Shipboard Scientific Party, 1998. Interstitial water chemistry of deeply buried sediments from the southwest African margin: a preliminary synthesis of results from Leg 175. *In* Wefer, G., Berger, W.H., and Richter, C., et al., *Proc. ODP, Init. Repts.*, 175: College Station, TX (Ocean Drilling Program), 547–553.
- Murray, R.W., Christensen, B.A., Kalbas, J.L., and Kryc, K.A., in press. Pliocene export production and terrigenous provenance of the Southern Cape Basin, southwest African margin. *Mar. Geol.*
- Nelson, D.M., Tréguer, P., Brzezinski, M.A., Leynaert, A., and Queguiner, B., 1995. Production and dissolution of biogenic silica in the ocean: revised global estimates, comparison with regional data and relationship to biogenic sedimentation. *Global Biogeochem. Cycles*, 9:359–372.
- Neumann, G., and Pierson, W.J., Jr., 1966. *Principles of Physical Oceanography*: Englewood Cliffs, NJ (Prentice-Hall).
- Oberhänsli, H., 1991. Upwelling signals at the northeastern Walvis Ridge during the past 500,000 years. *Paleoceanography*, 6:53–71.
- Parker, F.L., and Berger, W.H., 1971. Faunal and solution patterns of planktonic foraminifera in surface sediments of the South Pacific. *Deep-Sea Res., Part A*, 18:73–107.
- Peterson, R.G., and Stramma, L., 1991. Upper-level circulation in the South Atlantic Ocean. *Progr. Oceanogr.*, 26:1–73.
- Pufahl, P.K., Maslin, M.A., Anderson, L., Brüchert, V., Jansen, F., Lin, H., Perez, M., Vidal, L., and Shipboard Scientific Party, 1998. Lithostratigraphic summary for Leg 175: Angola–Benguela upwelling system. *In* Wefer, G., Berger, W.H., and Richter, C., et al., *Proc. ODP, Init. Repts.*, 175: College Station, TX (Ocean Drilling Program), 533–542.
- Ragueneau, O., Tréguer, P., Leynaert, A., Anderson, R.F., Brzezinski, M.A., DeMaster, D.J., Dugdale, R.C., Dymond, J., Fischer, G., Francois, R., Heinze, C., Maier-Reimer, E., Martin-Jézéquel, V., Nelson, D.M., and Quéguiner, B., 2000. A review of the Si cycle in the modern ocean: recent progress and missing gaps in the application of biogenic opal as a paleoproductivity proxy. *Global Planet. Change*, 26:317–365.
- Raymo, M.E., 1994. The Himalayas, organic carbon burial, and climate in the Miocene. *Paleoceanography*, 9:399–404.
- Sancetta, C., Heusser, L., and Hall, M.A., 1992. Late Pliocene climate in the Southeast Atlantic: preliminary results from a multi-disciplinary study of DSDP Site 532. *Mar. Micropaleontol.*, 20:59–75.
- Schmidt, H., Berger, W.H., Bickert, T., and Wefer, G., 1993. Quaternary carbon isotope record of pelagic foraminifers: Site 806, Ontong Java Plateau. *In* Berger, W.H., Kroenke, L.W., Mayer, L.A., et al., *Proc. ODP, Sci. Results*, 130: College Station, TX (Ocean Drilling Program), 397–409.
- Schmieder, F., von Dobeneck, T., and Bleil, U., 2000. The mid-Pleistocene climate transition as documented in the deep South Atlantic Ocean: initiation, interim state and terminal event. *Earth Planet. Sci. Lett.*, 179:539–549.
- Schneider, R.R., Müller, P.J., and Ruhland, G., 1995. Late Quaternary surface circulation in the east equatorial South Atlantic: evidence from alkenone sea surface temperatures. *Paleoceanography*, 10:197–219.
- Schneider, R.R., Müller, P.J., Ruhland, G., Meinecke, G., Schmidt, H., and Wefer, G., 1996. Late Quaternary surface temperatures and productivity in the east-equatorial South Atlantic: response to changes in trade/monsoon wind forcing and surface

- water advection. In Wefer, G., Berger, W.H., Siedler, G., and Webb, D. (Eds.), *The South Atlantic: Present and Past Circulation*: Berlin (Springer-Verlag), 527–551.
- Schneider, R.R., Price, B., Müller, P.J., Kroon, D., and Alexander, I., 1997. Monsoon-related variations in Zaire (Congo) sediment load and influence of fluvial silicate supply on marine productivity in the east equatorial Atlantic during the last 200,000 years. *Paleoceanography*, 12:463–481.
- Shackleton, N.J., and Kennett, J.P., 1975. Paleotemperature history of the Cenozoic and the initiation of Antarctic glaciation: oxygen and carbon isotope analyses in DSDP Sites 277, 279, and 281. In Kennett, J.P., Houtz, R.E., et al., *Init. Repts. DSDP*, 29: Washington (U.S. Govt. Printing Office), 743–755.
- Shackleton, N.J., Berger, A., and Peltier, W.A., 1990. An alternative astronomical calibration of the lower Pleistocene timescale based on ODP Site 677. *Trans. R. Soc. Edinburgh: Earth Sci.*, 81:251–261.
- Shannon, L.V., and Nelson, G., 1996. The Benguela: large scale features and processes and system variability. In Wefer, G., Berger, W.H., Siedler, G., Webb, D.J. (Eds.), *The South Atlantic: Present and Past Circulation*: Berlin (Springer-Verlag), 163–210.
- Shipboard Scientific Party, 1998a. Introduction: background, scientific objectives, and principal results for Leg 175 (Benguela Current and Angola-Benguela upwelling systems). In Wefer, G., Berger, W.H., and Richter, C., et al., *Proc. ODP, Init. Repts.*, 175: College Station, TX (Ocean Drilling Program), 7–25.
- , 1998b. Site 1075. In Wefer, G., Berger, W.H., and Richter, C., et al., *Proc. ODP, Init. Repts.*, 175: College Station, TX (Ocean Drilling Program), 49–86.
- , 1998c. Site 1076. In Wefer, G., Berger, W.H., and Richter, C., et al., *Proc. ODP, Init. Repts.*, 175: College Station, TX (Ocean Drilling Program), 87–113.
- , 1998d. Site 1077. In Wefer, G., Berger, W.H., and Richter, C., et al., *Proc. ODP, Init. Repts.*, 175: College Station, TX (Ocean Drilling Program), 115–141.
- , 1998e. Site 1078. In Wefer, G., Berger, W.H., and Richter, C., et al., *Proc. ODP, Init. Repts.*, 175: College Station, TX (Ocean Drilling Program), 143–176.
- , 1998f. Site 1079. In Wefer, G., Berger, W.H., and Richter, C., et al., *Proc. ODP, Init. Repts.*, 175: College Station, TX (Ocean Drilling Program), 177–199.
- , 1998g. Site 1081. In Wefer, G., Berger, W.H., and Richter, C., et al., *Proc. ODP, Init. Repts.*, 175: College Station, TX (Ocean Drilling Program), 223–272.
- , 1998h. Site 1082. In Wefer, G., Berger, W.H., and Richter, C., et al., *Proc. ODP, Init. Repts.*, 175: College Station, TX (Ocean Drilling Program), 273–312.
- , 1998i. Site 1083. In Wefer, G., Berger, W.H., and Richter, C., et al., *Proc. ODP, Init. Repts.*, 175: College Station, TX (Ocean Drilling Program), 313–337.
- , 1998j. Site 1084. In Wefer, G., Berger, W.H., and Richter, C., et al., *Proc. ODP, Init. Repts.*, 175: College Station, TX (Ocean Drilling Program), 339–384.
- , 1998k. Site 1085. In Wefer, G., Berger, W.H., and Richter, C., et al., *Proc. ODP, Init. Repts.*, 175: College Station, TX (Ocean Drilling Program), 385–428.
- , 1998m. Site 1086. In Wefer, G., Berger, W.H., and Richter, C., et al., *Proc. ODP, Init. Repts.*, 175: College Station, TX (Ocean Drilling Program), 429–455.
- Siesser, W.G., 1980. Late Miocene origin of the Benguela upwelling system off northern Namibia. *Science*, 208:283–285.
- Summerhayes, C.P., Emeis, K.C., Angel, M.V., Smith, R.L., and Zeitschel, B., 1995. *Upwelling in the Ocean: Modern Processes and Ancient Records*: New York (Wiley and Sons), Dahlem Workshop Reports, 422.
- Summerhayes, C.P., Prell, W.L., Emeis, K.C. (Eds.), 1992. *Upwelling Systems: Evolution Since the Early Miocene*. Spec. Publ.—Geol. Soc. London, 64.
- Tcherneria, P., 1980. *Descriptive Regional Oceanography*: New York (Pergamon Press).
- Tiedemann, R., Sarnthein, M., and Shackleton, N.J., 1994. Astronomic timescale for the Pliocene Atlantic  $\delta^{18}\text{O}$  and dust flux records of Ocean Drilling Program Site 659. *Paleoceanography*, 9:619–638.
- Tomczak, M., and Godfrey, J.S., 1994. *Regional Oceanography: An Introduction*: Oxford (Pergamon Press).

- Tréguer, P., Nelson, D.M., Van Bennekom, A.J., DeMaster, D.J., Leynaert, A., and Quéguiner, B., 1995. The silica balance in the world ocean: a reestimate. *Science*, 268:375–379.
- Vincent, E., and Berger, W.H., 1985. Carbon dioxide and polar cooling in the Miocene: the Monterey Hypothesis. In Sundquist, E.T., and Broecker, W.S. (Eds.), *The Carbon Cycle and Atmospheric CO<sub>2</sub>: Natural Variations Archean to Present*. Geophys. Monogr., Am. Geophys. Union, 32:455–468.
- von Dobeneck, T., and Schmieder, F., 1999. Using rock magnetic proxy records for orbital tuning and extended time series analyses into the super-and sub-Milankovitch bands. In Fischer, G., and Wefer, G. (Eds.), *Use of Proxies in Paleoceanography*: Berlin (Springer), 601–633.
- Wefer, G., Berger, W.H., Bickert, T., Donner, B., Fischer, G., Kemle-von Mücke, S., Meinencke, G., Müller, P.J., Mulitza, S., Niebler, H.-S., Pätzold, J., Schmidt, H., Schneider, R.R., and Segl, M., 1996. Late Quaternary surface circulation of the South Atlantic: the stable isotope record and implications for heat transport and productivity. In Wefer, G., Berger, W.H., Siedler, G., and Webb, D.J. (Eds.), *The South Atlantic: Present and Past Circulation*: Berlin (Springer-Verlag), 461–502.
- Wefer, G., Berger, W.H., Fischer, G., and Bijma, J., 1999. Clues to ocean history: a brief overview of proxies. In Fischer, G., Wefer, G. (Eds.), *Use of Proxies in Paleoceanography: Examples from the South Atlantic*: Berlin (Springer), 1–68.
- Wefer, G., Berger, W.H., and Richter, C., et al., 1998. *Proc. ODP, Init. Repts.*, 175 [CD-ROM]. Available from: Ocean Drilling Program, Texas A&M University, College Station, TX 77845-9547, U.S.A.
- Wefer, G., Berger, W.H., Richter, C., and Shipboard Scientific Party, 1998. Facies patterns and authigenic minerals of upwelling deposits off southwest Africa. In Wefer, G., Berger, W.H., and Richter, C., et al., *Proc. ODP, Init. Repts.*, 175: College Station, TX (Ocean Drilling Program), 487–504.
- Whitman, J.M., and Berger, W.H., 1992. Pliocene–Pleistocene oxygen isotope record of Site 586, Ontong Java Plateau. *Mar. Micropaleontol.*, 18:171–198.
- Winter, A., and Martin, K., 1990. Late Quaternary history of the Agulhas current. *Paleoceanography*, 5:479–486.
- Worthington, L.V., 1968. Genesis and evolution of water masses. *Meteorol. Monogr.*, 8:63–67.
- Young, R.W., 1991. Atmospheric iron inputs and primary productivity: phytoplankton responses in the North Pacific. *Global Biogeochem. Cycles*, 5:119–134.

## APPENDIX

## Summary of Holes Drilled during Leg 175

Hole	Latitude	Longitude	Water depth (mbsl)	Number of cores	Interval cored (m)	Core recovery (m)	Percent recovered (%)	Age of oldest sediment
1075A	4°47.1198'S	10°4.4989'E	2995.7	22	201.00	213.75	106.3	late Pliocene
1075B	4°47.1197'S	10°4.5025'E	2995.2	22	204.50	215.03	105.1	
1075C	4°47.1206'S	10°4.5100'E	2995.5	22	207.20	213.47	103.0	
Site 1075 totals:				66	612.70	642.25	104.8	
1076A	5°4.1316'S	11°6.0917'E	1404.2	22	204.30	217.47	106.4	early Pleistocene
1076B	5°4.1344'S	11°6.0922'E	1402.1	7	60.90	25.87	42.5	
1076C	5°4.1309'S	11°6.1048'E	1402.4	22	203.10	216.80	106.7	
1076D	5°4.1312'S	11°6.1150'E	1401.0	12	113.50	118.41	104.3	
Site 1076 totals:				63	581.80	578.55	99.4	
1077A	5°10.7969'S	10°26.1960'E	2380.0	22	204.50	208.99	102.2	early Pleistocene
1077B	5°10.7977'S	10°26.1831'E	2381.2	22	205.10	211.53	103.1	
1077C	5°10.7995'S	10°26.1687'E	2385.2	3	22.80	16.46	72.2	
Site 1077 totals:				47	432.40	436.98	101.1	
1078A	11°55.2145'S	13°24.0134'E	427.2	9	77.10	70.28	91.2	late Pleistocene
1078B	11°55.2318'S	13°24.0172'E	426.1	14	130.10	125.80	96.7	
1078C	11°55.2474'S	13°24.0161'E	426.0	18	165.20	149.58	90.5	
1078D	11°55.2661'S	13°24.0165'E	427.4	14	126.80	116.71	92.0	
Site 1078 totals:				55	499.20	462.37	92.6	
1079A	11°55.7785'S	13°18.5433'E	737.9	14	121.00	124.61	103.0	late Pleistocene
1079B	11°55.7676'S	13°18.5393'E	738.2	14	128.30	129.70	101.1	
1079C	11°55.7969'S	13°18.5607'E	737.9	14	126.80	129.90	102.4	
Site 1079 totals:				42	376.10	384.21	102.2	
1080A	16°33.5803'S	10°49.2029'E	2765.8	7	52.10	55.57	106.7	early Pleistocene
1080B	16°33.5963'S	10°49.2043'E	2767.9	5	38.20	40.06	104.9	
Site 1080 totals:				12	90.30	95.63	105.9	
1081A	19°37.1818'S	11°19.1598'E	794.1	49	452.70	393.48	86.9	late Miocene
1081B	19°37.1981'S	11°19.1588'E	793.1	21	187.60	195.87	104.4	
1081C	19°37.2128'S	11°19.1620'E	793.8	17	155.20	160.94	103.7	
Site 1081 totals:				87	795.50	750.29	94.3	
1082A	21°5.6373'S	11°49.2361'E	1279.3	64	600.60	502.01	83.6	late Miocene
1082B	21°5.6517'S	11°49.2326'E	1280.4	14	127.00	133.17	104.9	
1082C	21°5.6690'S	11°49.2342'E	1282.1	24	202.00	217.83	107.8	
Site 1082 totals:				102	929.60	853.01	91.8	
1083A	20°53.6841'S	11°13.0720'E	2178.1	22	201.30	185.32	92.1	late Pliocene
1083B	20°53.7004'S	11°13.0738'E	2183.1	22	202.30	206.41	102.0	
1083C	20°53.7138'S	11°13.0734'E	2178.9	1	9.50	9.78	102.9	
1083D	20°53.7138'S	11°13.0734'E	2178.3	21	196.10	201.94	103.0	
Site 1083 totals:				66	609.20	603.45	99.1	
1084A	25°30.8345'S	13°1.6668'E	1991.9	65	605.00	511.56	84.6	early Pliocene
1084B	25°30.8206'S	13°1.6665'E	1992.8	20	182.80	186.60	102.1	
1084C	25°30.8037'S	13°1.6670'E	1991.8	22	207.60	217.82	104.9	
Site 1084 totals:				107	995.40	915.98	92.0	
1085A	29°22.4665'S	13°59.4064'E	1713.2	64	604.00	594.39	98.4	middle Miocene
1085B	29°22.4657'S	13°59.3898'E	1713.0	35	321.20	326.51	101.7	
Site 1085 totals:				99	925.20	920.90	99.5	
1086A	31°33.1608'S	15°39.6235'E	781.1	22	206.20	211.09	102.4	late Miocene
1086B	31°33.1588'S	15°39.6047'E	784.5	23	208.50	212.09	101.7	
Site 1086 totals:				45	414.70	423.18	102.0	
1087A	31°27.8813'S	15°18.6541'E	1371.6	27	255.20	252.38	98.9	early Oligocene/ late Eocene
1087B	31°27.8975'S	15°18.6541'E	1371.8	8	72.50	74.83	103.2	
1087C	31°27.9137'S	15°18.6541'E	1374.2	53	491.90	478.30	97.2	
1087D	31°27.9299'S	15°18.6541'E	1383.5	15	128.80	130.92	101.6	
Site 1087 totals:				103	948.40	936.43	98.7	
Leg 175 totals:				894	8210.50	8003.23	97.5	

Figure F1. South Atlantic circulation and areas of high productivity (hatched). Stippled areas = shallower than 3 km. From Berger and Wefer (1996a), after Peterson and Stramma (1991) and Tomczak and Godfrey (1994), modified according to chlorophyll distribution as seen in satellite images (see Berger and Wefer, 1996a, fig. 4).

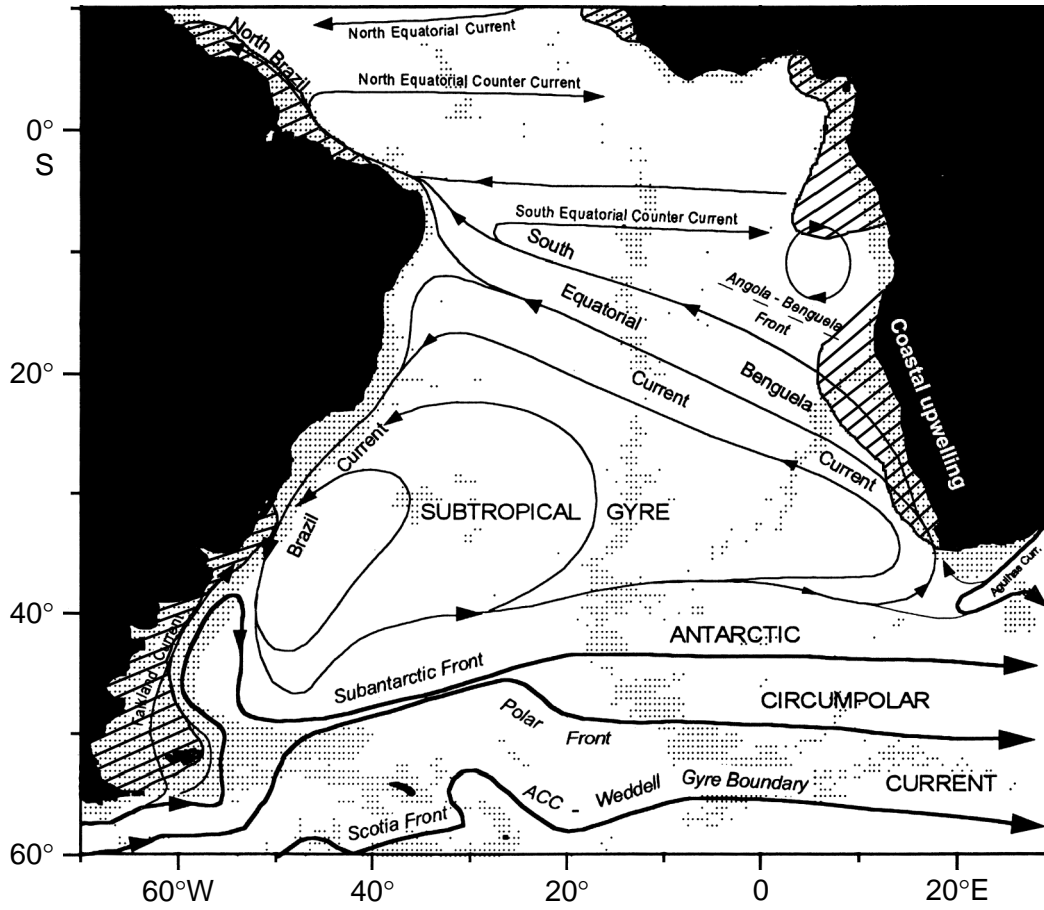


Figure F2. Locations of Sites 1075–1087, Leg 175 of the Ocean Drilling Program.

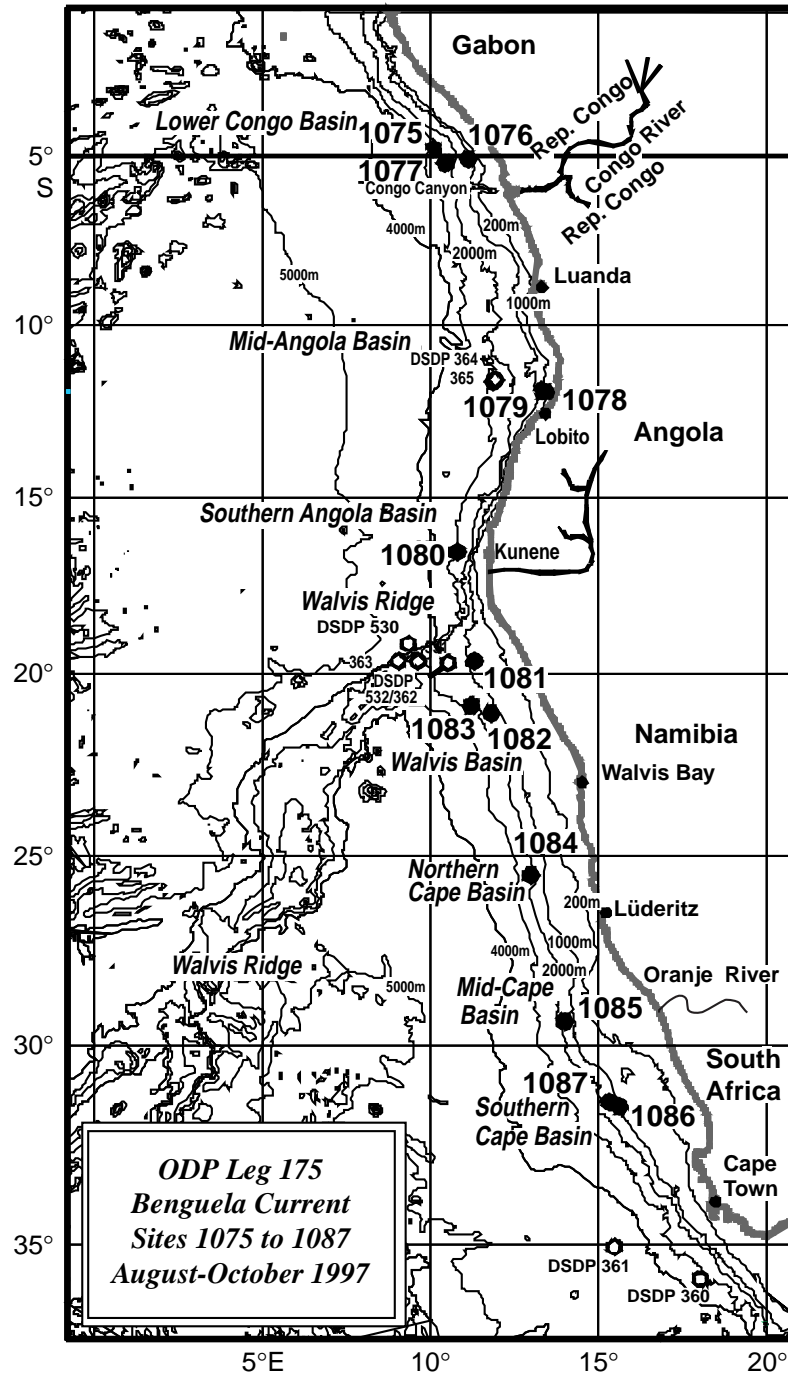
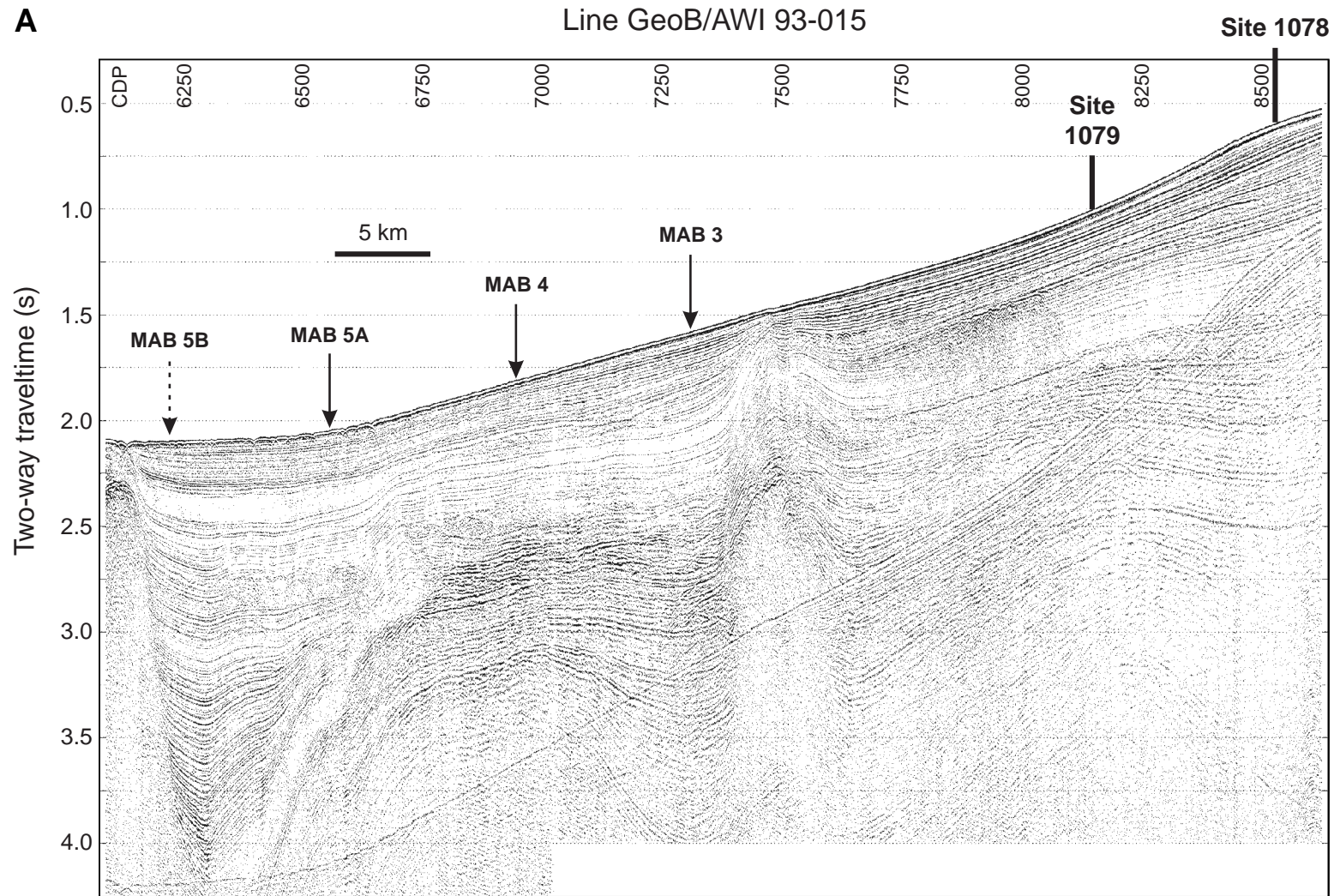


Figure F3. Nature of deposition north and south of the Walvis Ridge, with and without salt tectonics. A. North of Ridge. MAB3 to MAB5B = Mid-Angola site proposals. (Continued on next page.)



**Figure F3 (continued). B.** South of Ridge; note numerous small faults. From Shipboard Scientific Party (1998e, 1998f, 1998h). Seismic lines by V. Spiess; processing courtesy of the Alfred-Wegener-Institut, Bremerhaven. CDP = common depth point.

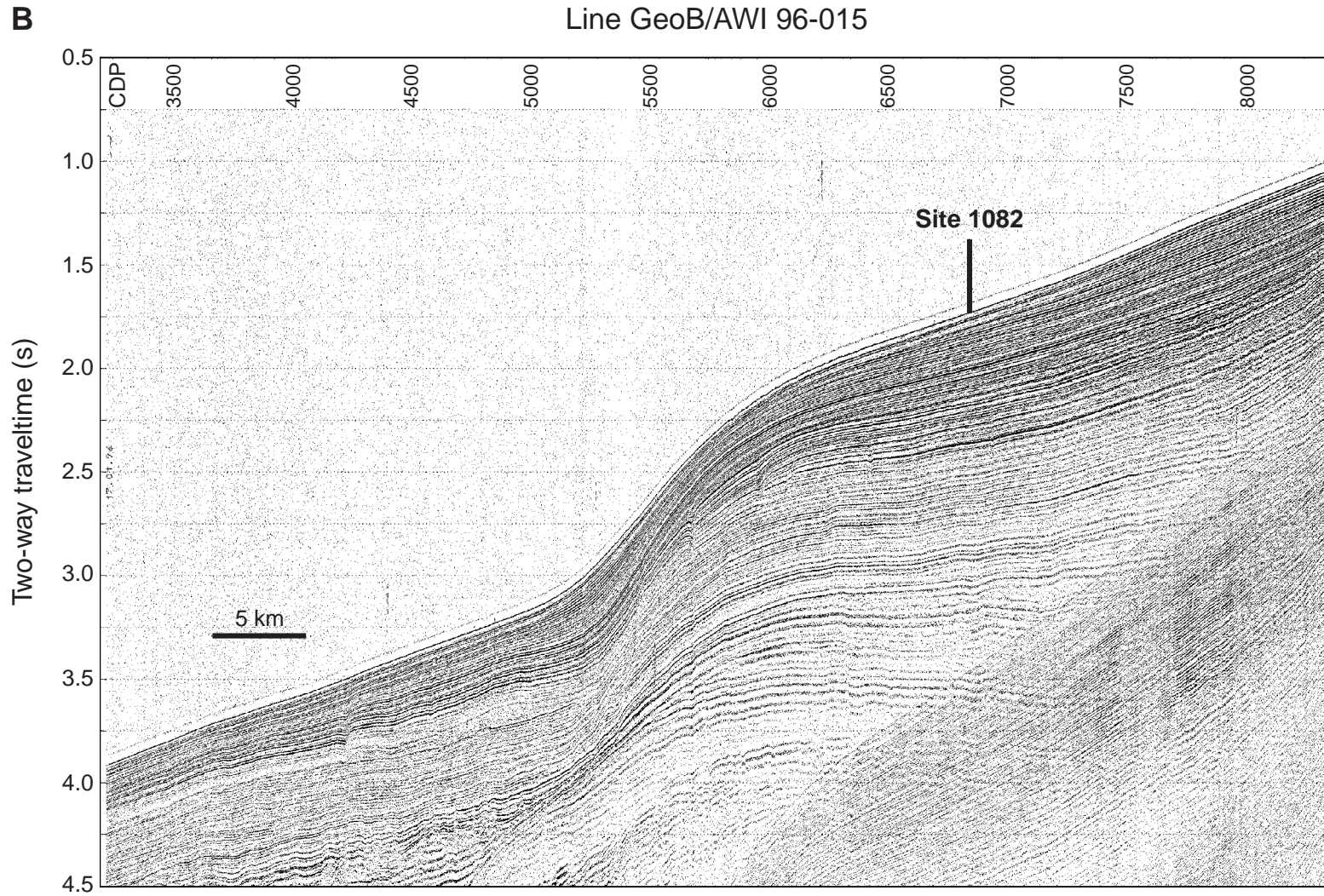


Figure F4. Silicate and phosphate patterns in subsurface waters of the South Atlantic (from Herzfeld and Berger, 1993). A. Silicate concentrations at 100-m depth ( $\mu\text{M}/\text{kg}$ ). B. Phosphate concentrations at 100-m depth ( $\mu\text{M}/\text{kg}$ ).

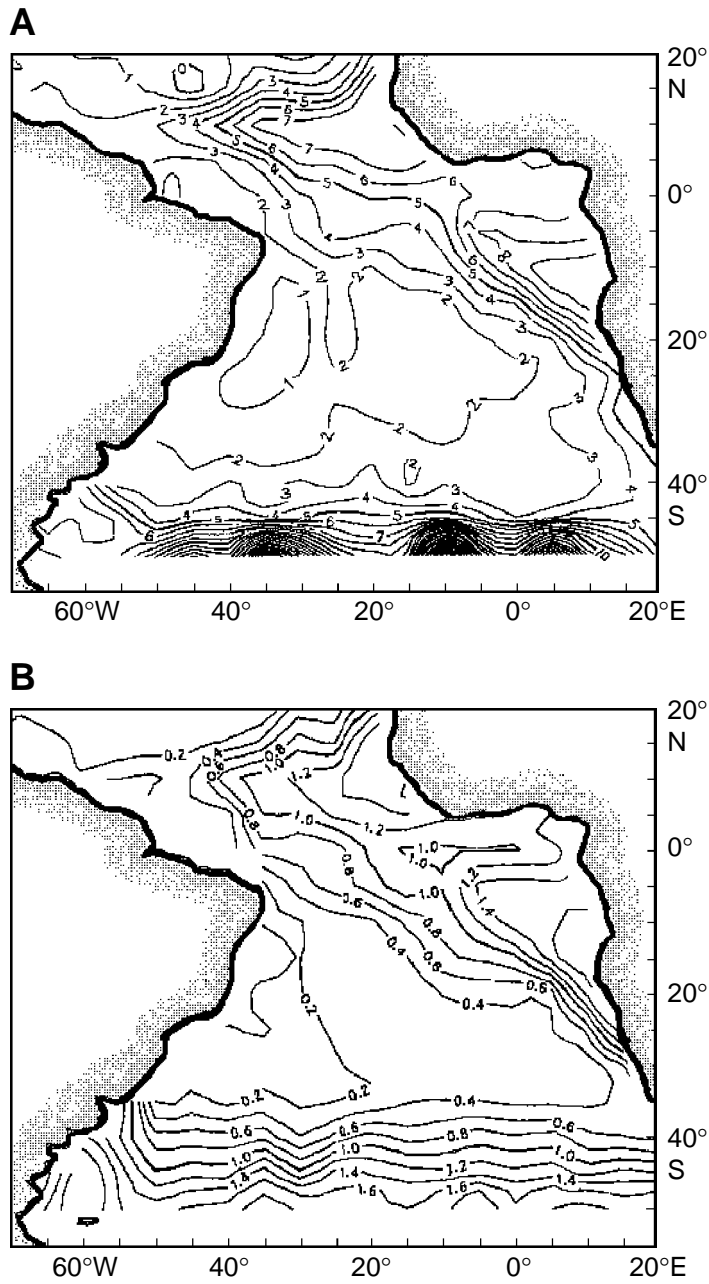
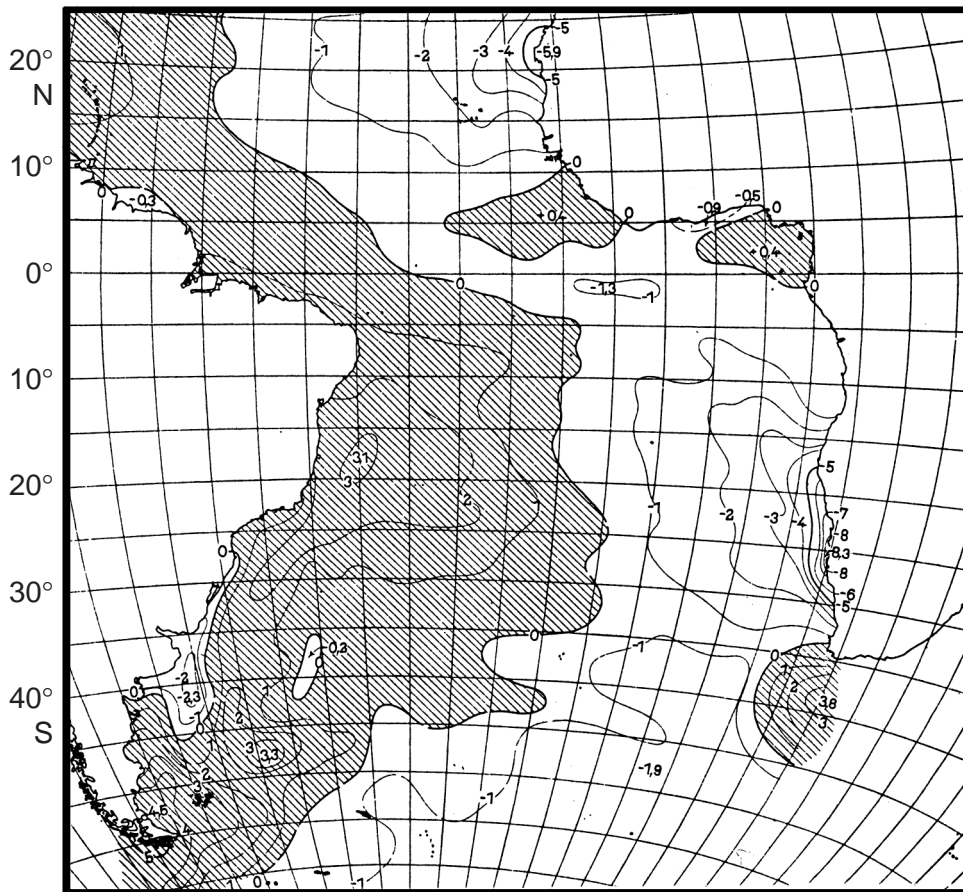


Figure F5. Annual mean of surface temperature anomalies in degrees Celsius relative to zonal averages for 2° latitude in the South Atlantic. From Neumann and Pierson (1966), after Böhnecke (1936). Shaded area = warmer than average for this latitude.



**Figure F6.** Deepwater circulation in the Atlantic Ocean, as seen in the distribution of salinity. Leg 175 sites are between 5° and 32°S along the eastern margin. Surface salinities are marked across the top axis. From Tchernia (1980).

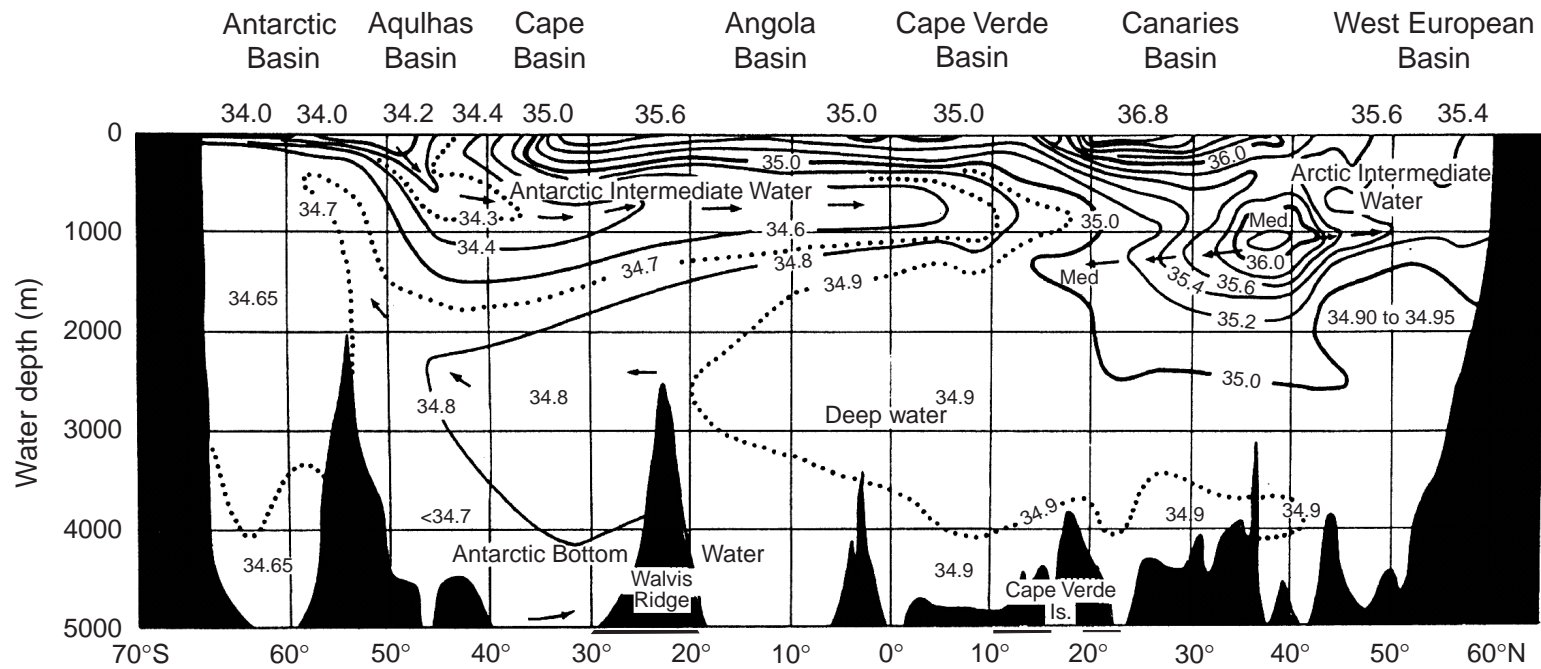


Figure F7. Summary of major facies patterns recovered during Leg 175. From Pufahl et al. (1998).

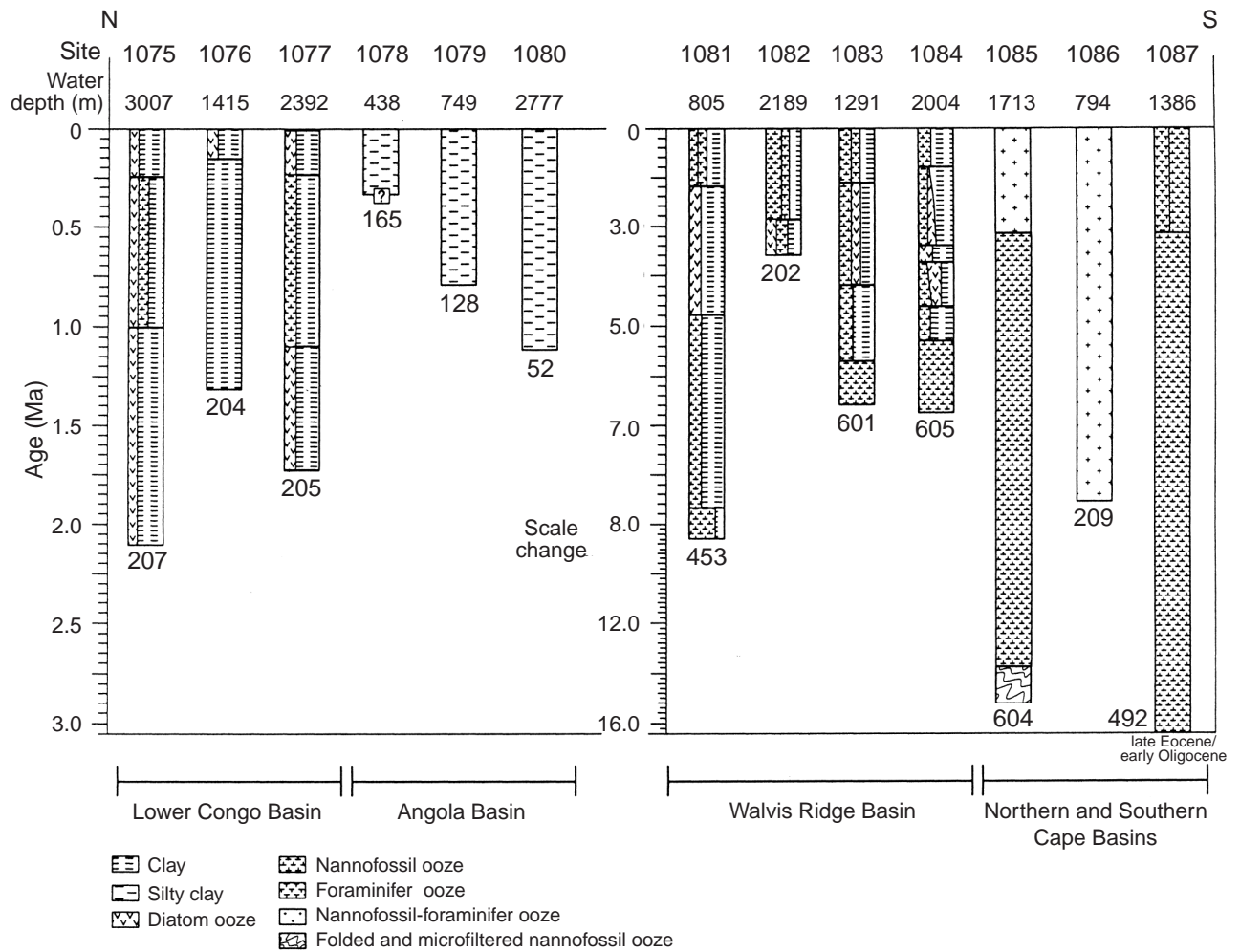


Figure F8. Graphic age models for Sites (A) 1075, (B) 1076, and (C) 1077 (Congo Fan). Line connecting control points = best guess for age-depth model, "Nanno" = biostratigraphy (Giraudeau et al., 1998), "Pmag" = magnetic reversals (Shipboard Scientific Party, 1998b, 1998c, 1998d), "Cycles" = based on sequencing color cycles and magnetic susceptibility (Berger et al., 1998b), heavy line = estimated sedimentation rate (secondary y-axis).

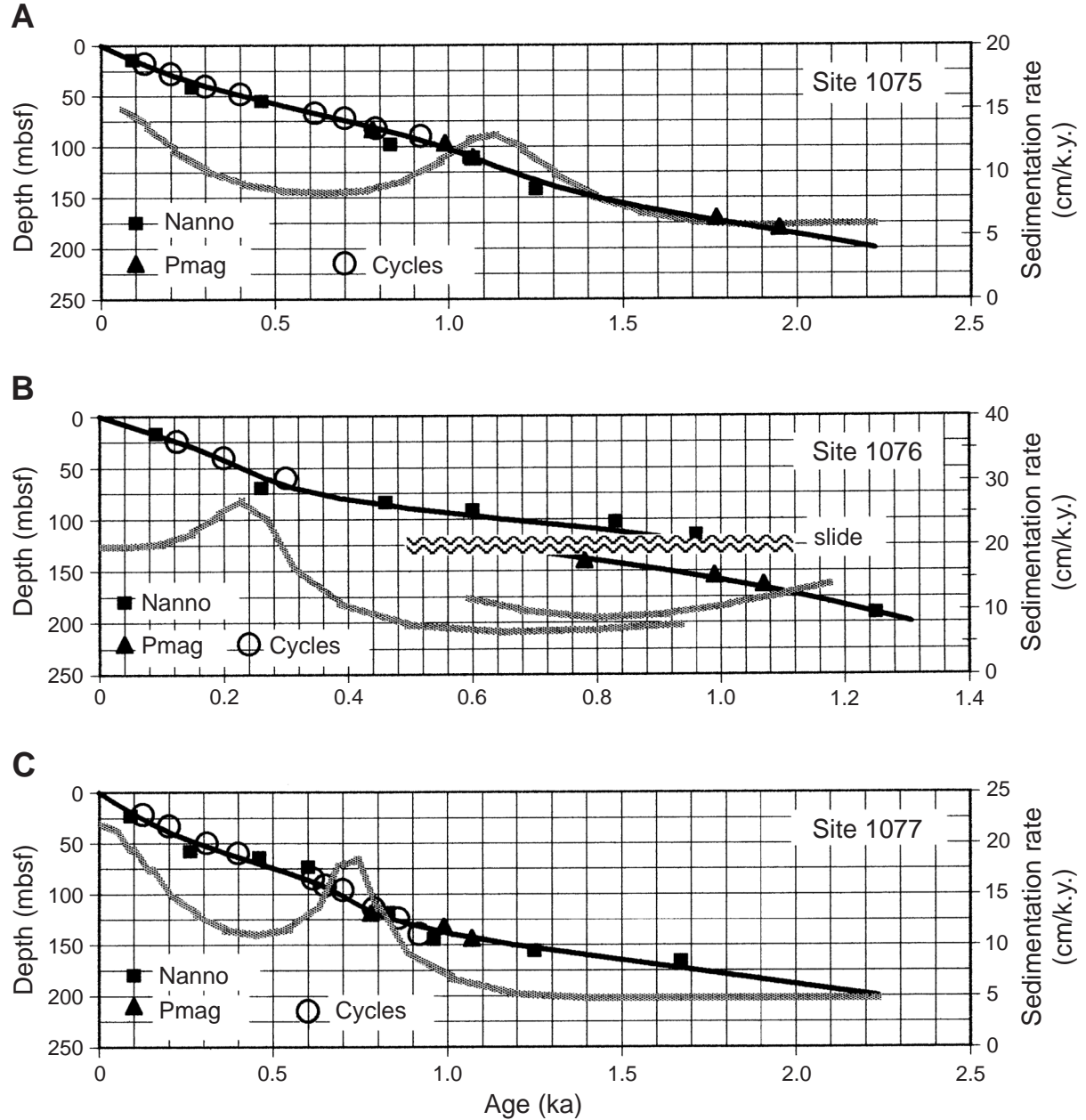


Figure F9. Graphic age models for Sites (A) 1078 and (B) 1079 (Angola). Line connecting control points = best guess for age-depth model. "Nanno" = biostratigraphy (Giraudeau et al., 1998; Shipboard Scientific Party, 1998e, 1998f). Heavy line = estimated sedimentation rate (secondary y-axis), "Ox. iso." = data in Pérez et al., Chap. 19 (this volume).

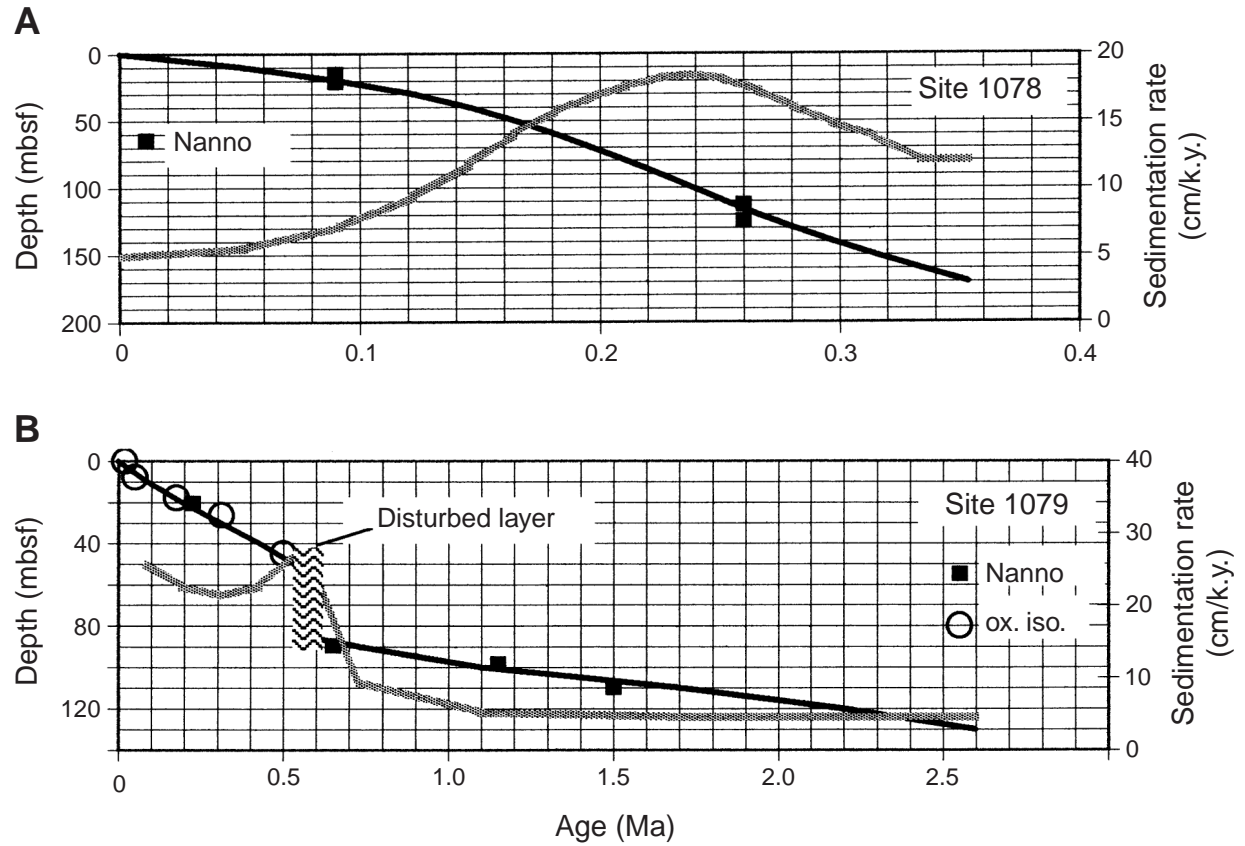


Figure F10. Graphic age models for Sites (A, C) 1081 (Walvis Ridge) and (B, D) 1082 (Walvis Basin). Line connecting control points = best guess for age-depth model. "Nanno" = biostratigraphy (Giraudeau et al., 1998), "Pmag" = magnetic reversals (Shipboard Scientific Party, 1998g, 1998h), "Cycles" = based on inspection of variations in magnetic susceptibility, heavy line = estimated sedimentation rate (secondary y-axis). Upper and lower panels of each pair (A, C and B, D) differ in scale plotted (not in data points).

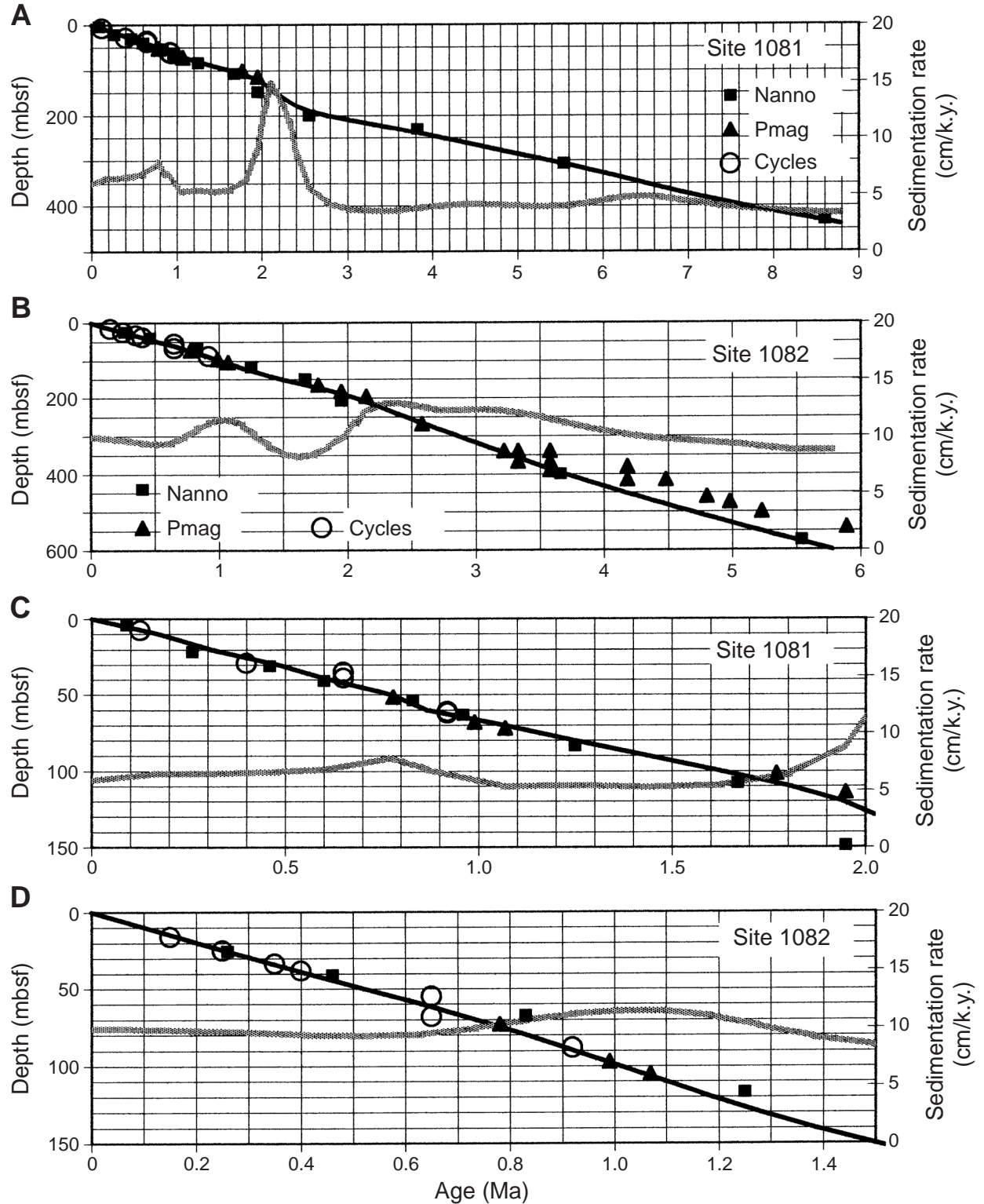


Figure F11. Graphic age models for Sites (A) 1083 (Walvis Bay) and (B, C) 1084 (Lüderitz Bay). Line connecting control points = best guess for age-depth model. "Nanno" = biostratigraphy (Giraudeau et al., 1998), "Pmag" = magnetic reversals (Shipboard Scientific Party, 1998i, 1998j). Heavy line = estimated sedimentation rate (secondary y-axis). Site 1084 panels (B, C) differ in scale plotted (not in data points).

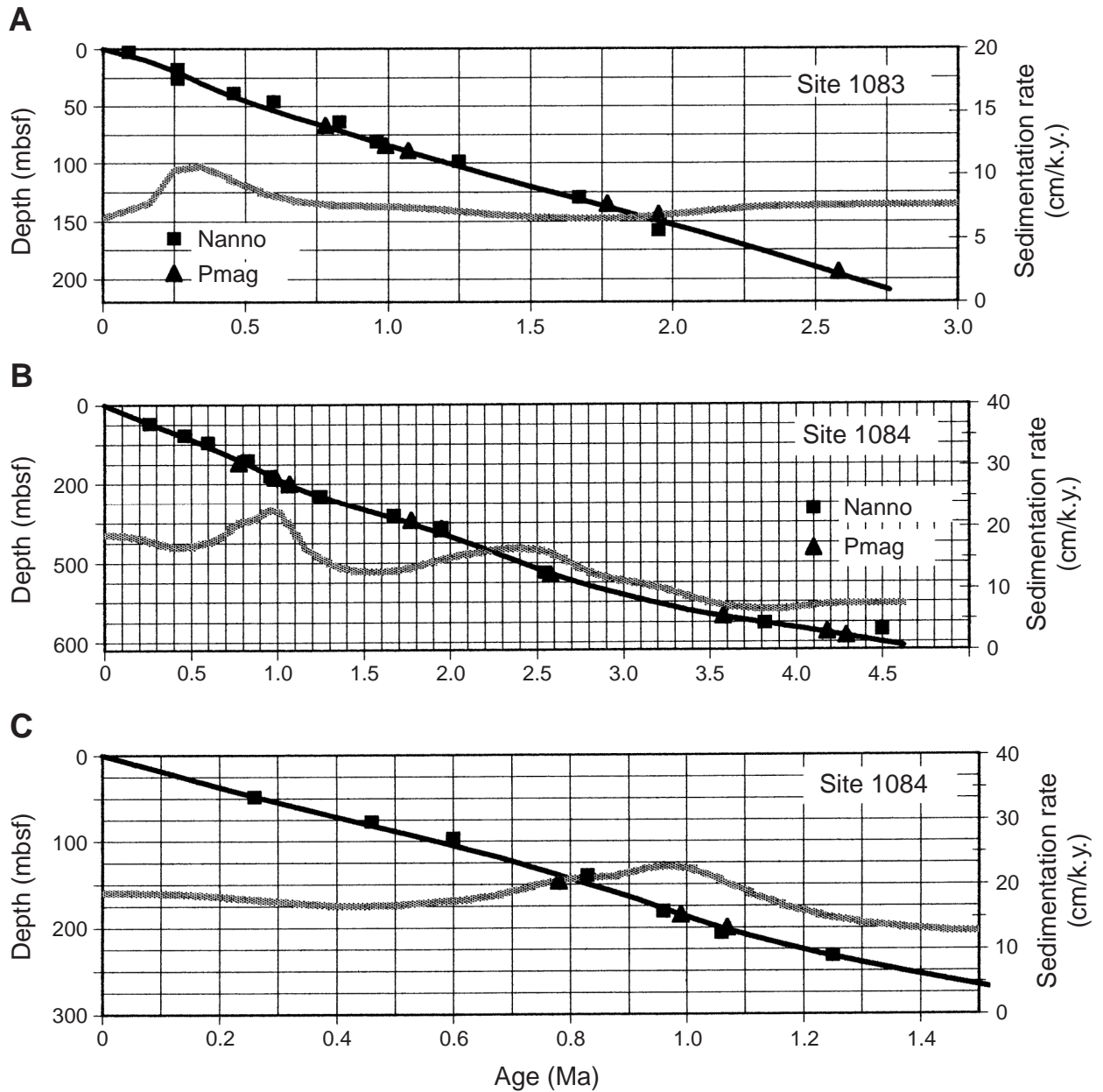


Figure F12. Graphic age models for Sites (A, B) 1085 and (C) 1086. (Continued on next page.)

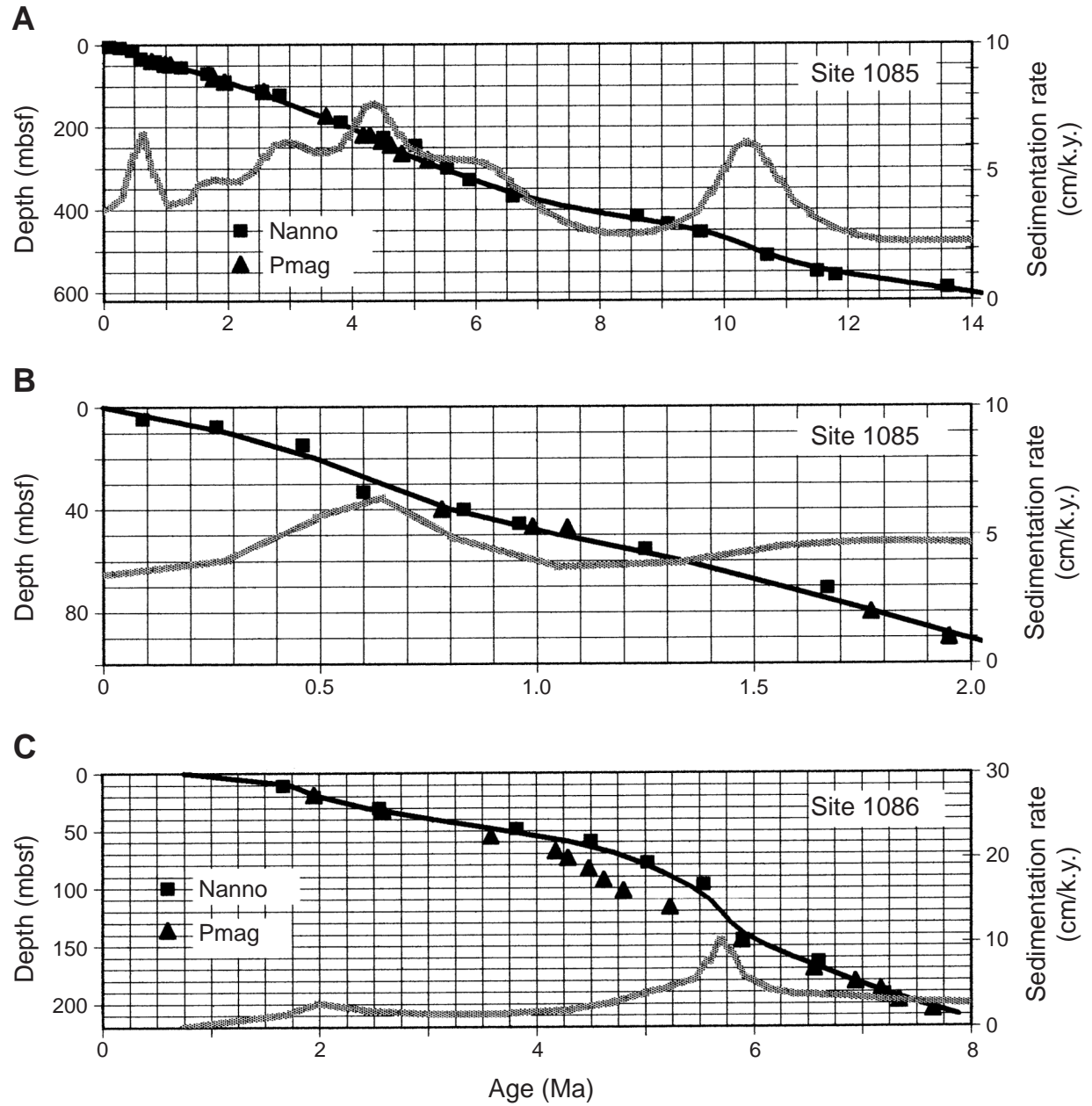


Figure F12 (continued). (D, E) 1087 (Cape Basin). Line connecting control points = best guess for age-depth model. "Nanno" = biostratigraphy (Giraudeau et al., 1998), "Pmag" = magnetic reversals (Shipboard Scientific Party, 1998i, 1998j), heavy line = estimated sedimentation rate (secondary y-axis). Upper and lower panels of each pair (A, B and D, E) differ in scale plotted (not in data points).

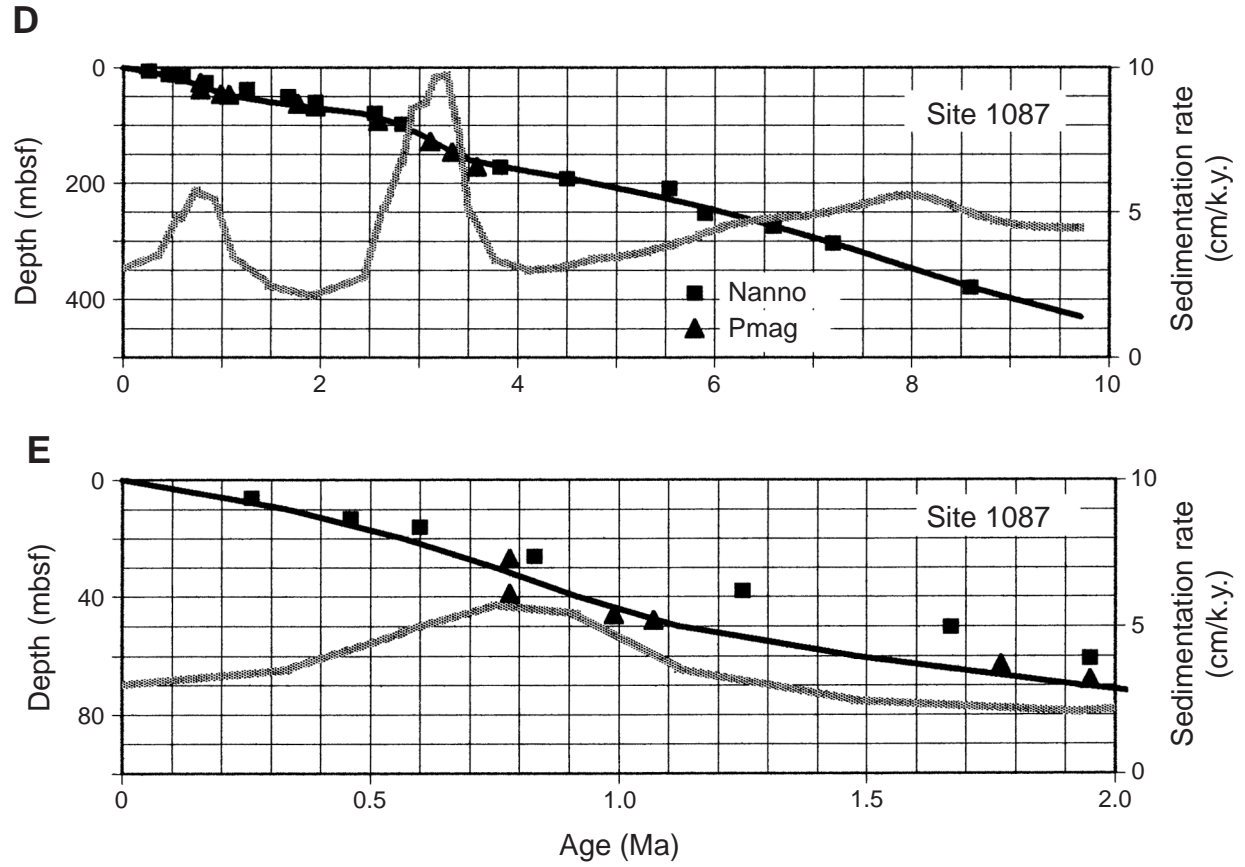
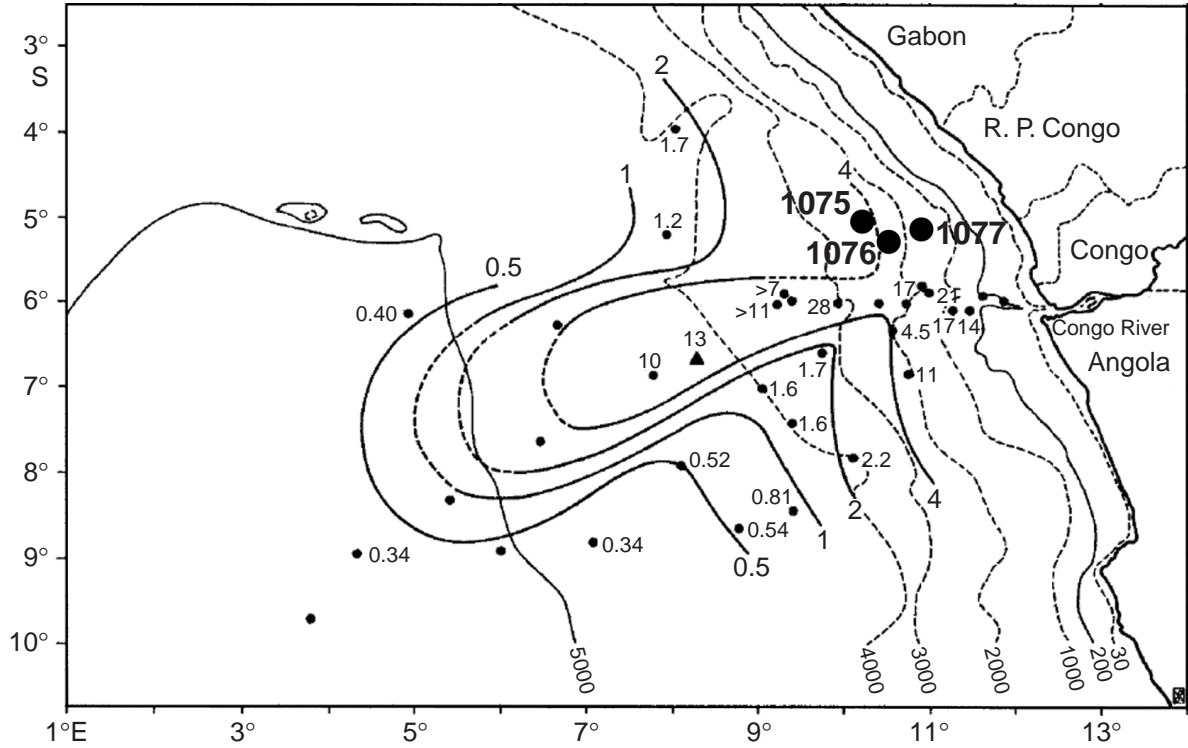
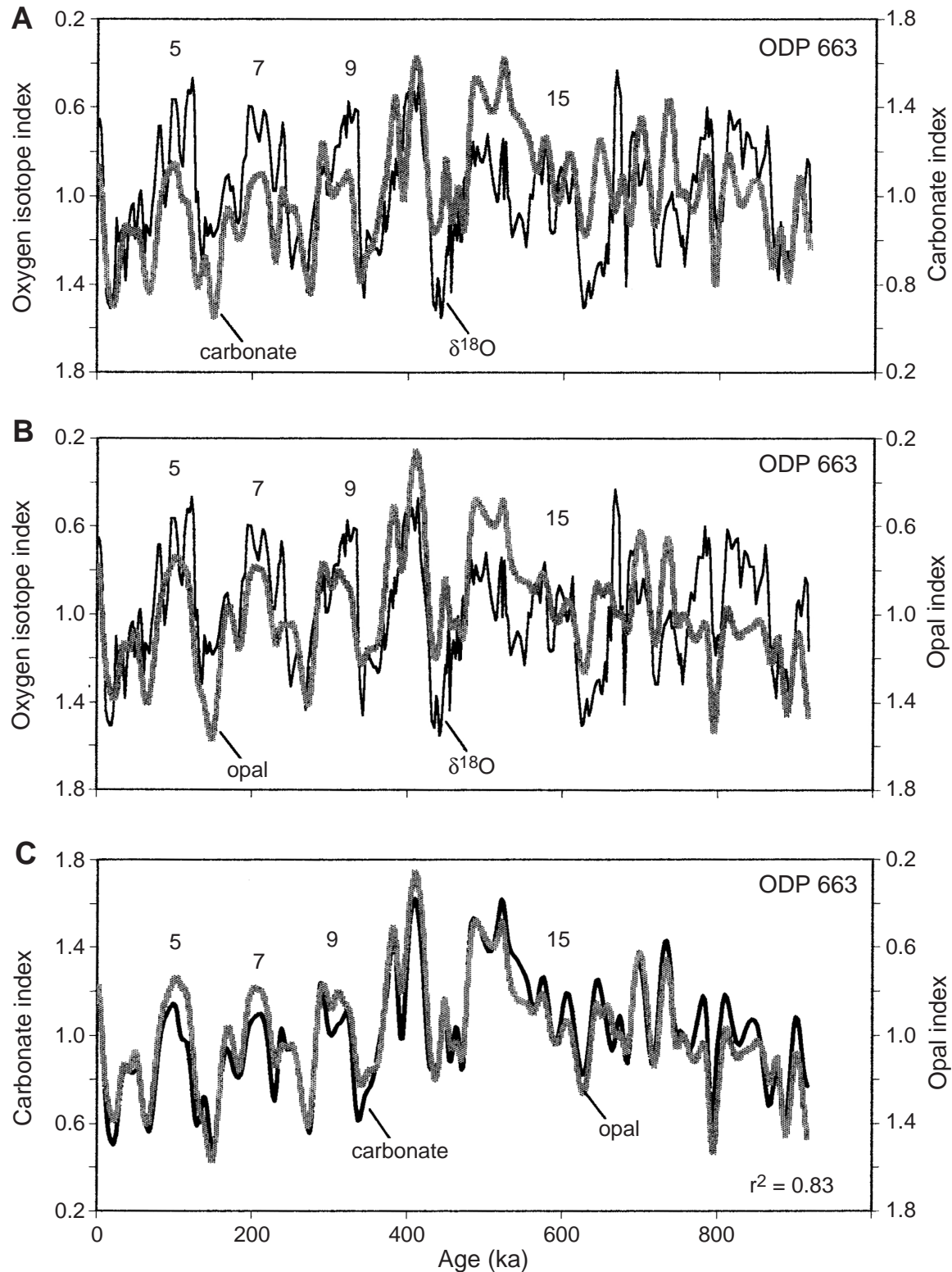


Figure F13. Position of Congo group sites relative to the present-day sedimentation rates (in centimeters per thousand years) on the Congo Fan. Base map is from Jansen et al. (1984).



**Figure F14.** The record of carbonate and opal at Site 663 from the eastern equatorial Atlantic for comparison with similarly cyclic fluctuations off the Congo. Site 663 data are from deMenocal et al. (1993). A. Oxygen isotope index, standardized permil data, and carbonate index, negative log of noncarbonate, standardized. B. Opal index, log percent of opal, standardized. C. High values of opal coincide with low values of carbonate (see **"Background: Deepwater Record,"** p. 16).



**Figure F15.** Record of (A) carbonate, (B) marine organic carbon, and (C) opal in core GeoB1008, Congo Fan. Data are from Schneider et al. (1997). Note the transform of the opal data (to get a fit to marine carbon). Black boxes = position along the oxygen isotope curve of unusually high carbonate values, arrows = position of maximal obliquity of Earth's axis, unmarked line in middle panel = oxygen isotopes of *G. ruber* (standardized), Ox. iso. = standard curve of Imbrie et al. (1984).

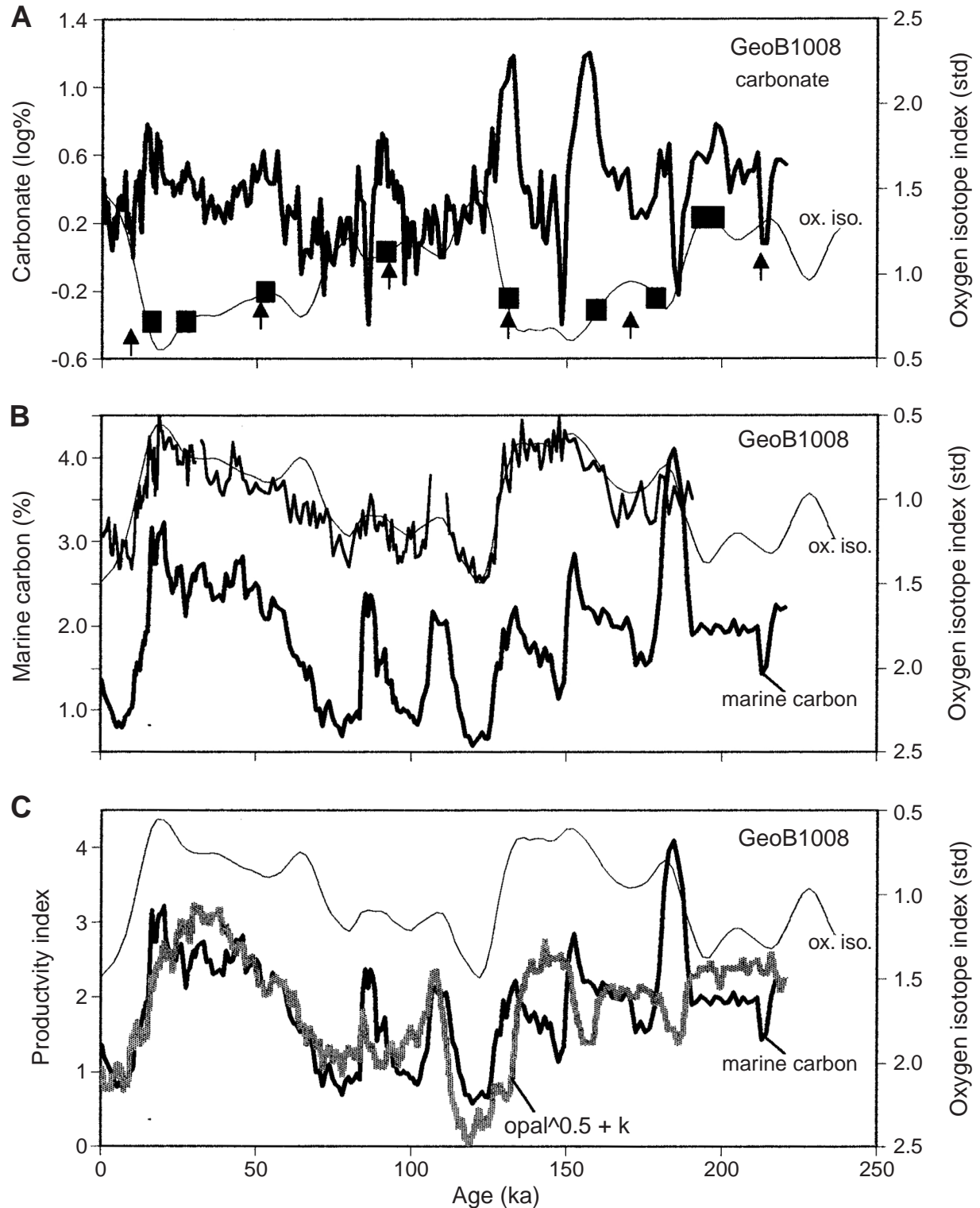


Figure F16. Patterns of carbonate sedimentation at the Congo group sites, based on shipboard results (data from Wefer, Berger, Richter, et al., 1998). A. Carbonate plotted as log of carbonate/noncarbonate ratio (standardized to mean = unity; std. = 0.25). B. Visual nannofossil abundance index, standardized. 8 = isotope stage (glacial).

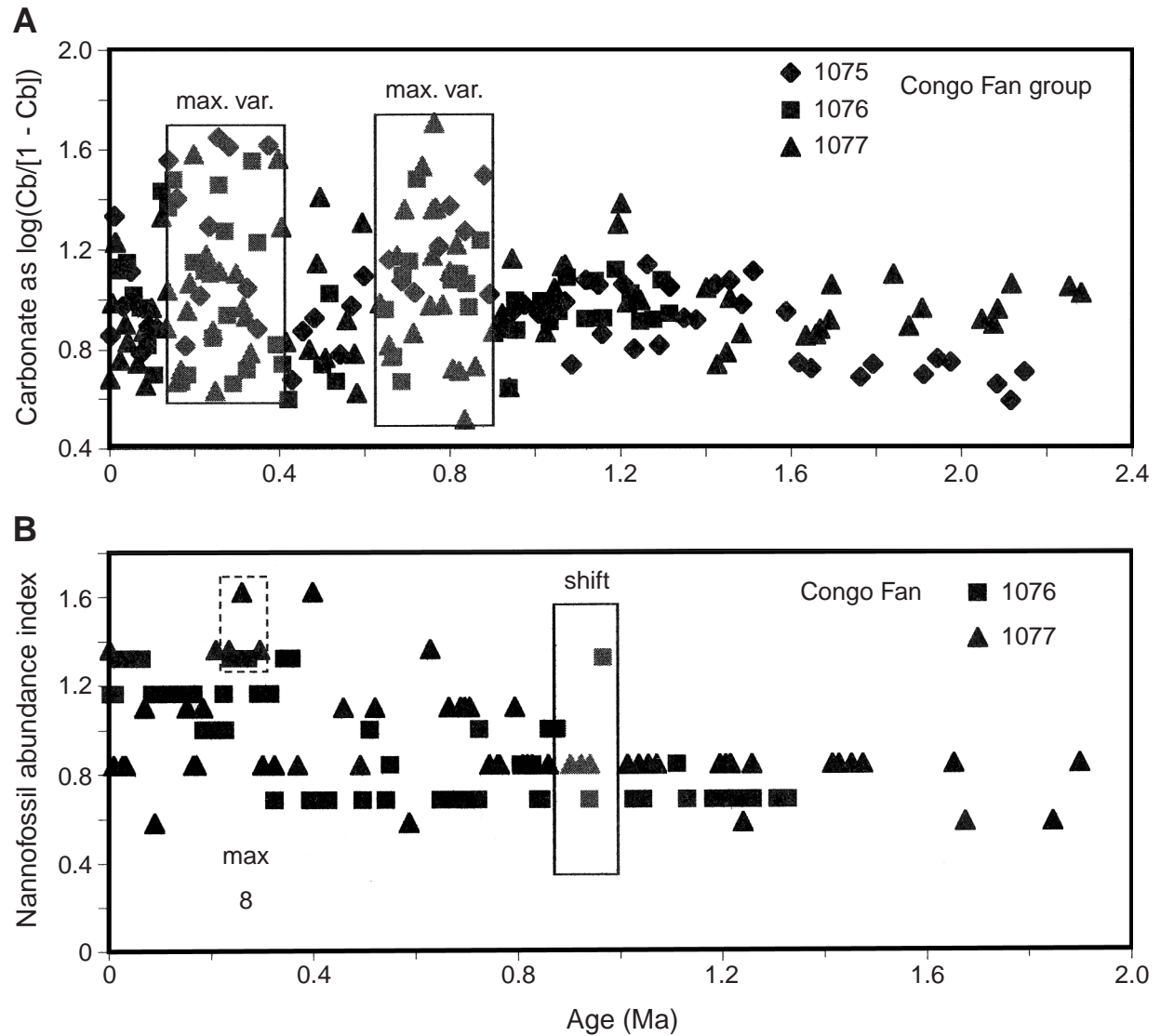
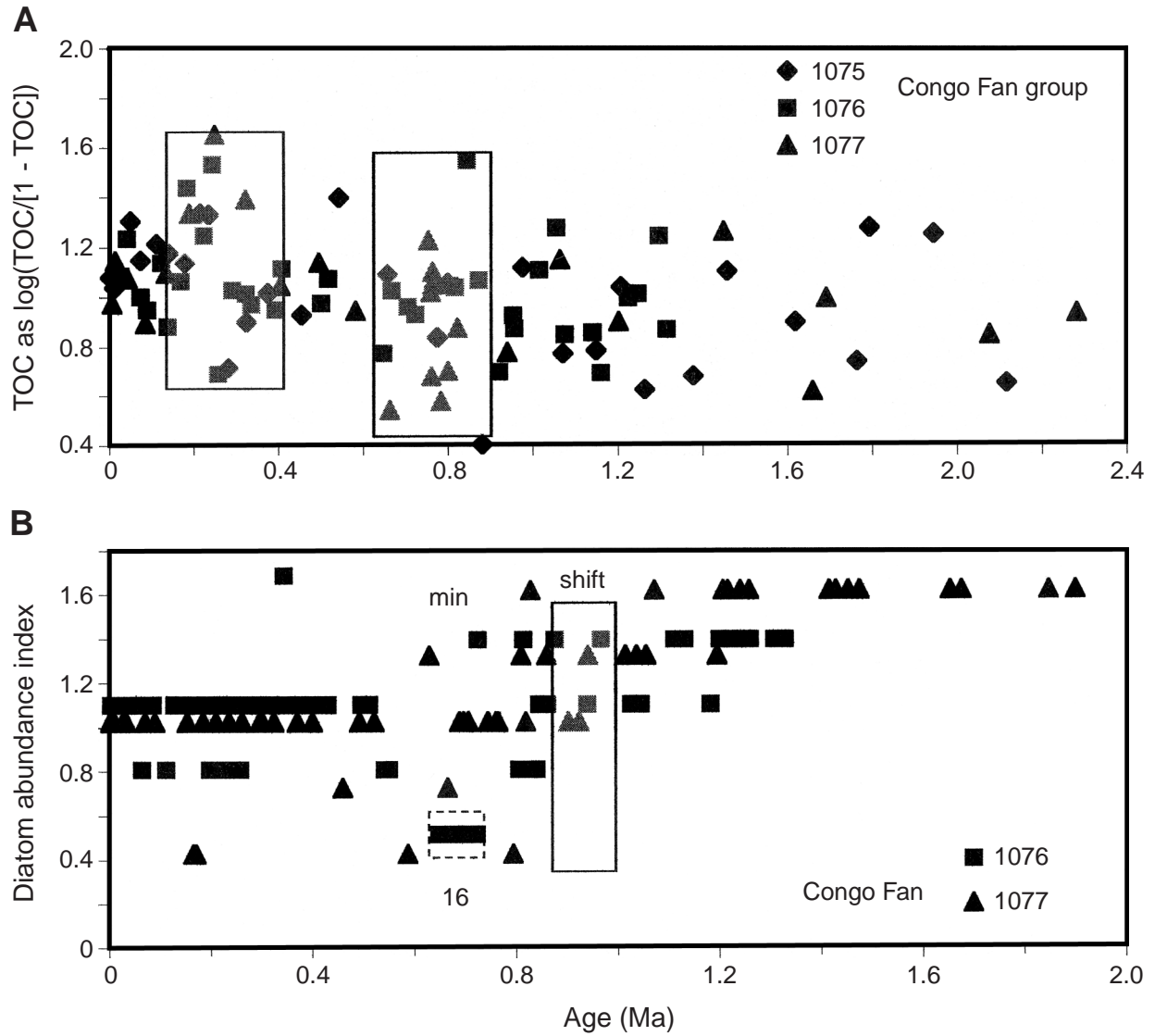


Figure F17. Patterns of organic carbon and of diatom abundance at the Congo group sites, based on ship-board results (data from Wefer, Berger, Richter, et al., 1998). A. TOC is plotted as the log of  $TOC/(1-TOC)$ , standardized. B. Visual diatom abundance index, standardized. 16 = isotope stage (glacial).



**Figure F18.** Productivity fluctuations in core GeoB1016 off Mid-Angola, as seen in organic matter and opal content. **A.** Comparison with core GeoB1008 off the Congo (C[1008]). The unlabeled curve is the oxygen isotope curve of Imbrie et al. (1984). **B.** Comparison of carbon and opal record in core GeoB1016. Arrows in the lower panel mark the position of evidence for anticorrelation of total organic carbon (TOC) and opal on the precessional timescale. (Continued on next page.)

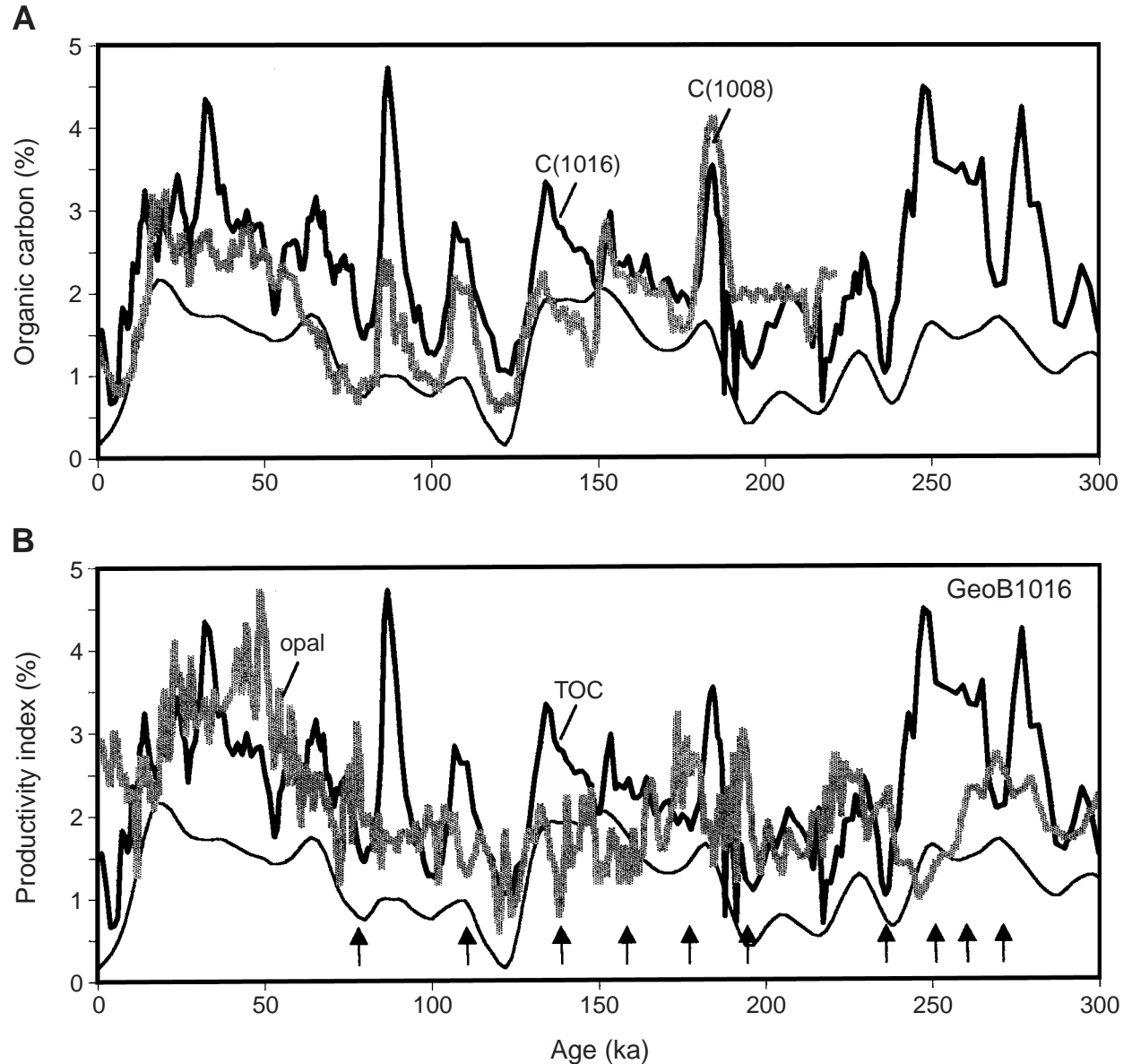


Figure F18 (continued). C. Modeling the organic carbon abundance, using a global  $\delta^{18}\text{O}$  curve (OJsox96) (Berger et al., 1996) and the insolation at  $15^\circ\text{N}$  in July (Berger and Loutre, 1991) (weights adjusted for best fit). D. Demonstration that the model for organic carbon deposition does not work for opal. Data for TOC, opal, and timescale are from Schneider et al. (1997).

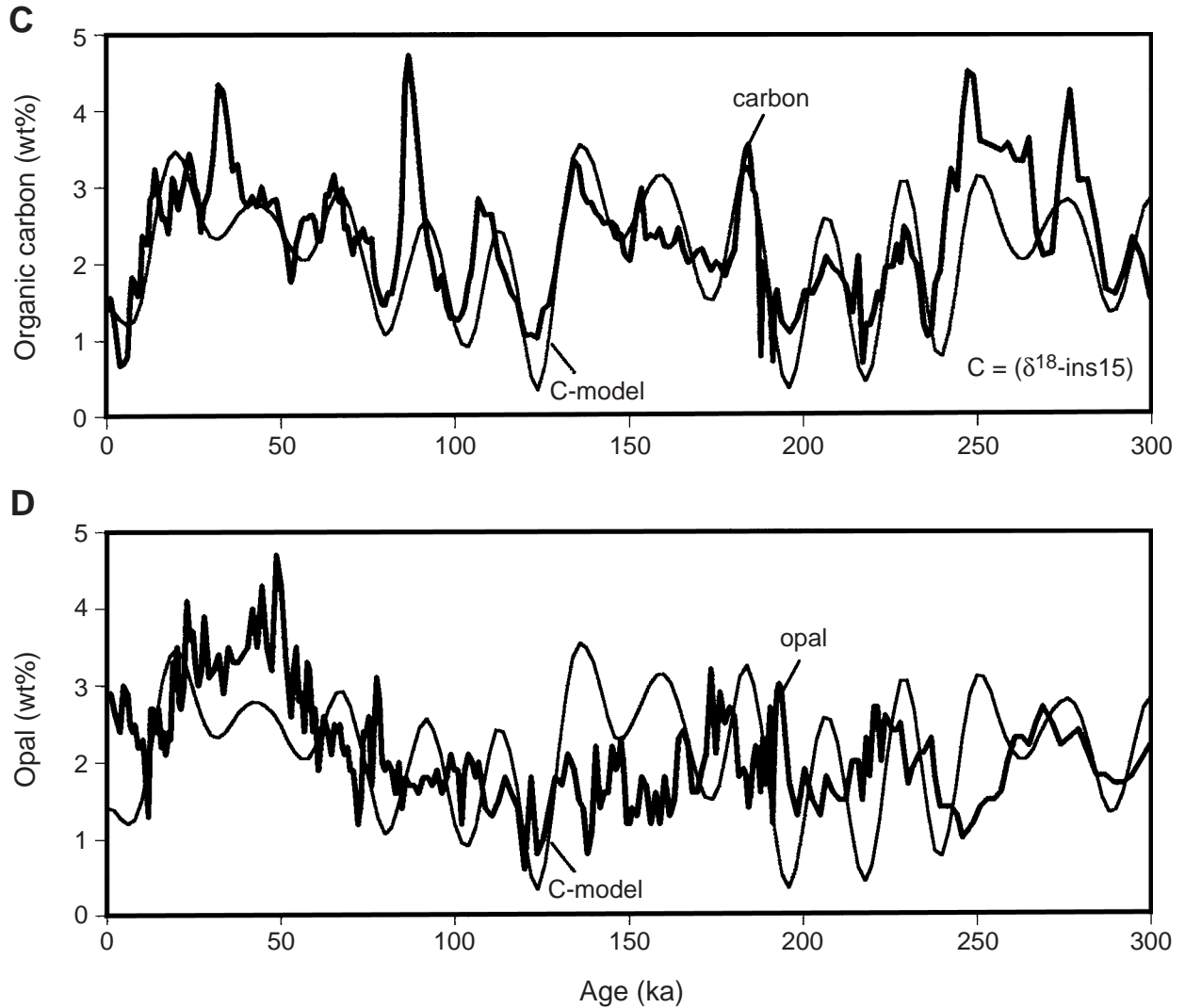


Figure F19. (A) Carbonate and (B) organic carbon at Sites 1078 and 1079. (Abundances as log of ratios, standardized.) Data source: Shipboard data, Wefer, Berger, Richter, et al. (1998).

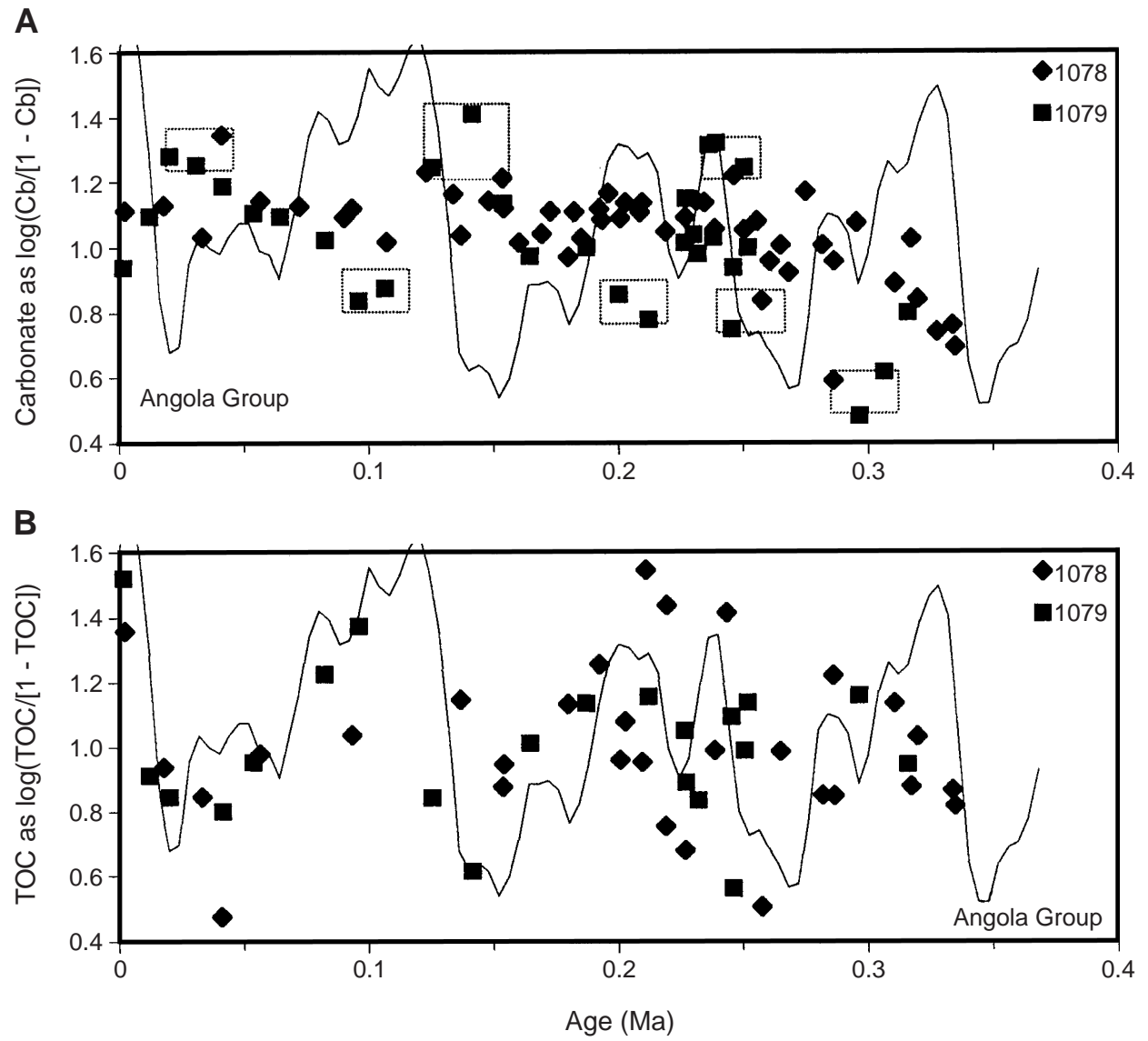
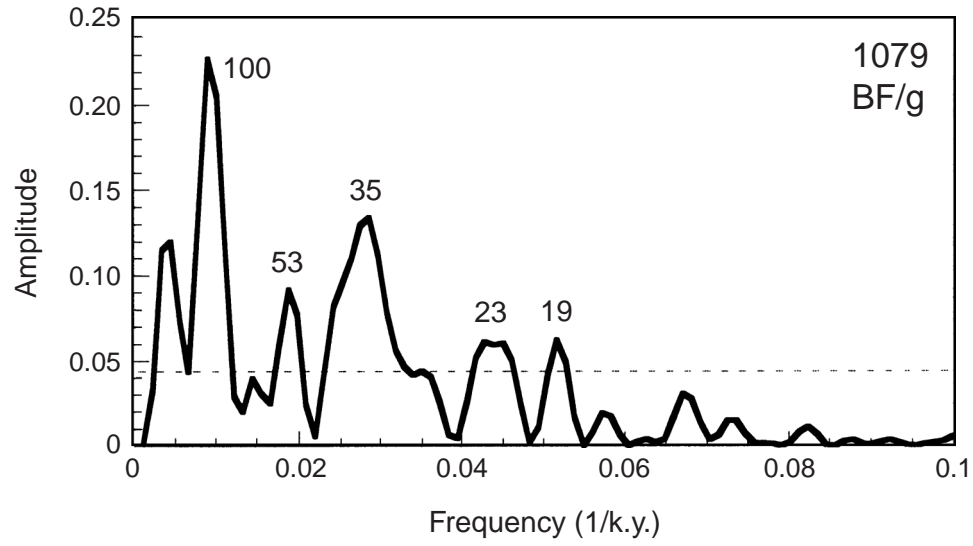
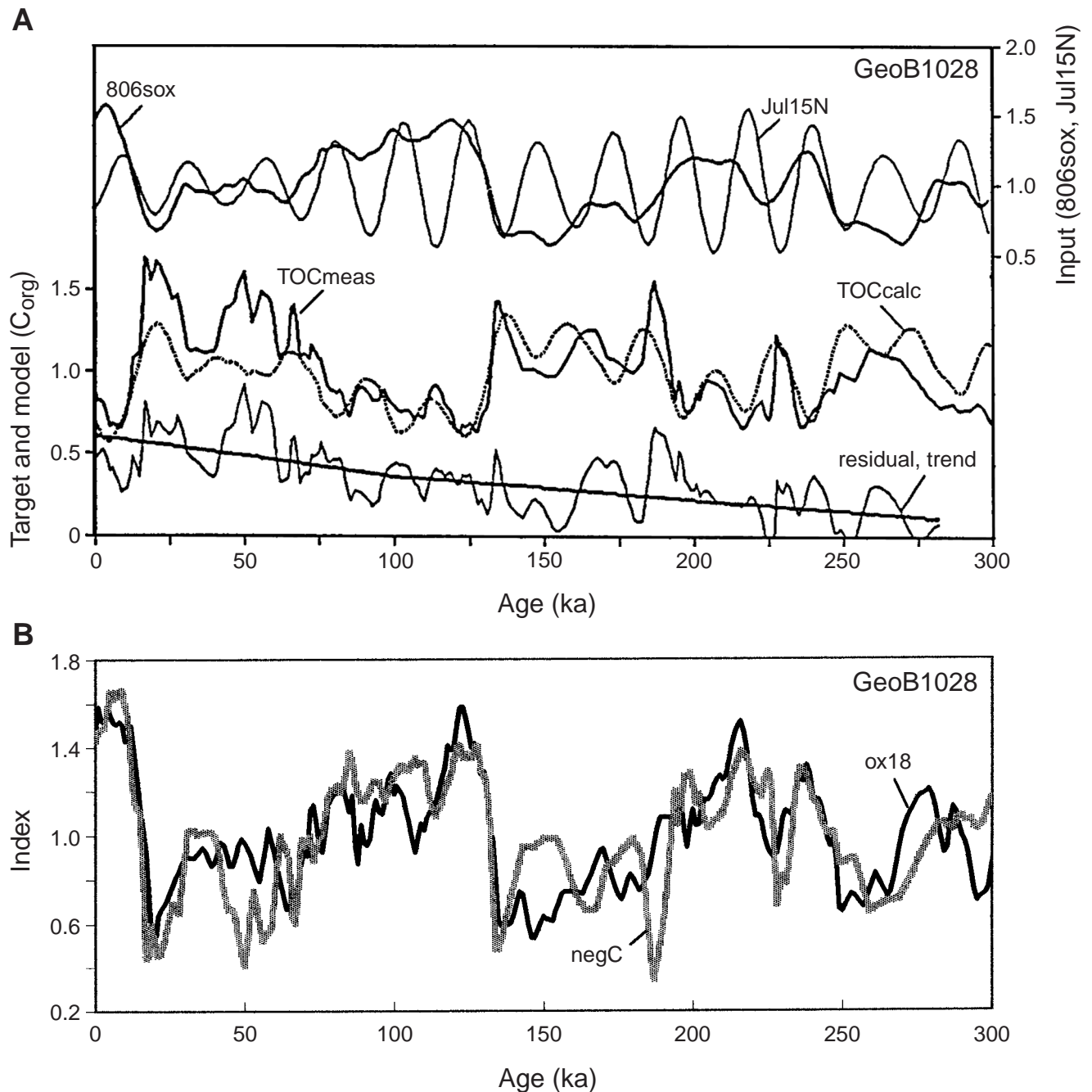


Figure F20. Spectrum of productivity cycles at Site 1079 in the latest Quaternary. Proxy is BF/g. From Pérez et al., [Chap. 19](#) (this volume).



**Figure F21.** Match of total organic matter ( $C_{org}$ ) with glacial–interglacial climate fluctuations. **A.** Statistical modeling of TOC content in core GeoB1028 taken on Walvis Ridge. Input is global sea level, as reflected in a global oxygen-isotope signal (806sox) and July insolation at 15°N (Jul15N). From Berger, Wefer, Richter, et al. (1998). **B.** Direct match of TOC and oxygen isotope index within core GeoB1028, based on *Globigerinoides ruber*. TOC is plotted upside down (negC). (Both series standardized to mean = unity and std. = 0.25.) Data are from Geowissenschaften Bremen (analysts: R. Schneider and H. Schmidt).



**Figure F22.** (A) Benthic foraminifer abundance (BF/g) and (B) organic matter content (TOC) (standardized and plotted upside down as negBF and negC) in core GeoB1028, on Walvis Ridge. Ox18 = isotope stratigraphy of the core (*G. ruber*), standardized. Data are from Geowissenschaften Bremen (analysts: R. Schneider and H. Schmidt).

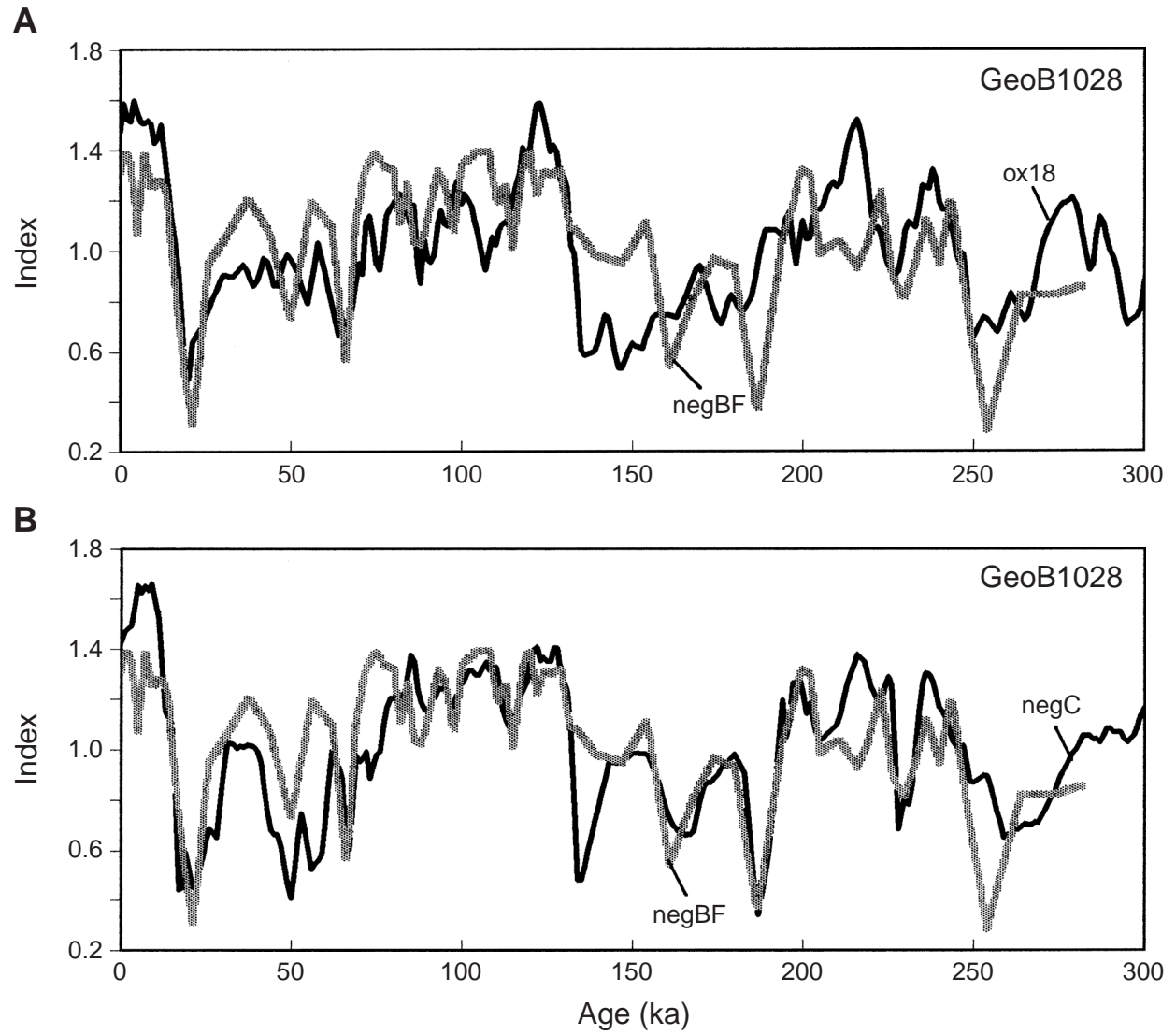


**Figure F23.** Glacial–interglacial cycles in the late Pliocene, Site 532. **A.** Heavy line = deepwater oxygen isotopes (*Uvigerina*). Other lines are obliquity band– and precession band–filtered sequence (based on peak width in spectrum). **B.** Spectrum of oxygen isotope record, carbonate content, and opal at Site 532, late Pliocene. Data are from Sancetta et al. (1992). (Ages adjusted by matching to scale of Bickert et al., 1997).

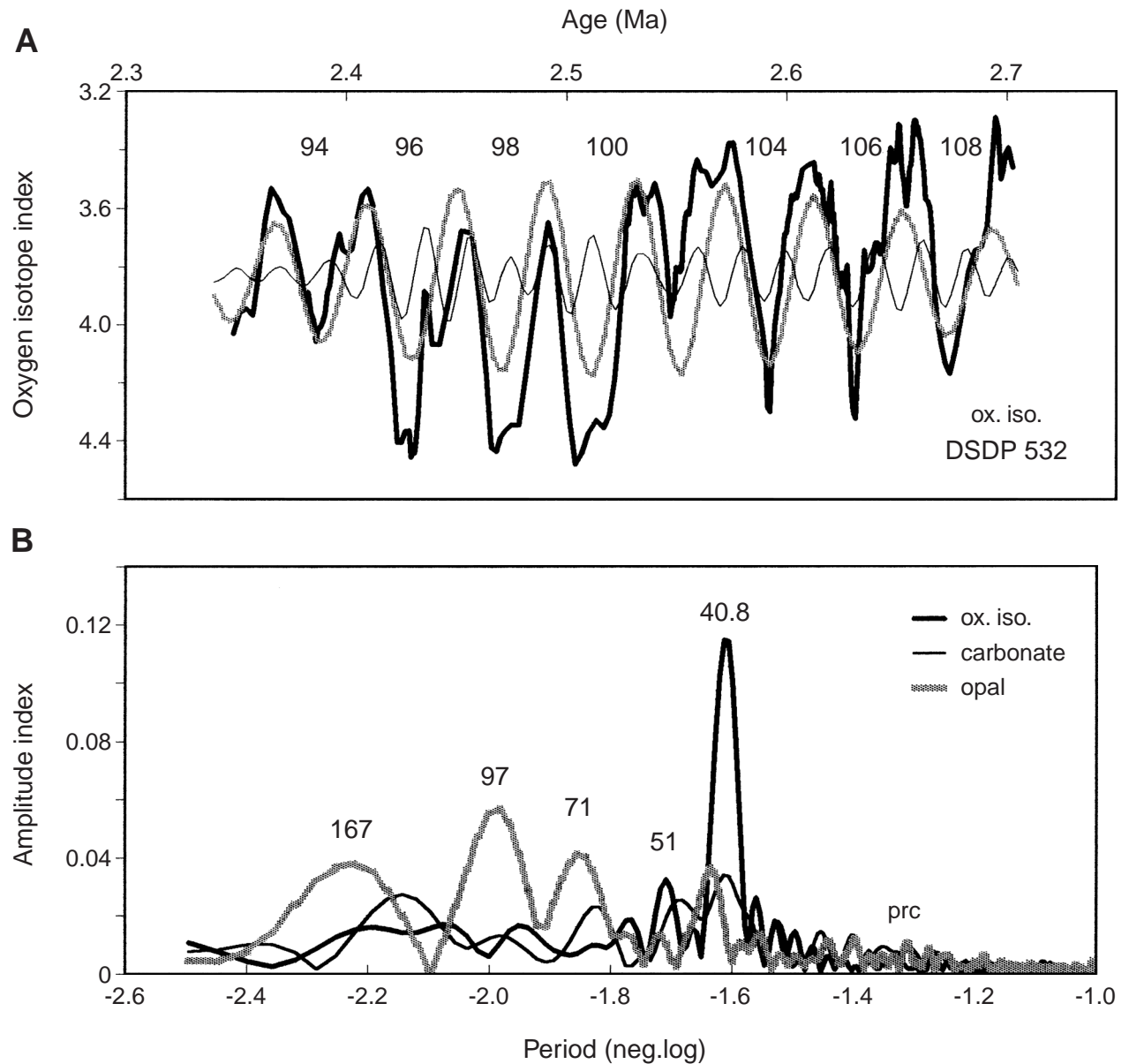
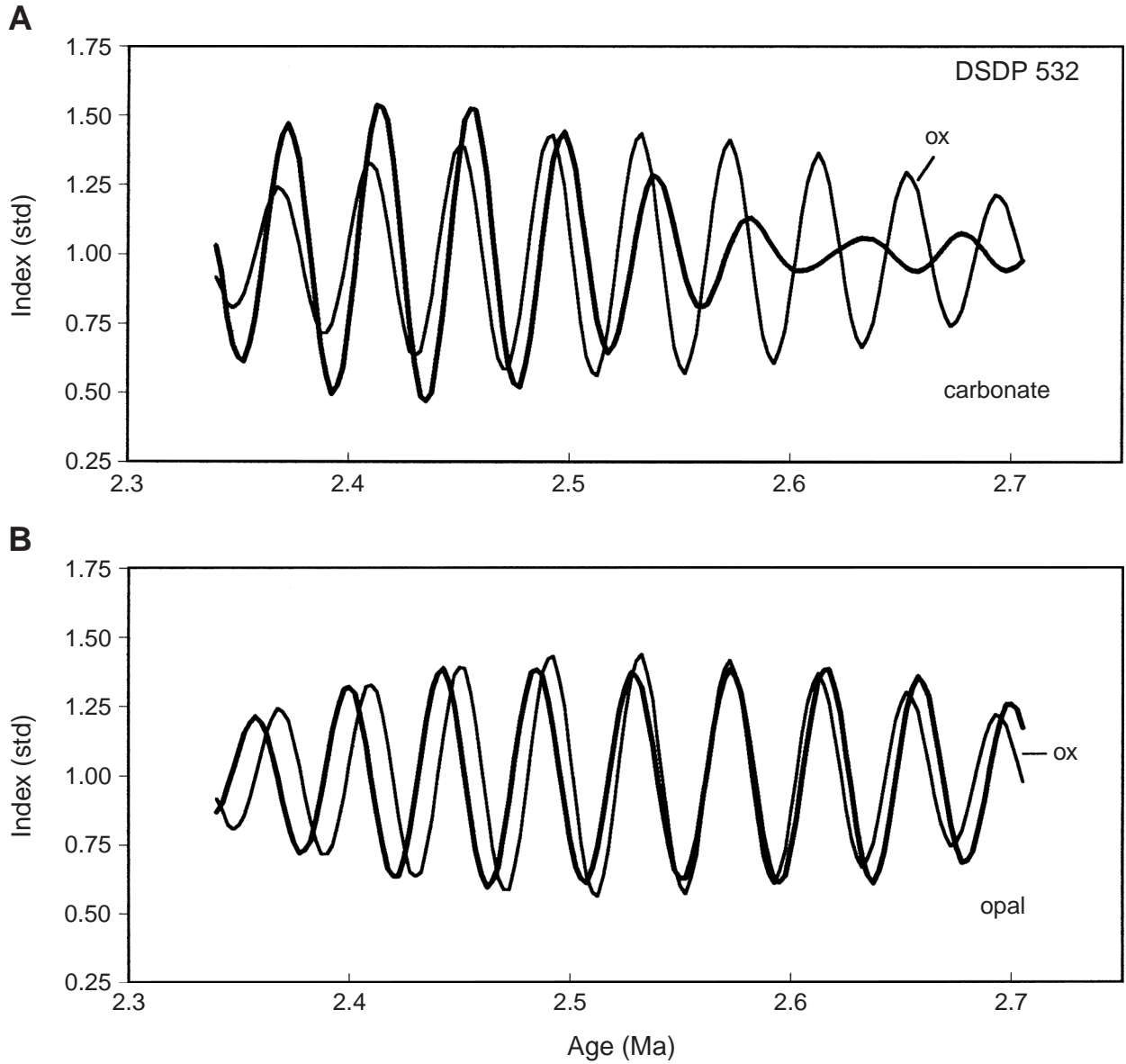


Figure F24. Record of oxygen isotopes (ox) and (A) carbonate and (B) opal content at Site 532, late Pliocene, filtered for obliquity band. Data are from Sancetta et al. (1992). (Ages are adjusted by matching to scale of Bickert et al., 1997).



**Figure F25.** Discovery of the Namibia Opal Paradox: maximum coastal upwelling (in the Quaternary) is not congruent with maximum overall diatom abundance at the sites off Namibia. *Proboscia barboi* indicates a cold-water influence, as does *P. curvirostris*. *Thalassiothrix*-rich sediments and mats are ascribed to varying supply from strong frontal systems with a coastal, Antarctic/subantarctic, and open ocean component. *Cycladophora plicenica* and *P. barboi* in this system suggest Southern Ocean influence. *Chaetoceros* spores are taken as indicating upwelling, and especially coastal upwelling. A. Sites 1081 and 1082. (Continued on next page.)

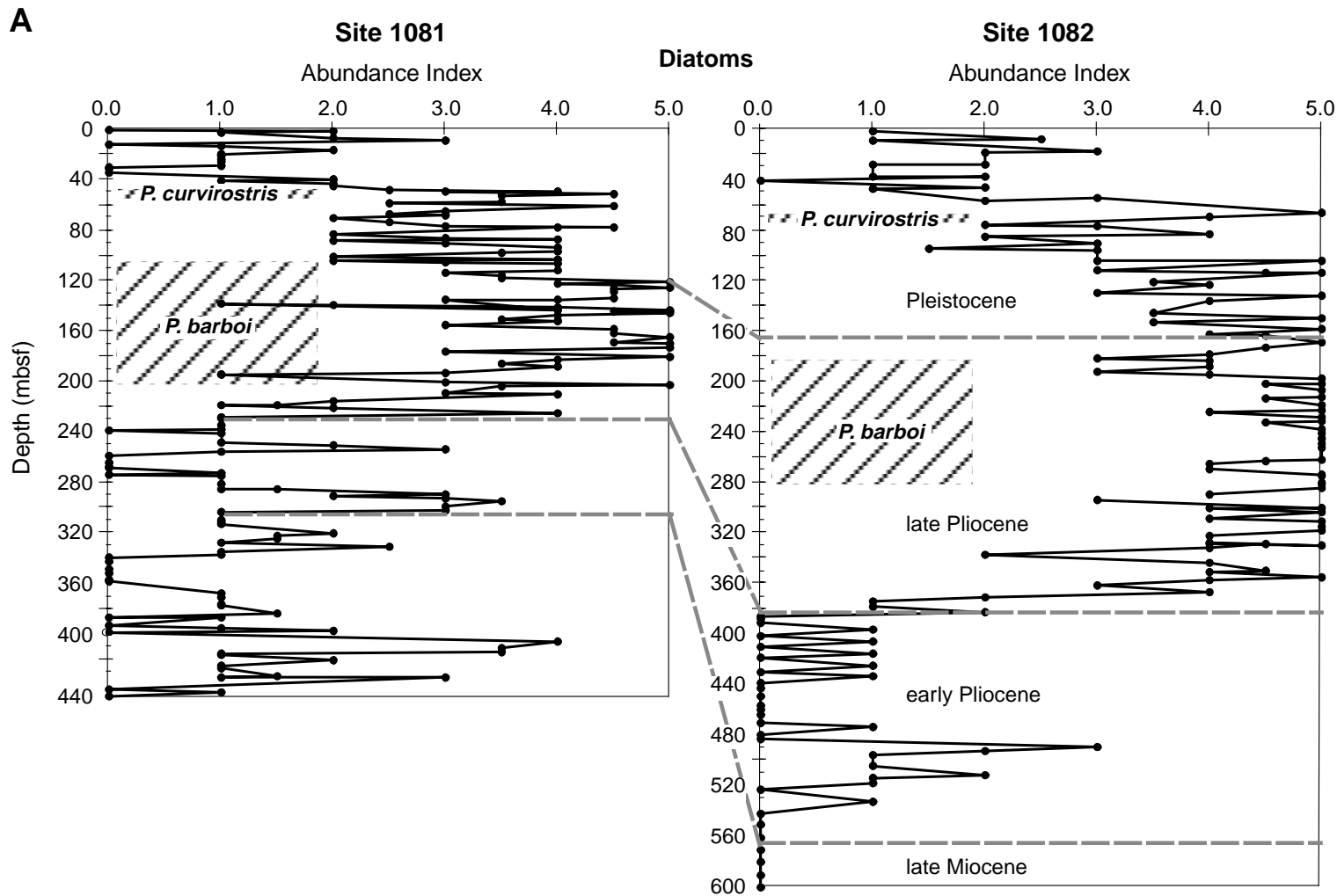
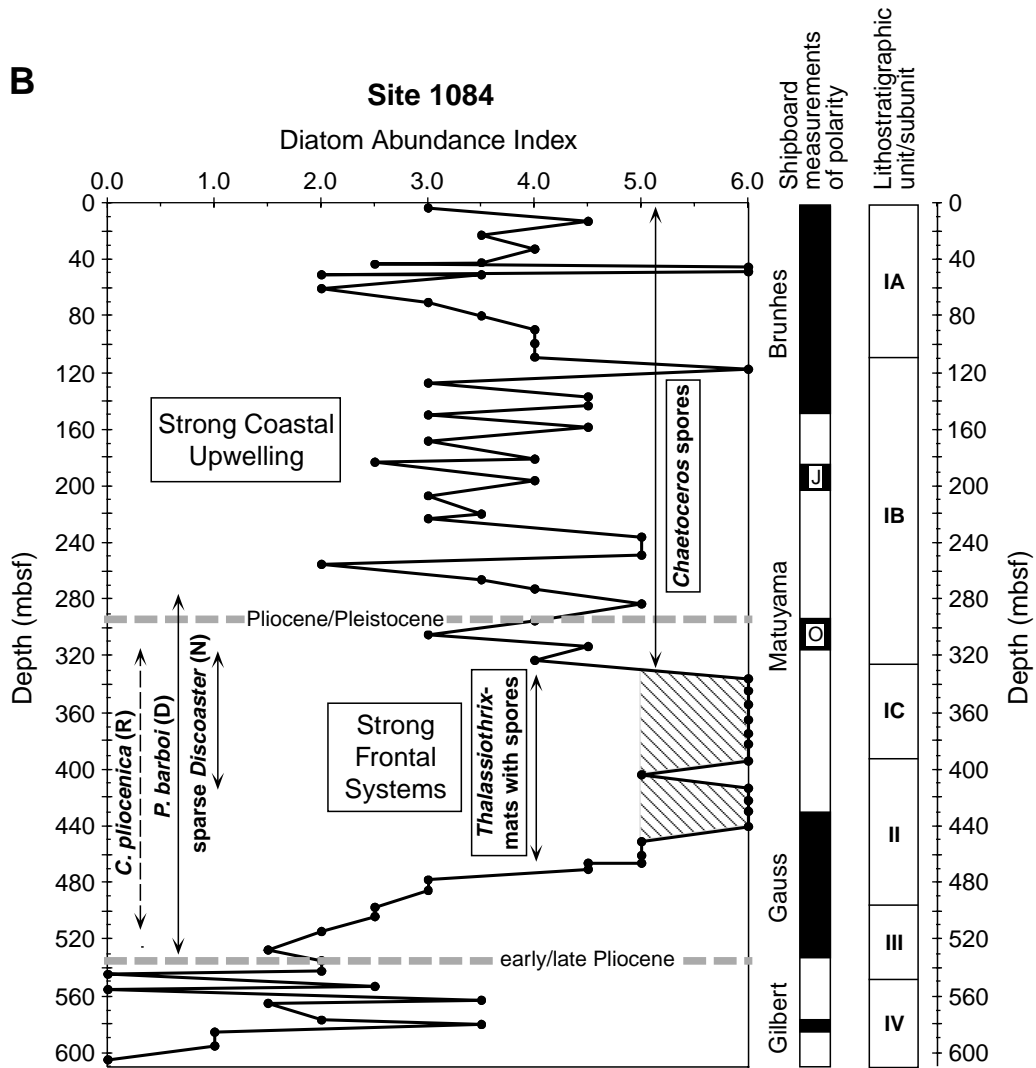
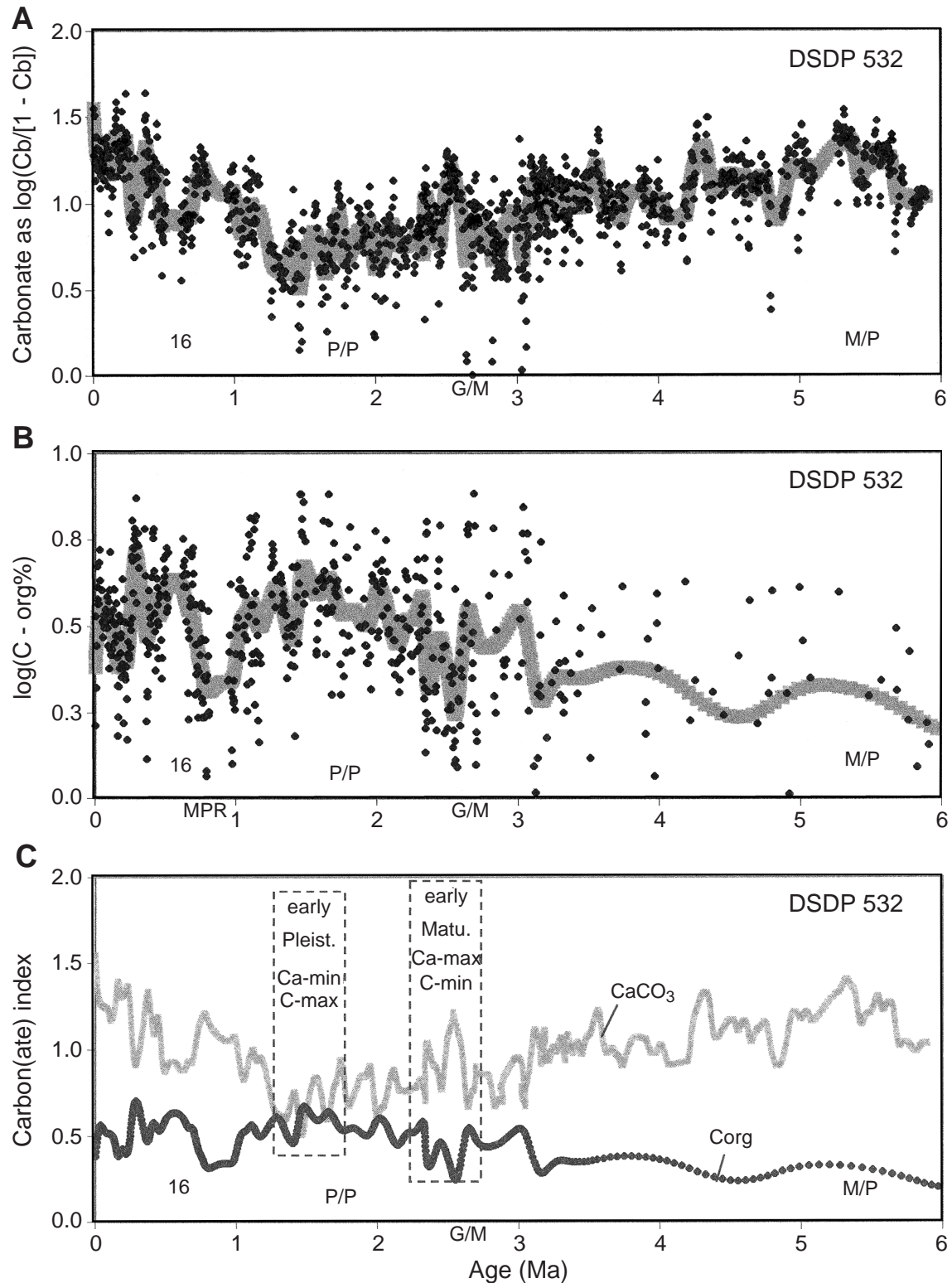


Figure F25 (continued). B. Site 1084. The graphs are from Shipboard Scientific Party, 1998h, 1998j). J = Jamarillo, O = Olduvai. R = radiolarian, D = diatom, N = nannofossil.



**Figure F26.** (A) Carbonate and (B) organic carbon stratigraphy and (C) carbonate index for Site 532. Carbonate values are taken as the ratio of carbonate to noncarbonate and are log transformed to avoid the artificial ceiling near 100%. 16 = Stage 16, P/P = Pliocene/Pleistocene boundary, G/M = Gauss/Matuyama reversal, M/P = Miocene/Pliocene boundary. Organic carbon values are transformed to log values to emphasize factors over increments. Data are from Gardner et al. (1984) (age model adjusted).



**Figure F27.** Characterization of climate regimes as seen in deep-ocean sediments. **A.** Oxygen isotope record of the benthic foraminifer *Cibicides wuellerstorfi* at ODP Sites 925 and 926 on Ceara Rise. Data are from Bickert et al. (1997; back to 2.6 Ma) and unpublished (courtesy of Torsten Bickert, Geowissenschaften Bremen). **B.** Relationship between oxygen and carbon isotopes recorded in benthic foraminifers at ODP Site 849. Window of comparison = 100 k.y.  $C(\text{std})/O(\text{std})$  is the ratio between the variability of carbon and oxygen isotopes (offset by 0.7 for clarity),  $r^2$  is the correlation coefficient,  $C(\text{std}) \times O(\text{std})$  is the product (amplified for clarity). Data are from Mix et al. (1995).

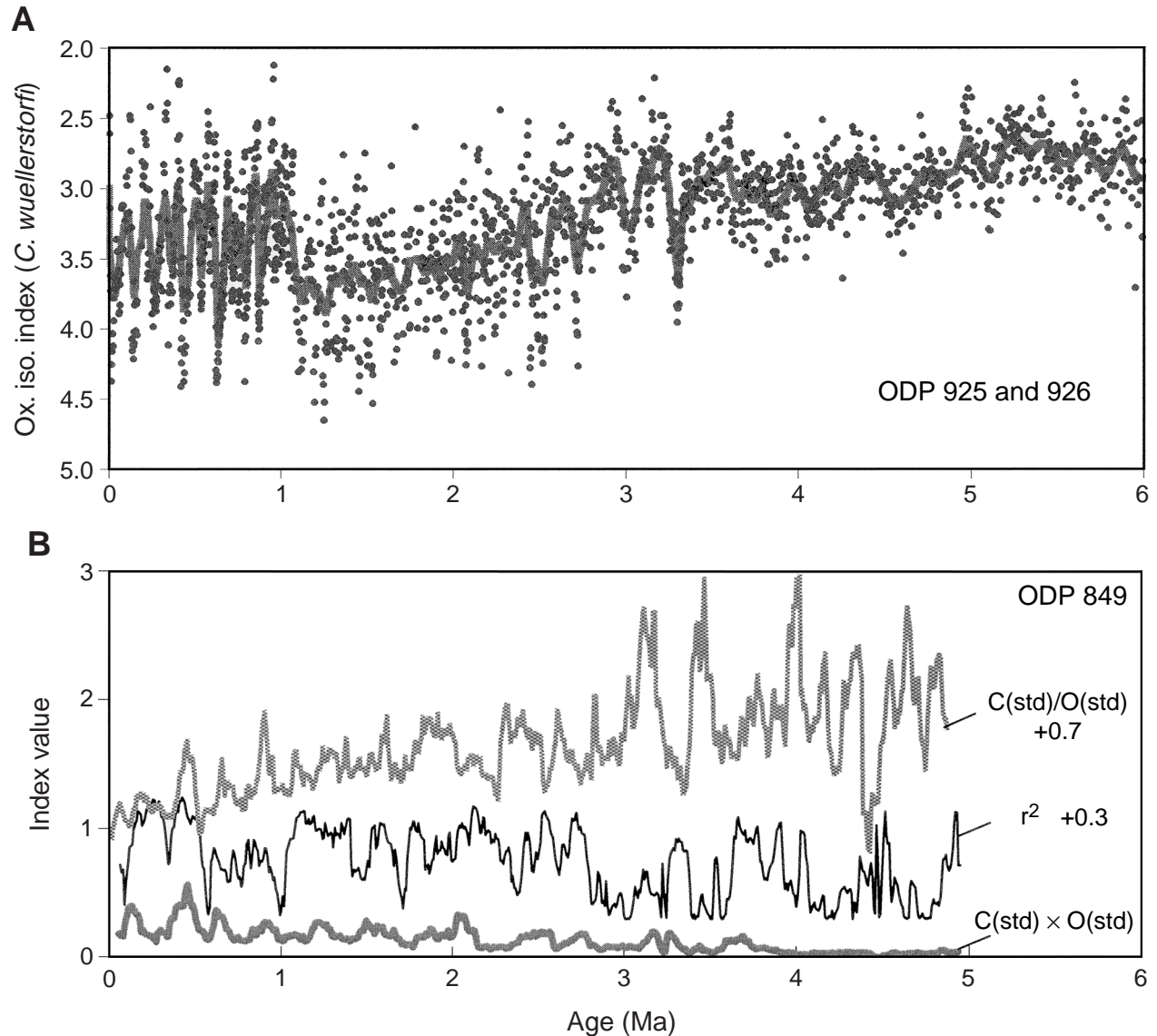
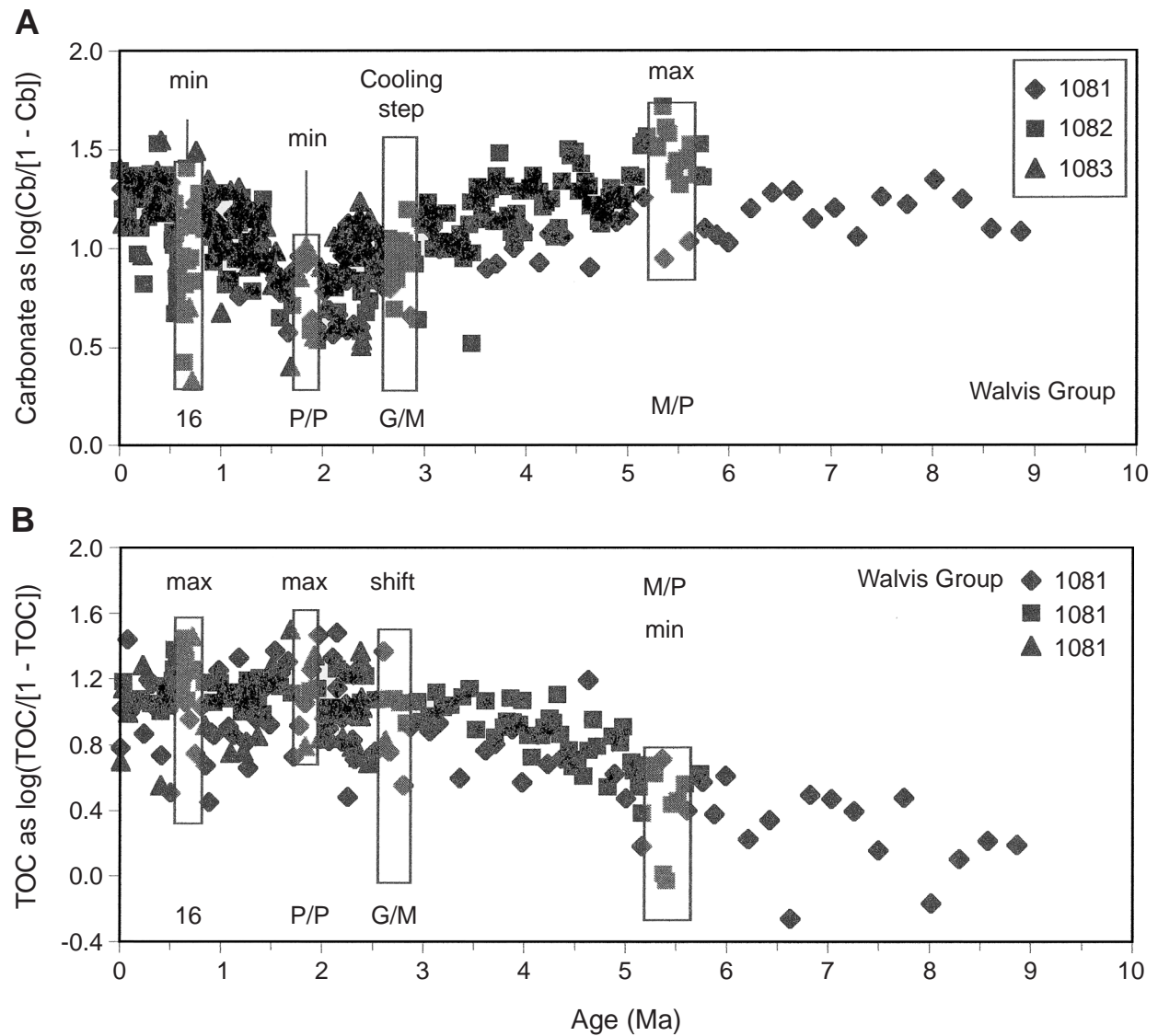


Figure F28. Overall patterns of carbon sedimentation at the Walvis group sites. A. Carbonate. B. Total organic carbon (TOC). Shipboard data (Wefer, Berger, Richter, et al., 1998); ages as in "Age Assignments and Sedimentation Rates," p. 9. 16 = Stage 16, P/P = Pliocene/Pleistocene boundary, G/M = Gauss/Matuyama reversal, M/P = Miocene/Pliocene boundary.



**Figure F29.** Comparison of diatom abundance, carbonate, and total organic carbon (TOC) content at Site 1084. **A.** Diatom smear slide abundance (Shipboard Scientific Party, 1998g, 1998h, 1998i, 1998j) for Walvis group sites (1081, 1082, and 1083) and Lüderitz Site (1084), showing the early Matuyama Diatom Maximum, centered on 2.2 to 2.3 Ma. The diatom regimes (oceanic types dominate, transition, and upwelling indicators dominate) are based on diatom taxonomy as interpreted in Lange et al. (1999). **B.** Shipboard carbonate data. **C.** Shipboard organic carbon data. Ages were reassigned based on age models in this report. Max = maximum, min = minimum, P/P = Pliocene/Pleistocene boundary, G/M = Gauss/Matuyama boundary, 11 = Stage 11.

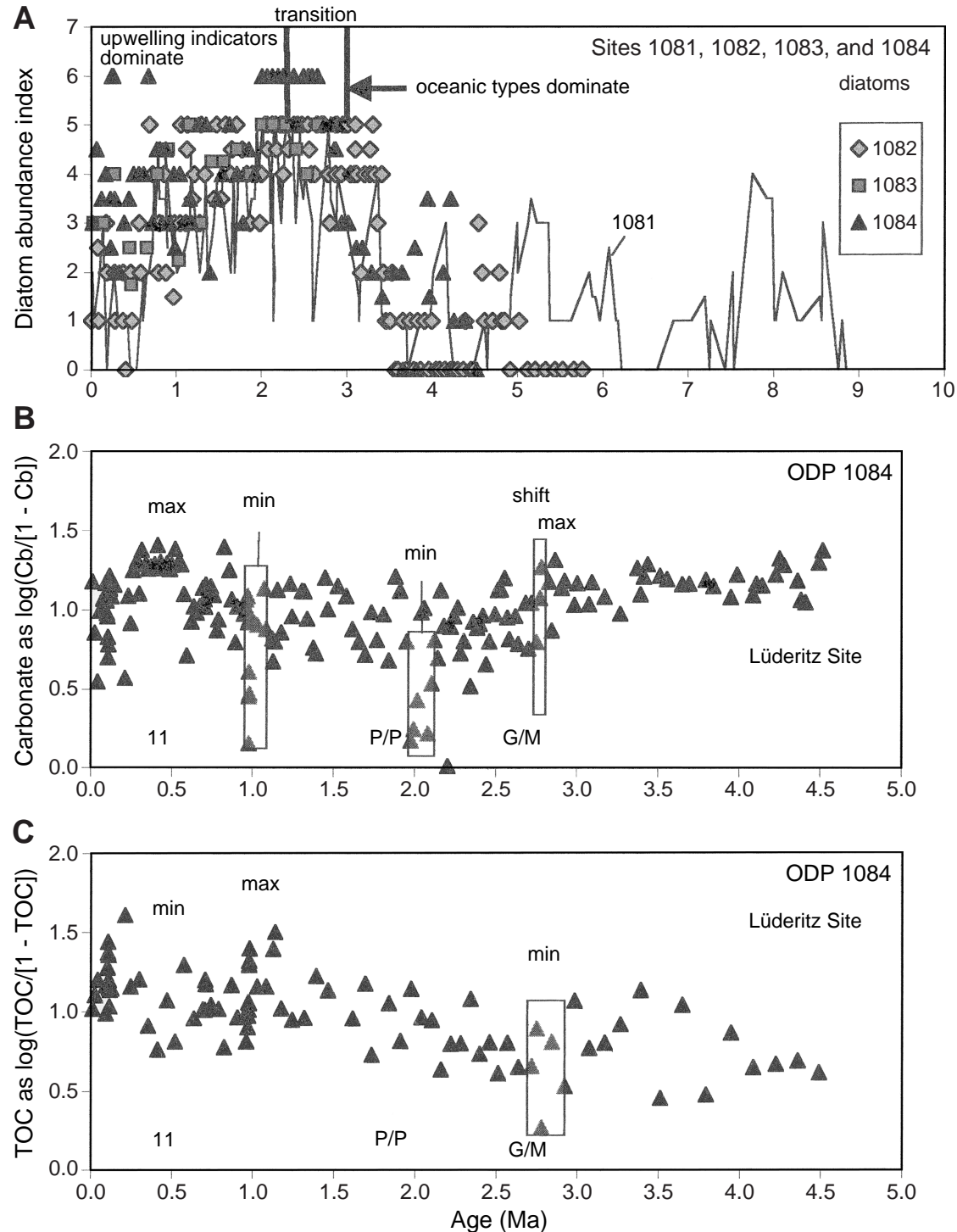
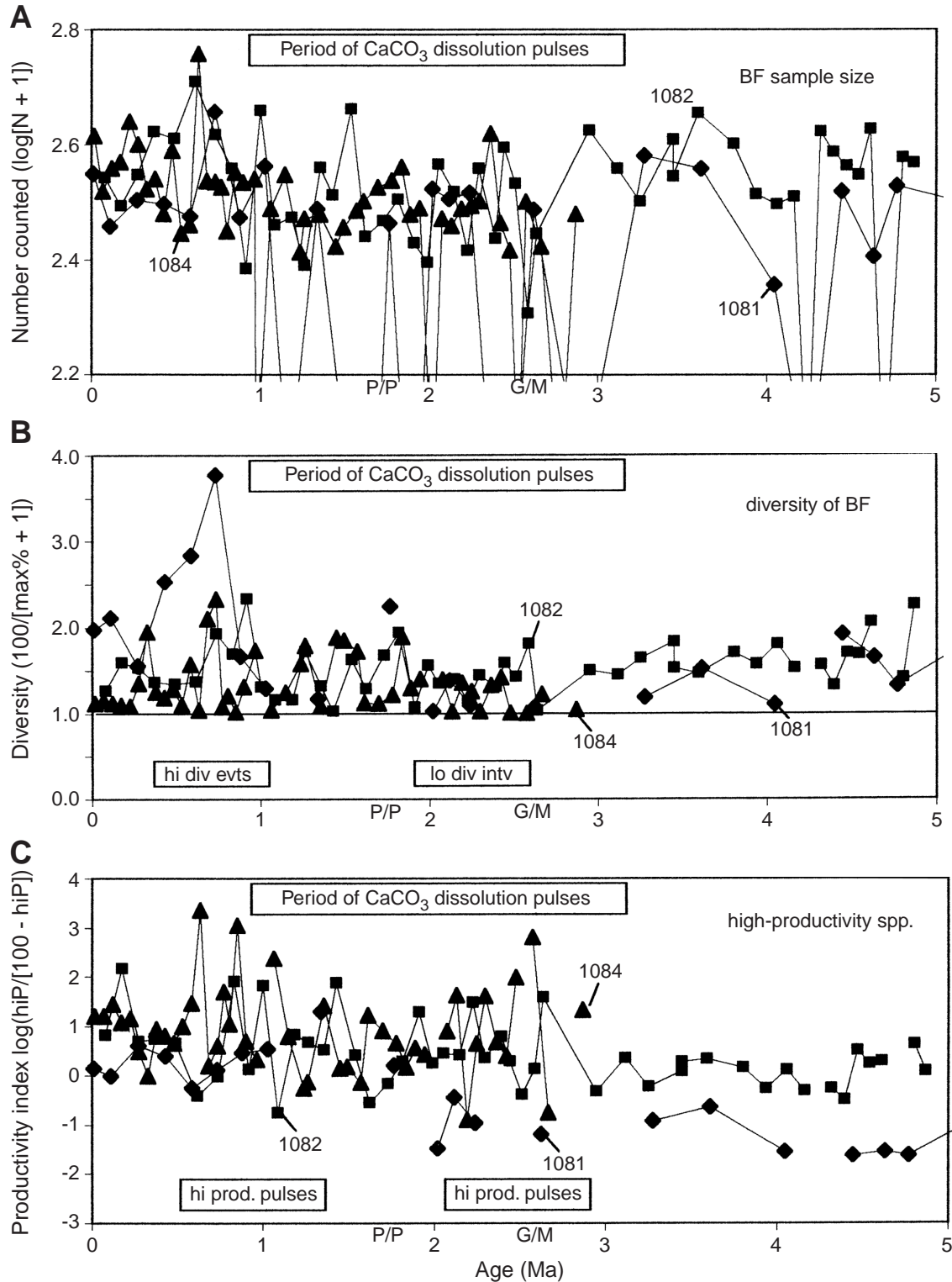
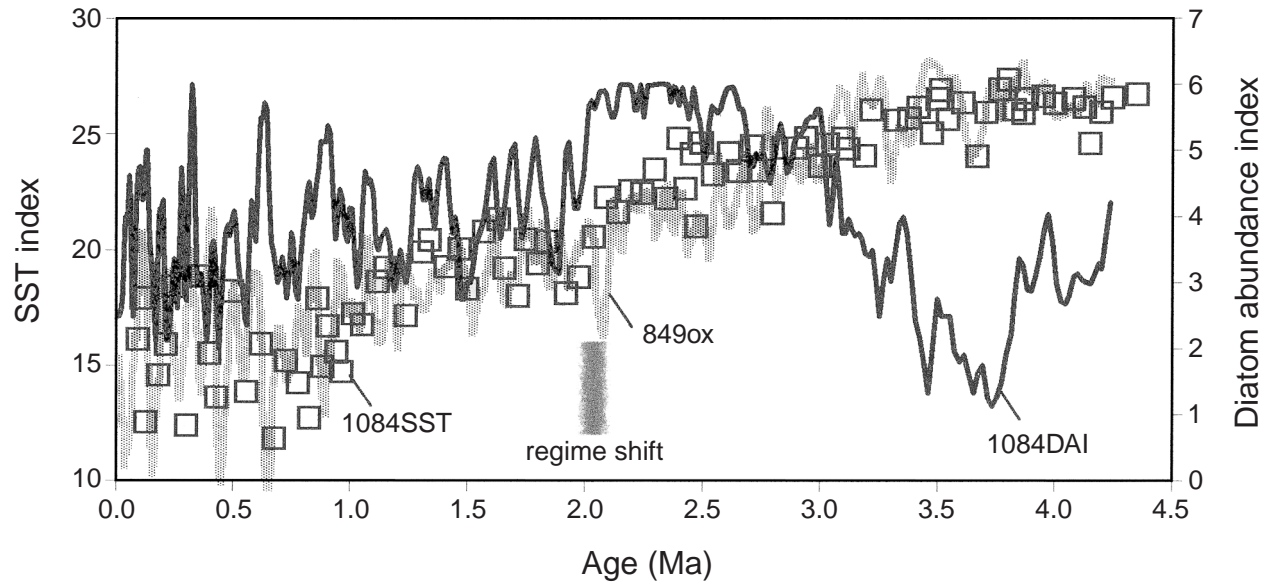


Figure F30. Productivity indices based on benthic foraminifers at Site 1084 and at two Walvis group sites. A. Number of tests counted for determination of species assemblage. B. Diversity of assemblages, calculated as  $1/\text{dominance}$  and expressed as a logarithm. C. Sum percentage of the taxa *Bolivina*, *Bulimina*, *Globobulimina*, and *Praeglobobulimina*. All counts are by Otto Hermelin (Shipboard Scientific Party, 1998g, 1998h, 1998j). hi div evts = high-diversity events, lo div intv = low-diversity interval, hi prod. = high productivity.



**Figure F31.** Comparison of diatom abundance (smear slide visual index, ranging from 0 to 6) with alkenone-derived sea-surface temperature (SST) series and an “expected” temperature series based on deepwater oxygen isotopes in the eastern equatorial Pacific. The series labeled “1084DAI,” “1084SST,” and “849ox” are derived from the original data by methods including repositioning and smoothing (see “[Early Matuyama Diatom Maximum: Search for Mechanisms](#),” p. 33). The raw data for the three series are from Lange et al. (1999), Marlow et al. (2000), and Mix et al. (1995), respectively.



**Figure F32.** Conceptual model of the Matuyama Diatom Maximum (MDM) between 2.6 and 2.1 Ma. The input parameter is the system state  $x$ , represented by deepwater oxygen isotopes ( $\delta^{18}\text{O}$  of benthic foraminifers from Site 849, eastern equatorial Pacific; Mix et al., 1995), greatly smoothed. A frontal zone optimum is defined as those numbers of  $x$  that lie within the interval MDM. The model depends on  $x$  itself (taken as a proxy for upwelling) and on the absolute difference of  $x$  to the nearest value within the frontal zone optimum. All such difference values are increased by 0.5 and then inverted to write the two-dimensional equation (see “[Early Matuyama Diatom Maximum: Search for Mechanisms](#),” p. 33). The Site 1084 diatom abundance index (DAI) data are from Lange et al. (1999); the sea-surface temperature (SST) index (y-axis) is based on transforming  $x$  to the mean and range of the Site 1084 alkenone SST of Marlow et al. (2000).

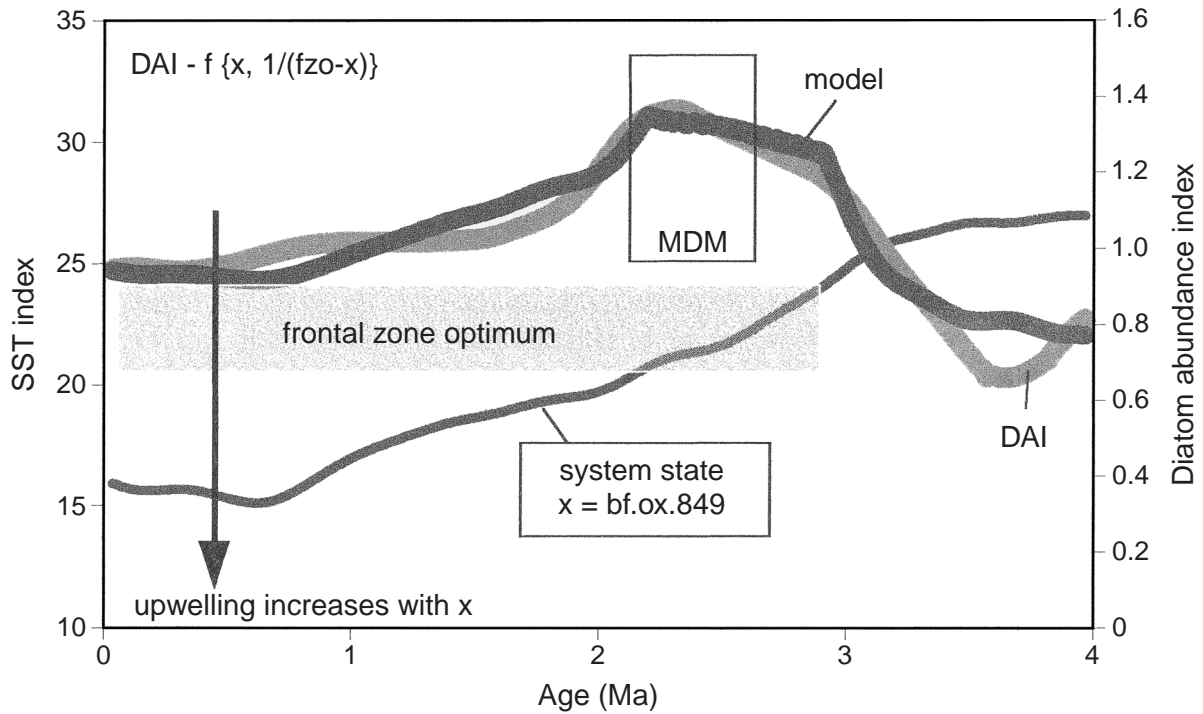
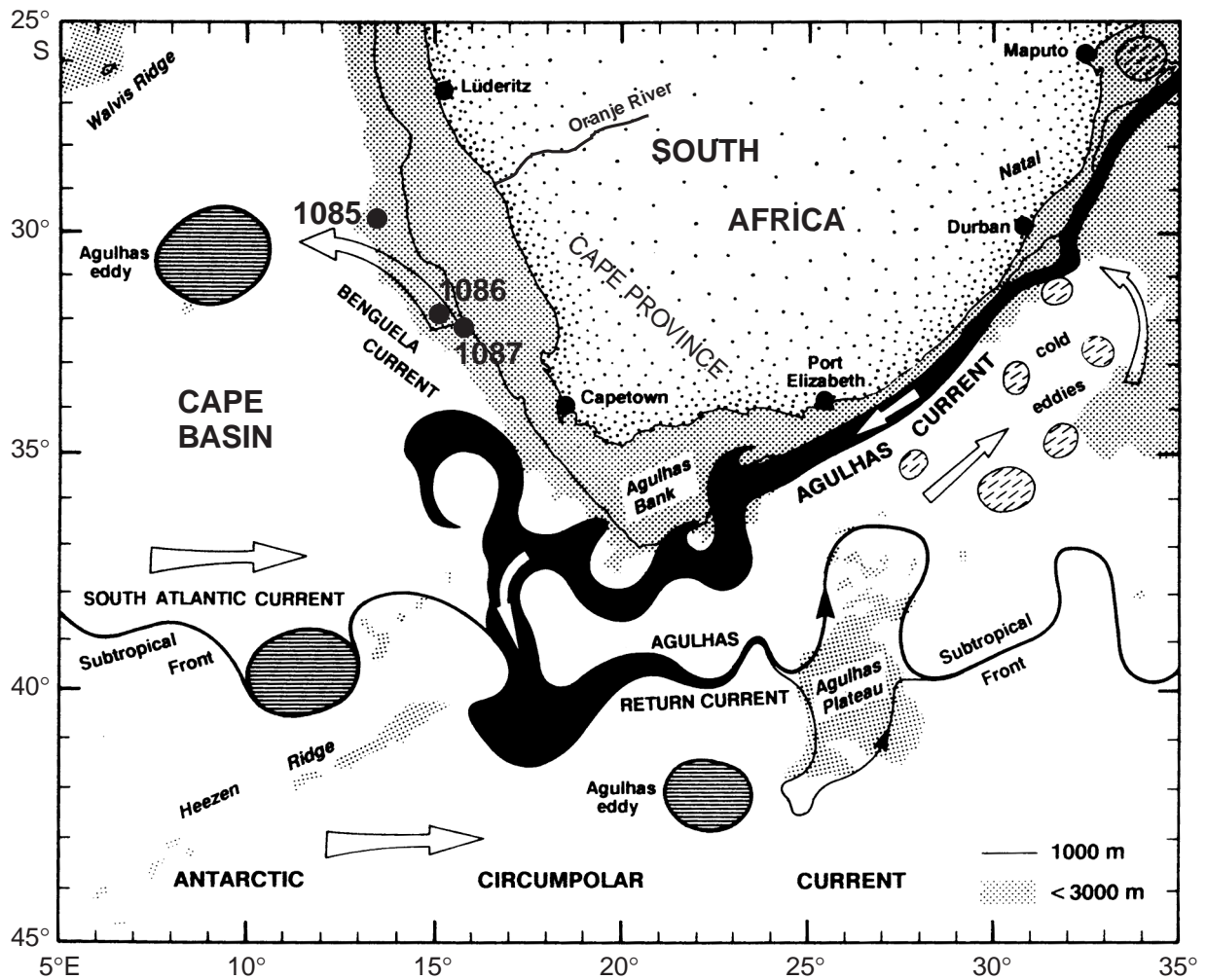


Figure F33. Location of the Cape group sites (1085, 1086, and 1087) off the Cape Province off South Africa and at the eastern margin of the Cape Basin. Note the various water masses combining here to form the beginning of the Namibia Current ("Benguela Current").



**Figure F34.** Carbon record of the Cape group sites (1085, 1086, and 1087). A. Carbonate is plotted as the logarithm of the ratio between carbonate and noncarbonate (see “Carbonate and Organic Carbon Record,” p. 36). Events are identified and labeled (“CI,” Carbonate Event Roman One, etc.), for ease of reference. B. Organic carbon is similarly plotted as log of ratio. Unity is added to avoid negative numbers. The Carbonate Event Numbers are retained as is for comparison. The boxes are specific to the organic carbon. Data are from Shipboard Scientific Party 1998k, 1998m) and from the data report of Meyers and Robinson (Chap. 2, this volume). P/P = Pliocene/Pleistocene boundary, G/M = Gauss/Matuyama reversal, M/P = Miocene/Pliocene boundary, T/M = Tortonian/Messinian boundary, ItM = late Miocene, ItM/mM = late Miocene/middle Miocene boundary.

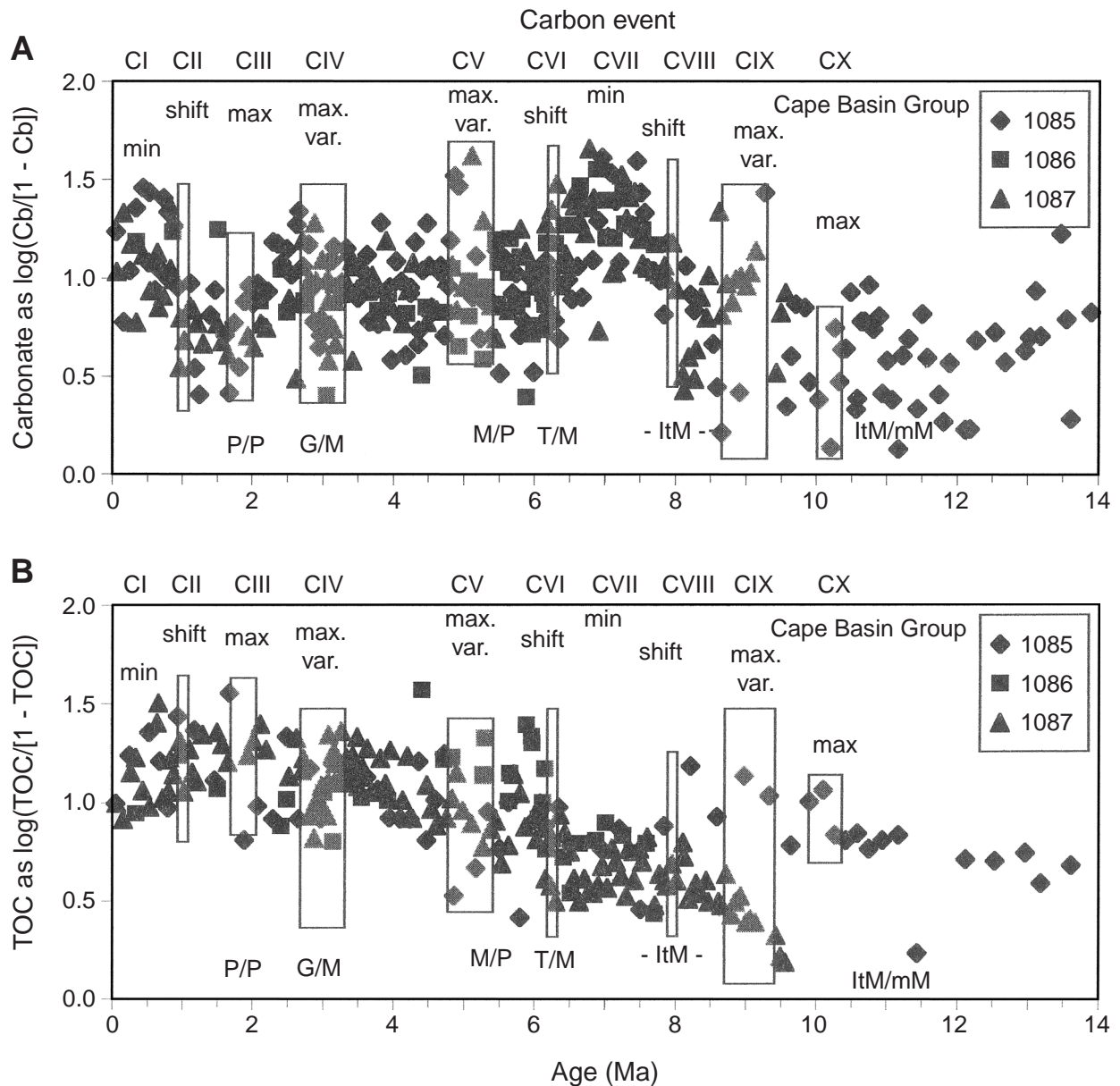
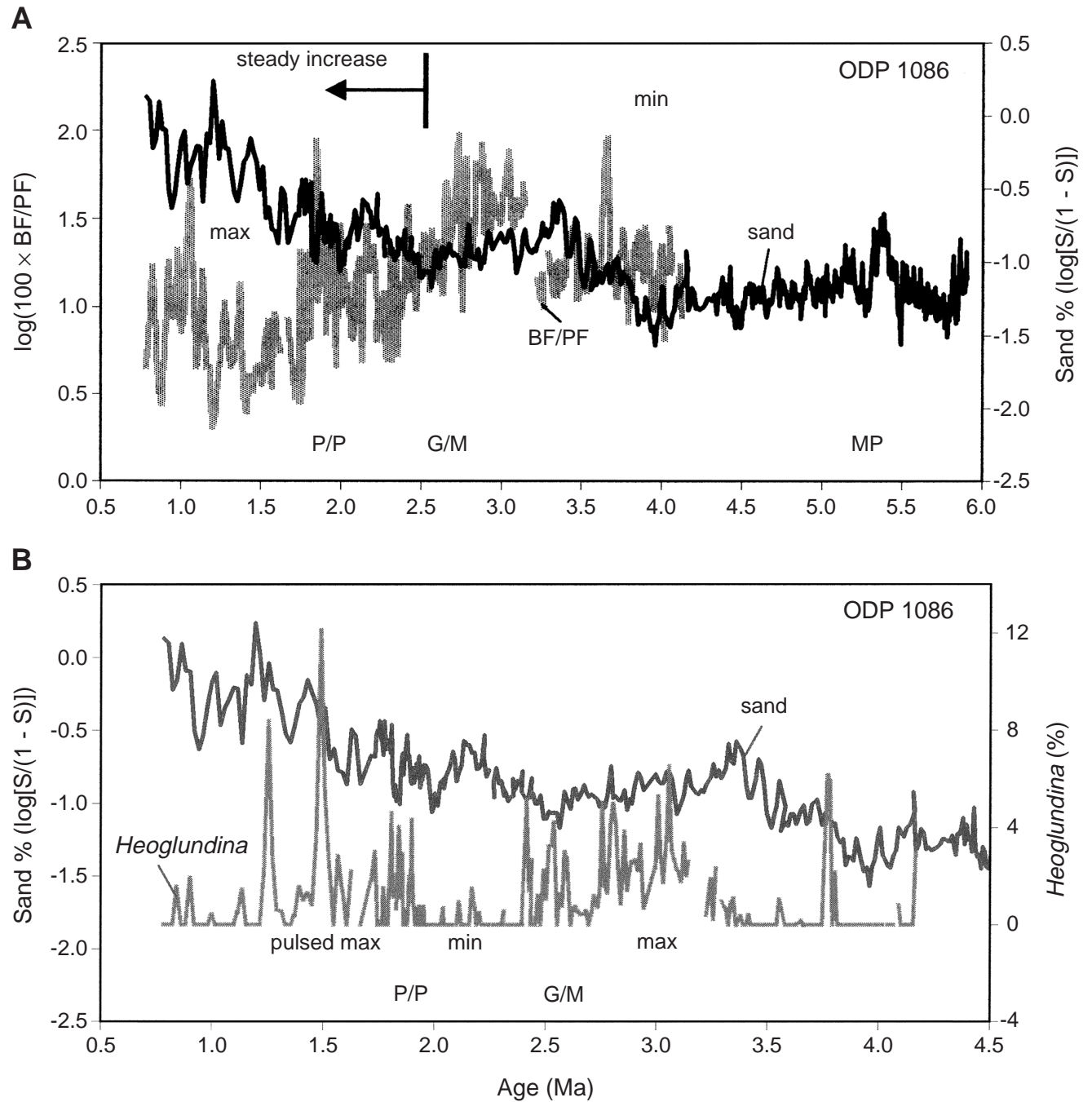
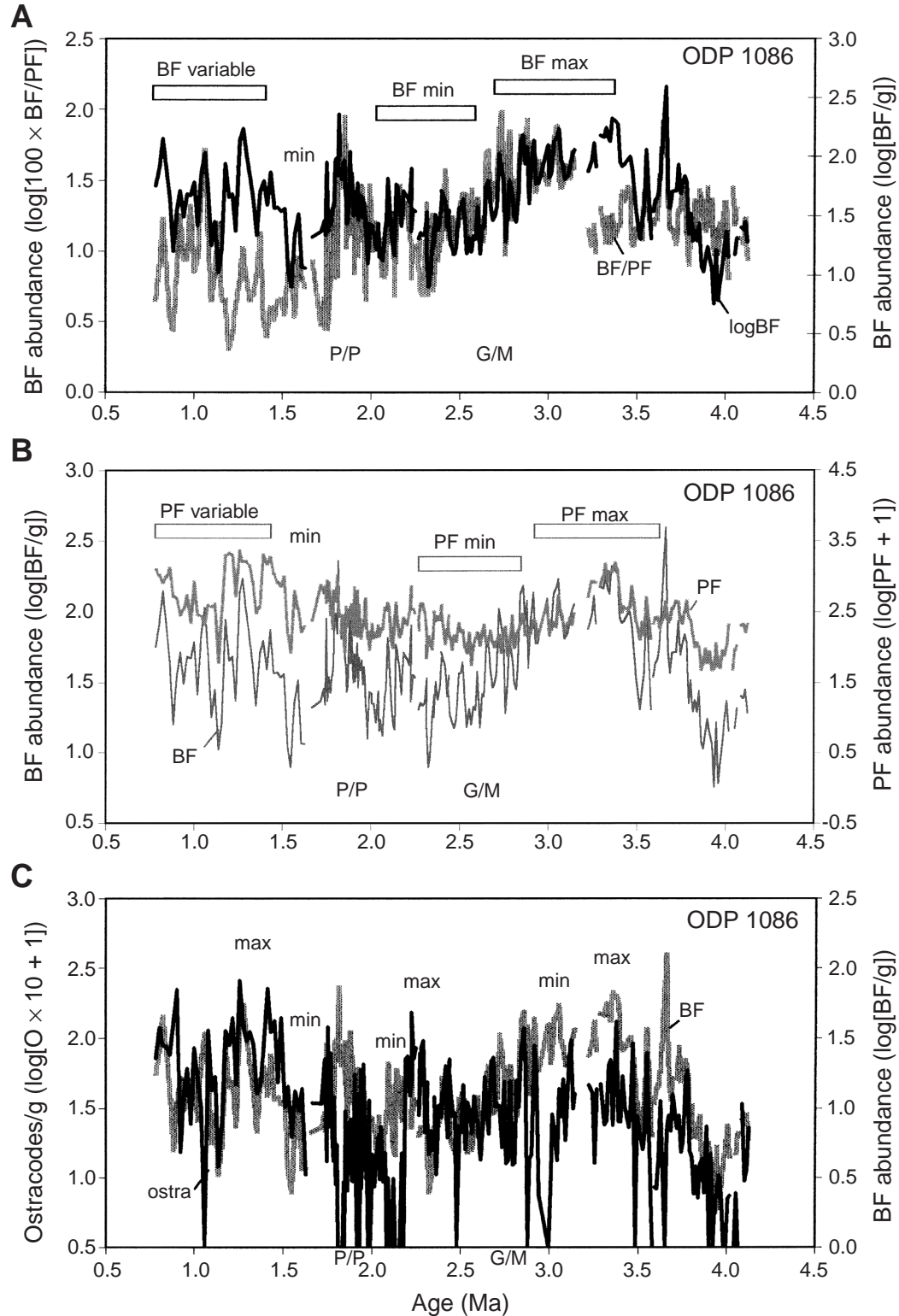


Figure F35. Sand content at Site 1086 for the last 6 m.y., compared with (A) the ratio of benthic to planktonic foraminifers and with (B) the abundance of *Hoeglundina elegans*, an aragonitic benthic species. Note the shorter time span in B. P/P = Pliocene/Pleistocene boundary, G/M = Gauss/Matuyama reversal, BF = benthic foraminifer, PF = planktonic foraminifer, MP = Miocene/Pliocene boundary.



**Figure F36.** Comparison of the abundance of benthic foraminifers (BF), planktonic foraminifers (PF), and benthic ostracodes (ostra) in the upper section of Site 1086 (last 4 m.y.). **A.** BF/PF vs. BF/g. **B.** BF/g vs. PF/g. The minima and maxima are similarly positioned in the two indices. **C.** Abundance pattern of ostracodes compared with BF/g. (All indices are on log scale.) P/P = Pliocene/Pleistocene boundary, G/M = Gauss/Matuyama reversal.



**Figure F37.** Productivity reconstruction from benthic foraminifers (BF): taxon indices. **A.** Abundance of *Uvigerina* compared with the BF/PF ratio. **B.** Abundance of the sum of *Bolivina* and *Bulimina* (BoBu) and that of *Cibicides* (Cib). **C.** *Uvigerina* abundance compared with the ratio BoBu/Cib, a highly sensitive productivity index. PF = planktonic foraminifers, P/P = Pliocene/Pleistocene boundary, G/M = Gauss/Matuyama reversal.

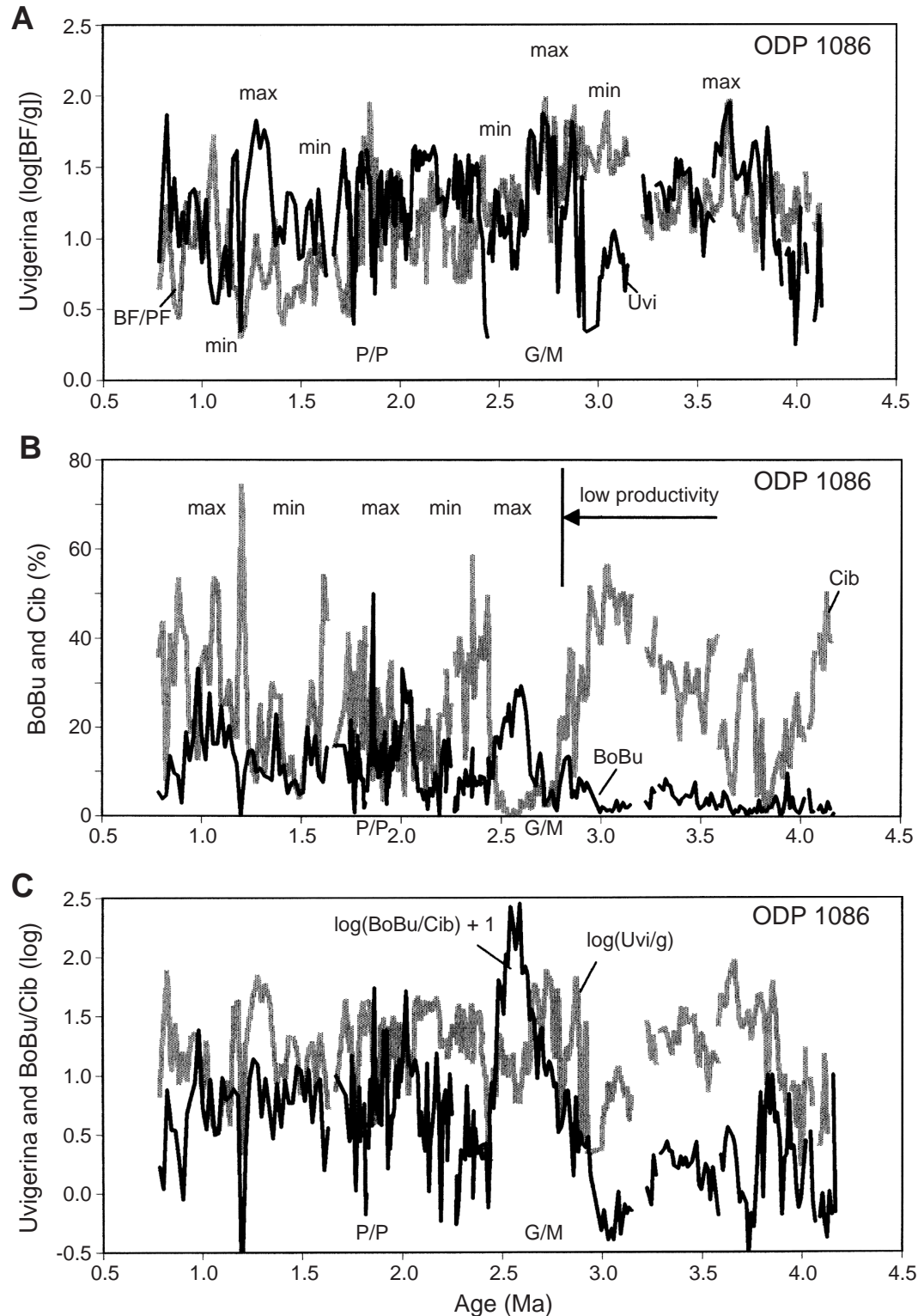
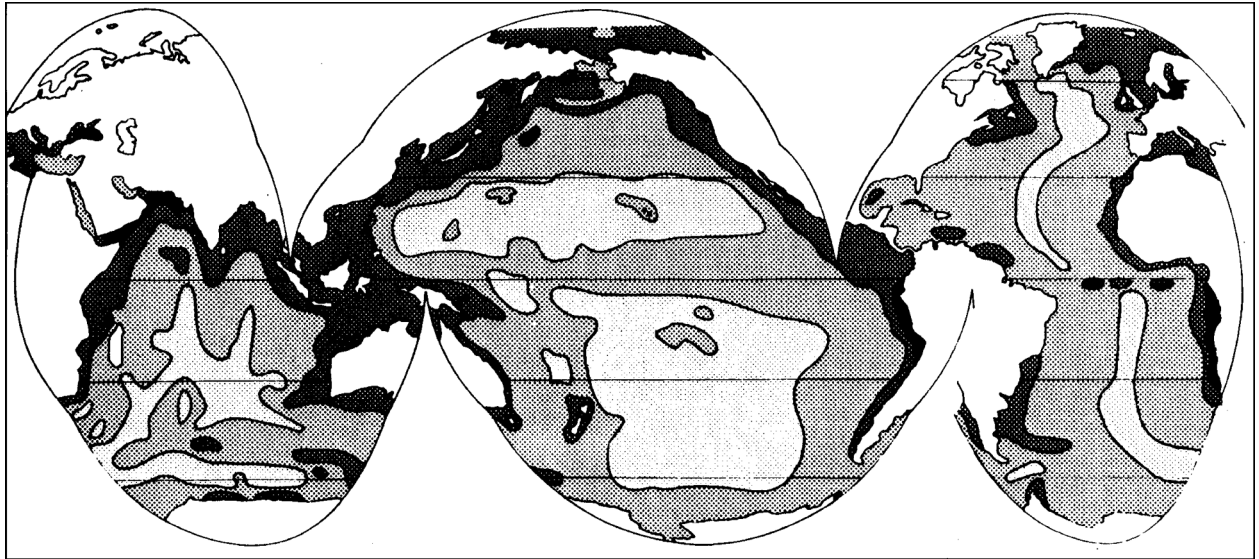


Figure F38. Present-day patterns of distribution of organic matter and opal on the seafloor. From Berger and Herguera (1992). A. Percent  $C_{org}$ . B. Siliceous microfossils and opal flux.

A



B

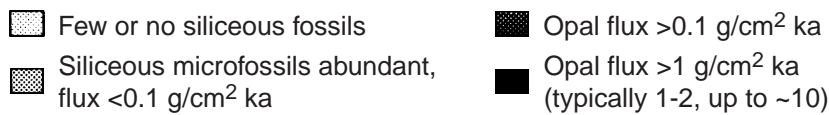
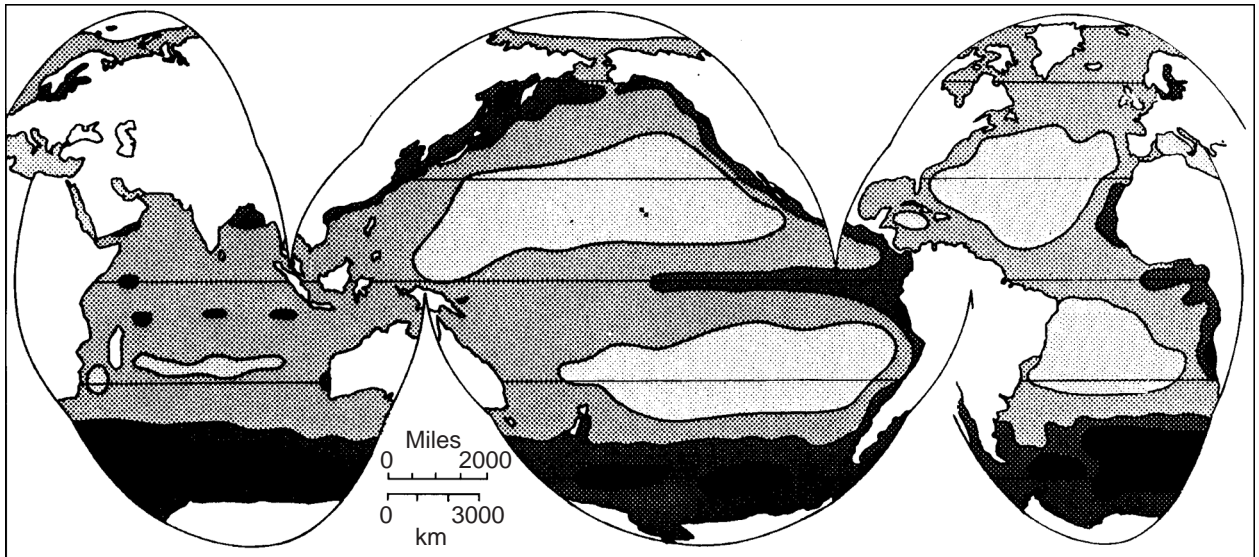


Table T1. Age models for Congo and Angola sites.

Depth (mbsf)	Age (Ma)				
	Site 1075	Site 1076	Site 1077	Site 1078	Site 1079
0	0	0	0	0	0
10	0.064	0.051	0.045	0.052	0.035
20	0.133	0.101	0.094	0.091	0.078
30	0.211	0.150	0.149	0.122	0.124
40	0.302	0.193	0.210	0.145	0.171
50	0.409	0.230	0.281	0.164	0.213
60	0.524	0.267	0.364	0.181	Disturbed
70	0.644	0.314	0.456	0.196	Disturbed
80	0.765	0.386	0.547	0.211	0.227
90	0.878	0.496	0.629	0.225	0.293
100	0.978	0.645	0.691	0.238	0.439
110	1.062	0.805	0.743	0.252	0.680
120	1.138	0.935	0.799	0.266	0.878
130	1.217	0.680	0.888	0.281	1.039
140	1.308	0.797	1.014	0.297	
150	1.420	0.912	1.187	0.315	
160	1.556	1.013	1.397	0.334	
170	1.714	1.100	1.607	0.353	
180	1.887	1.175	1.817		
190	2.062	1.243	2.027		
200	2.224	1.307	2.237		

Notes: Assignments of ages to depths below seafloor are based on nannofossil stratigraphy and paleomagnetic reversals, with information from cyclic stratigraphy, in cases (see Figs. F8, p. 63, F9, p. 64, F10, p. 65, F11 p. 66, F12, p. 67). The assignments are not precise. Decimal digits are given to preserve apparent sedimentation rates. Errors of age assignment are routinely of the magnitude 0.01 m.y. and greater.

Table T2. Age models for Namibia and South Africa sites.

Depth (mbsf)	Age (Ma)						
	Site 1081	Site 1082	Site 1083	Site 1084	Site 1085	Site 1086	Site 1087
0	0	0	0	0	0	0.75	0
10	0.171	0.101	0.153	0.053	0.291	1.731	0.333
20	0.309	0.203	0.257	0.107	0.492	1.989	0.566
30	0.482	0.307	0.347	0.161	0.643	2.432	0.750
40	0.612	0.413	0.444	0.216	0.800	3.038	0.916
50	0.774	0.521	0.553	0.272	1.049	3.719	1.119
60	0.867	0.629	0.676	0.330	1.333	4.312	1.475
70	1.066	0.734	0.806	0.389	1.558	4.727	1.927
80	1.245	0.831	0.938	0.449	1.776	5.003	2.437
90	1.435	0.923	1.072	0.509	1.980	5.231	2.643
100	1.627	1.011	1.208	0.568	2.204	5.434	2.829
110	1.803	1.098	1.349	0.625	2.410	5.589	2.941
120	1.940	1.186	1.496	0.682	2.596	5.694	3.062
130	2.032	1.280	1.648	0.734	2.766	5.787	3.168
140	2.100	1.385	1.802	0.783	2.928	5.920	3.270
150	2.167	1.499	1.952	0.830	3.089	6.119	3.373
160	2.242	1.621	2.096	0.879	3.254	6.369	3.514
170	2.321	1.743	2.234	0.925	3.425	6.635	3.781
180	2.415	1.859	2.368	0.968	3.600	6.906	4.104
190	2.559	1.964	2.500	1.012	3.772	7.201	4.452
200	2.762	2.058	2.632	1.058	3.935	7.530	4.750
210	3.026	2.143	2.763	1.109	4.084	7.884	5.044
220	3.304	2.224		1.166	4.221		5.327
230	3.587	2.302		1.228	4.350		5.593
240	3.856	2.379		1.297	4.480		5.841
250	4.111	2.457		1.370	4.617		6.071
260	4.355	2.535		1.446	4.766		6.289
270	4.594	2.615		1.524	4.927		6.500
280	4.836	2.696		1.603	5.098		6.709
290	5.087	2.777		1.682	5.275		6.916
300	5.343	2.859		1.759	5.455		7.119
310	5.597	2.941		1.833	5.636		7.318
320	5.841	3.022		1.904	5.818		7.511
330	6.069	3.103		1.972	6.001		7.698
340	6.283	3.184		2.038	6.186		7.878
350	6.489	3.266		2.103	6.377		8.056
360	6.697	3.349		2.167	6.583		8.236
370	6.914	3.433		2.229	6.811		8.424
380	7.144	3.519		2.291	7.073		8.621
390	7.389	3.605		2.352	7.373		8.829
400	7.648	3.694		2.412	7.712		9.046
410	7.919	3.785		2.473	8.084		9.268
420	8.201	3.877		2.534	8.473		9.492
430	8.492	3.972		2.597	8.860		9.716
440		4.068		2.663	9.222		9.940
450		4.166		2.734	9.539		10.165
460		4.266		2.811	9.803		10.390
470		4.367		2.893	10.018		10.616
480		4.469		2.980	10.197		10.842
490		4.572		3.071	10.359		11.068
500		4.677		3.164	10.521		11.294
510		4.782		3.263	10.696		
520		4.888		3.371	10.894		
530		4.995		3.493	11.126		
540		5.103		3.630	11.400		
550		5.212		3.779	11.725		
560		5.324		3.934	12.102		
570		5.438		4.083	12.521		
580		5.552		4.217	12.961		
590		5.667		4.352	13.401		
600		5.781		4.487	13.840		
610				4.622	14.280		

Notes: Assignments of ages to depths below seafloor are based on nannofossil stratigraphy and paleomagnetic reversals with information from cyclic stratigraphy, in cases (see Figs. F8, p. 63, F9, p. 64, F10, p. 65, F11, p. 66, F12, p. 67). The assignments are not precise. Decimal digits are given to preserve apparent sedimentation rates. Errors of age assignment are routinely of the magnitude 0.01 m.y. and greater.

**Table T3.** Approximate percentages for integrated core expansion.

Depth (mbsf)	Core expansion (%)											
	Congo and Angola Sites					Walvis and Cape Basin Sites						
	Site 1075	Site 1076	Site 1077	Site 1078	Site 1079	Site 1081	Site 1082	Site 1083	Site 1084	Site 1085	Site 1086	Site 1087
50	5	10	8	5.5	4.5	11	10	10	15.5	12	10	11
100	9	11	8	6	5	8.5	10	10	17	11	9	12
150	11	12	7			8.5	10	11	18	11	9	12
200	13	12	7			6.5		10.5	18	9.5	10.5	12
300									11	9		

Note: Based on composite depth profiles from physical properties (from shipboard data: Wefer, Berger, Richter, et al., 1998).

**Table T4.** Average ages of events defined and effectively used in present age-depth graphs, Congo and Angola sites.

Biostratigraphic event	Age (Ma)			N
	Shipboard defined	Effectively used weighted	Effectively used unweighted	
N FO <i>Emiliana huxleyi</i> acme	0.09	0.09	0.09	7
N FO <i>Emiliana huxleyi</i>	0.26	0.30	0.30	6
N <i>Gephyrocapsa caribbeanica</i> acme	0.26	0.30	0.30	6
N LO <i>Pseudoemiliana lacunosa</i>	0.46	0.41	0.43	4
R LO <i>Axoprunum angelinum</i>	0.46	0.38	0.38	3
N Small <i>Gephyrocapsa</i> acme	0.6	0.59	0.58	3
S LO <i>Bachmannocena quadrangula</i>	0.8	0.87	0.86	2
N LO <i>Reticulofenestra asanoi</i>	0.83	0.82	0.82	3
D LO <i>Nitzschia fossilis</i>	0.92	1.07	1.07	1
N Small <i>Gephyrocapsa</i> acme	0.96	0.91	0.93	3
N FO <i>Reticulofenestra asanoi</i>	1.06	1.07	1.07	1
R LO <i>Lamprocyrtis neoheteroporos</i>	1.07	1.43	1.37	2
N LO <i>Helicosphaera sellii</i>	1.25	1.29	1.30	4
N LO <i>Calcidiscus macintyreii</i>	1.67	1.52	1.56	2

Notes: N = nannofossil, R = radiolarian, S = silicoflagellate, D = diatom. FO = first occurrence, LO = last occurrence. N = number of samples. Estimated age weighted according to narrowness of age range, and unweighted. Average effective ages of biostratigraphic events are as used in the age models. Weighted = estimated age weighted according to narrowness of age range, unweighted = not so weighted. (Differences between shipboard-assigned age and effectively used age arise from a number of sources such as sampling interval vs. sedimentation rate, intensity of search for presence and absence of a nannofossil, and problems of preservation. Thus, the data do not necessarily reflect real differences in assigned ages of events and their occurrence at the sites occupied. They do give an idea about the consistency of biostratigraphic shipboard assignments in the circumstances of Leg 175.)

Table T5. Average effective ages of biostratigraphic events as used in the age models of Sites 1081–1084 (Walvis sites).

Biostratigraphic event	Age (Ma)			N
	Shipboard defined	Effectively used weighted	Effectively used unweighted	
N FO <i>Emiliana huxleyi</i> acme	0.09	0.06	0.06	2
N FO <i>Emiliana huxleyi</i>	0.26	0.27	0.28	5
N <i>Gephyrocapsa caribbeanica</i> acme	0.26	0.27	0.28	5
R LO <i>Axoprunum angelinum</i>	0.46	0.39	0.38	3
N LO <i>Pseudoemiliana lacunosa</i>	0.46	0.44	0.45	4
N Small <i>Gephyrocapsa</i> acme	0.60	0.56	0.56	3
D LO <i>Nitzschia reinholdii</i>	0.69	0.61	0.63	2
S LO <i>Bachmannocena quadrangula</i>	0.80	0.74	0.71	4
N LO <i>Reticulofenestra asanoi</i>	0.83	0.76	0.76	4
D LO <i>Nitzschia fossilis</i>	0.92	0.64	0.64	1
N Small <i>Gephyrocapsa</i> acme	0.96	0.97	0.96	3
N FO <i>Reticulofenestra asanoi</i>	1.06	1.09	1.09	1
R LO <i>Lamprocyrtis neoheteroporos</i>	1.07	0.97	0.92	3
D LO <i>Rhizosolenia matuyama</i>	1.10	1.07	1.06	3
N LO <i>Helicosphaera sellii</i>	1.25	1.23	1.23	4
D LO <i>Rhizosolenia praebergonii</i> (robust)	1.65	1.61	1.75	2
N LO <i>Calcidiscus macintyreii</i>	1.67	1.63	1.63	4
D LO <i>Proboscia barboi</i>	1.68	1.69	1.66	4
R LO <i>Cycladophora pliocenica</i>	1.83	1.79	1.80	4
D LO <i>Fragilariopsis doliolus</i>	1.88	1.51	1.51	1
N LO <i>Discoaster brouweri</i>	1.95	2.07	2.05	4
D LO <i>Thalassiosira kolbei</i>	1.96	1.67	1.67	1
D LO <i>Thalassiosira convexa</i>	2.19	2.39	2.41	2
N LO <i>Discoaster surculus</i>	2.55	2.70	2.67	2
R FO <i>Cycladophora davisiana</i>	2.70	2.61	2.56	3
D FO <i>Rhizosolenia praebergonii</i>	3.12	2.95	2.95	2
N LO <i>Sphenolithus</i> spp.	3.66	3.70	3.70	1
N LO <i>Reticulofenestra pseudoumbilicus</i>	3.82	3.84	3.73	2
N LO <i>Amaurolithus tricorniculatus</i>	4.50	4.09	4.09	1
R FO <i>Spongurus pylomaticus</i>	5.20	5.11	5.06	2
N LO <i>Discoaster quinqueramus</i>	5.54	5.50	5.50	2
N FO <i>Discoaster quinqueramus</i>	8.60	8.50	8.50	1

Notes: N = nannofossil, R = radiolarian, S = silicoflagellate, D = diatom. FO = first occurrence, LO = last occurrence. N = number of samples. Estimated age weighted according to narrowness of age range, and unweighted. Average effective ages of biostratigraphic events are as used in the age models. Weighted = estimated age weighted according to narrowness of age range, unweighted = not so weighted. (Differences between shipboard-assigned age and effectively used age arise from a number of sources such as sampling interval vs. sedimentation rate, intensity of search for presence and absence of a nannofossil, and problems of preservation. Thus, the data do not necessarily reflect real differences in assigned ages of events and their occurrence at the sites occupied. They do give an idea about the consistency of biostratigraphic shipboard assignments in the circumstances of Leg 175.)

**Table T6.** Average ages of events defined and effectively used in present age-depth graphs, Sites 1085–1087 (Cape Basin sites).

Biostratigraphic event	Age (Ma)			N
	Shipboard defined	Effectively used weighted	Effectively used unweighted	
N FO <i>Emiliana huxleyi</i> acme	0.09	0.15	0.15	1
N FO <i>Emiliana huxleyi</i>	0.26	0.23	0.23	2
N <i>Gephyrocapsa caribbeanica</i> acme	0.26	0.23	0.23	2
R LO <i>Axoprunum angelinum</i>	0.46	0.48	0.48	1
N LO <i>Pseudoemiliana lacunosa</i>	0.46	0.42	0.42	2
N Small <i>Gephyrocapsa</i> acme	0.60	0.64	0.60	2
N LO <i>Reticulofenestra asanoi</i>	0.83	0.75	0.75	2
N Small <i>Gephyrocapsa</i> acme	0.96	0.93	0.93	1
N LO <i>Helicosphaera sellii</i>	1.25	1.08	1.06	2
N LO <i>Calcidiscus macintyreii</i>	1.67	1.35	1.52	3
N LO <i>Discoaster brouweri</i>	1.95	1.93	1.85	3
D LO <i>Thalassiosira convexa</i>	2.19	2.07	2.07	1
N LO <i>Discoaster surculus</i>	2.55	2.45	2.46	3
R FO <i>Cycladophora davisiana</i>	2.70	2.47	2.47	1
N LO <i>Discoaster tamalis</i>	2.83	2.71	2.72	2
N LO <i>Reticulofenestra pseudoumbilicus</i>	3.82	3.81	3.78	3
N LO <i>Amaurolithus tricorniculatus</i>	4.50	4.41	4.39	3
N FO <i>Discoaster asymmetricus</i>	5.02	4.66	4.77	2
N LO <i>Discoaster quinquerramus</i>	5.54	5.29	5.29	3
N LO <i>Amaurolithus amplifucus</i>	5.90	6.05	6.05	3
N FO <i>Amaurolithus amplifucus</i>	6.60	6.65	6.61	3
N FO <i>Amaurolithus primus</i>	7.20	7.24	7.24	2
N FO <i>Discoaster quinquerramus</i>	8.60	8.41	8.43	2
N LO <i>Discoaster bollii</i>	9.10	9.05	9.05	1
N LO <i>Discoaster hamatus</i>	9.63	9.67	9.67	1
N FO <i>Discoaster hamatus</i>	10.70	10.70	10.70	1

Notes: N = nannofossil, R = radiolarian, S = silicoflagellate, D = diatom. FO = first occurrence, LO = last occurrence. N = number of samples. Estimated age weighted according to narrowness of age range, and unweighted. Average effective ages of biostratigraphic events are as used in the age models. Weighted = estimated age weighted according to narrowness of age range, unweighted = not so weighted. (Differences between shipboard-assigned age and effectively used age arise from a number of sources such as sampling interval vs. sedimentation rate, intensity of search for presence and absence of a nannofossil, and problems of preservation. Thus, the data do not necessarily reflect real differences in assigned ages of events and their occurrence at the sites occupied. They do give an idea about the consistency of biostratigraphic shipboard assignments in the circumstances of Leg 175.)

**Table T7.** Comparison of average effective ages of biostratigraphic events for Congo, Walvis, and Cape Basin sites.

Biostratigraphic event		Age (Ma)									
		Shipboard age	Congo sites			Walvis sites			Cape Basin sites		
			Age range (weighted)	Age range (unweighted)	N	Age range (weighted)	Age range (unweighted)	N	Age range (weighted)	Age range (unweighted)	N
N	FO <i>Emiliana huxleyi</i> acme	0.09	0.09	0.09	7	0.06	0.06	2	0.15	0.15	1
N	FO <i>Emiliana huxleyi</i>	0.26	0.30	0.30	6	0.27	0.28	5	0.23	0.23	2
N	<i>Gephyrocapsa caribbeanica</i> acme	0.26	0.30	0.30	6	0.27	0.28	5	0.23	0.23	2
R	LO <i>Axoprunum angelinum</i>	0.46	0.38	0.38	3	0.39	0.38	3	0.48	0.48	1
N	LO <i>Pseudoemiliana lacunosa</i>	0.46	0.41	0.43	4	0.44	0.45	4	0.42	0.42	2
N	Small <i>Gephyrocapsa</i> acme	0.6	0.59	0.58	3	0.56	0.56	3	0.64	0.60	2
N	LO <i>Reticulofenestra asanoi</i>	0.83	0.82	0.82	3	0.76	0.76	4	0.75	0.75	2
D	LO <i>Nitzschia fossilis</i>	0.92	1.07	1.07	1	0.64	0.64	1			
N	Small <i>Gephyrocapsa</i> acme	0.96	0.91	0.93	3	0.97	0.96	3	0.93	0.93	1
N	FO <i>Reticulofenestra asanoi</i>	1.06	1.07	1.07	1	1.09	1.09	1			
R	LO <i>Lamprocyrtis neoheteroporos</i>	1.07	1.43	1.37	2	0.97	0.92	3			
N	LO <i>Helicosphaera sellii</i>	1.25	1.29	1.30	4	1.23	1.23	4	1.08	1.06	2
N	LO <i>Calcidiscus macintyreii</i>	1.67	1.52	1.56	2	1.63	1.63	4	1.35	1.52	3
N	LO <i>Discoaster brouweri</i>	1.95				2.07	2.05	4	1.93	1.85	3
D	LO <i>Thalassiosira convexa</i>	2.19				2.39	2.41	2	2.07	2.07	1
N	LO <i>Discoaster brouweri</i>	2.55				2.70	2.67	2	2.45	2.46	3
R	FO <i>Cycladophora davisiana</i>	2.70				2.61	2.56	3	2.47	2.47	1
N	LO <i>Reticulofenestra pseudoumbilicus</i>	3.82				3.84	3.73	2	3.81	3.78	3
N	LO <i>Amaurolithus tricorniculatus</i>	4.50				4.09	4.09	1	4.41	4.39	3

Notes: N = nannofossil, R = radiolarian, S = silicoflagellate, D = diatom. FO = first occurrence, LO = last occurrence. N = number of samples. Estimated age weighted according to narrowness of age range, and unweighted. Average effective ages of biostratigraphic events are as used in the age models. Weighted = estimated age weighted according to narrowness of age range, unweighted = not so weighted. (Differences between shipboard-assigned age and effectively used age arise from a number of sources such as sampling interval vs. sedimentation rate, intensity of search for presence and absence of a nannofossil, and problems of preservation. Thus, the data do not necessarily reflect real differences in assigned ages of events and their occurrence at the sites occupied. They do give an idea about the consistency of biostratigraphic shipboard assignments in the circumstances of Leg 175.)